Summer 8-15-2018

The Mechanism of Hyper Daptomycin Resistance in Corynebacterium striatum and Daptomycin's Mechanism of Action

Nicholas Kevork Goldner
Washington University in St. Louis

WASHINGTON UNIVERSITY IN ST. LOUIS

Division of Biology and Biomedical Sciences
Molecular Cell Biology

Dissertation Examination Committee:
Gautam Dantas, Chair
Carey-Ann Burnham
Jeffery Henderson
Shabaana Khader
Rob Mitra
Paul Schlesinger

The Mechanism of Hyper Daptomycin Resistance in *Corynebacterium striatum* and Daptomycin's Mechanism of Action

by

Nicholas K. Goldner

A dissertation presented to
The Graduate School
of Washington University in
partial fulfillment of the
requirements for the degree
of Doctor of Philosophy

August 2018
St. Louis, Missouri

Table of Contents

List of Figures…….... v
List of Tables…… vii
List of Abbreviations……... viii
Acknowledgments……..... ix
Abstract of the Dissertation…… xiii
Chapter 1: Introduction to Daptomycin……. 1
1.1 References…… 8
Chapter 2: Mechanism of High-Level Daptomycin Resistance in *Corynebacterium striatum*.... 15
2.1 Abstract……... 16
2.2 Introduction ……..……...17
2.3 Results…….…… 20
2.3.1 PG synthase mutations in HLDR C. striatum strains…… 20
2.3.2 Minimal transcriptional changes in HLDR C. striatum…… 22
2.3.3 Lipidomics reveals loss of phosphatidylglycerol in the membrane…….. 23
2.3.4 Surface plasmon resonance indicates PG is the preferred target of daptomycin…… 25
2.3.5 CFLSA indicates PG's necessary and sufficient for daptomycin activity 26
2.3.6 CFLSA indicates PG's concentration predicts daptomycin activity *in vivo* ……27
2.4 Conclusions……. 28
2.5 Methods……... 29
2.5.1 Whole Genome Sequencing and Comparison…….. 29
2.5.2 Transcriptomic methods…… 30
2.5.3 Zeta potential measurement methods…… 31
2.5.4 Lipidomics methods…….. 31
2.5.5 Carboxyfluorescein liposome stability assay…… 32
2.5.6 Surface plasmon resonance……... 33
2.6 Main Text Figures……... 34
2.7 Supplemental Figures…….. 42
2.8 References……... 48
Chapter 3: Daptomycin Forms Pores in Phosphatidylglycerol-Containing Membranes *in vitro* and in *Corynebacterium striatum*……... 55
3.1 Abstract……... 56
3.2 Introduction……. 57
3.3 Results……. 60
3.3.1 Daptomycin disrupts membranes through a different mechanism than valinomycin…….... 60
3.3.2 Daptomycin binds and stably integrates into PG-containing membranes 61

3.3.3 Daptomycin binds to PG at a 1:1 ratio…….. 61
3.3.4 Daptomycin binds and integrates rapidly into phosphatidylglycerol containing membranes…….. 62
3.3.5 Daptomycin forms pores large enough to be inhibited by 148.2 kDa dextran which has a Stokes radius of ~8 nm……. 63
3.3.6 Daptomycin-treated C. striatum releases metabolites after treatment in a manner consistent with pore formation……. 63
3.4 Discussion…..……... 64
3.5 Materials and Methods…… 71
3.5.1 Planar lipid bilayer data collection and analysis……... 71
3.5.2 Surface plasmon resonance data collection and analysis…….. 71
3.5.3 Carboxyfluorescein liposome stability assay data collection and analysis ……... 73
3.5.4 *In vivo* daptomycin pore formation data collection and analysis……. 74
3.6 Figures……. 76
3.7 References……... 87
Chapter 4: Conclusions……..... 99
Appendix 1: Comparative transcriptomics elucidates adaptive phenol tolerance and utilization in lipid-accumulating Rhodococcus opacus PD630…….. 103
A1.1 Abstract…….. 103
A1.2 Introduction…… 104
A1.3 Materials and Methods……... 107
A1.3.1 Adaptive evolution…….. 107
A1.3.2 Lipid assay…….. 108
A1.3.3 Illumina library preparation…… 109
A1.3.4 Genome sequencing and SNP analysis……... 110
A1.3.5 RNA-Seq data analysis……... 110
A1.4 Results……..... 111
A1.4.1 Adaptive evolution of R. opacus PD630 using phenol as a sole carbon Source……. 111
A1.4.2 Phenotypic characterization of phenol-adapted strains…….. 112
A1.4.3 Deep whole-genome sequencing of phenol-adapted strains……... 114
A1.4.4 Transcriptomic analysis of phenol-adapted strains……. 115
A1.4.4.1 Stress adaptation in evol33 and evol40 compared to WT…… 115
A1.4.4.2 Phenol degradation and utilization genes were highly upregulated in adapted strains…….. 116
A1.4.4.3 Upregulation of transporter genes in phenol…… 119
A1.4.4.4 Lipid biosynthesis and metabolism genes were differentially regulated in adapted strains……. 120
A1.4.4.5 Effects of nitrogen limitation on R. opacus transcriptome….. 111

A1.5 Discussion…….. 112
A1.6 Tables and Figures……..... 129
A1.7 References…….. 165

List of Figures

Figure 2.1: All HLDR isolates have predicted nonfunctional mutations in pgsA2…… 34
Figure 2.2: Lipid metabolism pathway of Phosphatidylglycerol, observed SNPs and relative abundance changes of key lipids between WT and HLDR isolates……. 35
Figure 2.3: Lipidomic comparison of WT and resistant paired isolates across mutation types.. 36
Figure 2.4: Daptomycin binding across concentrations and liposome content…… 39
Figure 2.5: Daptomycin activity across concentrations and liposome content…… 40
Supplemental Figure 2.1: Nonsynonymous mutations in biosynthetic pathways…… 43
Supplemental Figure 2.2: Phosphatidylinositol lipid biosynthesis pathways…….. 44
Supplemental Figure 2.3: Structures of the key phospholipids…… 46
Supplemental Figure 2.4: Comparison of HLDR and WT lipid membranes and surface charge.47

Figure 3.1: Daptomycin disrupts membranes through a different mechanism than valinomycin.76
Figure 3.2: Daptomycin stably binds and integrates into PG-containing membranes…….. 78
Figure 3.2 – Supplement 1: Long term daptomycin binding and lipid of interest structures….. 79
Figure 3.3: The phosphatidylglycerol to daptomycin stoichiometric ratio is ~1:1……... 80
Figure 3.4: Daptomycin binds and integrates into phosphatidylglycerol-containing membranes rapidly and can saturate membranes with low phosphatidylglycerol content…….. 81
Figure 3.4 – Supplement 1: Daptomycin retention after 15, 30 and 60 second injections…….. 83
Figure 3.5: Daptomycin forms pores in PG-containing artificial membranes…….. 84
Figure 3.6: Mass spectrometry detects molecular features increased in culture supernatants by daptomycin treatment……. 85
Figure 3.6 – Supplement 1: Treated and untreated supernatant features and distributions…….. 86

Figure A1.1: Growth comparison between the two phenol-adapted strains and the WT strain in diverse growth conditions…….. 132
Figure A1.2: Characterization of lipid accumulation……. 133
Figure A1.3: Transcriptomic and genomic information of genes involved in phenol degradation and utilization……. 134
Figure A1.4: Pathway and genome maps showing genes involved in phenol degradation and utilization……... 135
Supplemental Figure A1.1: Experimental approach……... 136
Supplemental Figure A1.2: Characterization of IC50 values for WT and adapted strains……. 138
Supplemental Figure A1.3: Growth and phenol consumption profiles of WT and adapted strains. ……..140
Supplemental Figure A1.4: Correlation between Nile red fluorescence and total lipid content (% CDW lipid)……... 141
Supplemental Figure A1.5: Nile red fluorescence and growth kinetics of WT and adapted strains. ……142
Supplemental Figure A1.6: Lipid accumulation using lignin model compounds……. .143
Supplemental Figure A1.7: Principal component analysis plot…… 144
Supplemental Figure A1.8: Bubble plot representation of fold changes in phenol degradation and utilization genes in low phenol…….. 145
Supplemental Figure A1.9: Expression profiles of other annotated phenolic degradation genes. ……..147

Supplemental Figure A1.10: Phenolic degradation pathways present in R. opacus PD630……148
Supplemental Figure A1.11: Venn diagrams of genes ……...149
Supplemental Figure A1.12: Microscopy images of R. opacus PD630 under nitrogen-limited conditions…….. 151
Supplemental Figure A1.13: MA Plot Summary. ……...152
Supplemental Figure A1.14: Expression profile of Rsr and YRNA homologs in different growth conditions…….. 153
Supplemental Figure A1.15: Calibration curve…….. 155

List of Tables

Supplemental Table 2.1: Available *Corynebacterium striatum* isolates…….. 42
Table A1.1: Single nucleotide polymorphisms (SNPs) found in the adapted strains……. 129
Table A1.2: Summarized fold changes of selected genes……... 130
Supplemental Table A1.1: Comparison of WT, evol33, and evol40 maximum biomass accumulation…… 156
Supplemental Table A1.2: Comparison of WT, evol33, and evol40 lag phase…….. 157
Supplemental Table A1.3: Comparison of WT, evol33, and evol40 growth rates……. 158
Supplemental Table A1.4: Maximum Nile red fluorescence in stationary phase……... 159
Supplemental Table A1.5: Overall lipid productivity as measured by Nile red fluorescence… 160
Supplemental Table A1.7: Differentially regulated genes in WT and adapted strains……... 161
Supplemental Table A1.8: Annotation for phenolic degradation pathways present in R. opacus PD630 (Supplemental Figure S10)…….. 162
Supplemental Table A1.9: Growth rate, lag phase, and maximum optical density of best performing strains obtained from colony purification……. 163

List of Abbreviations

CAMHB – cation adjusted Mueller-Hinton broth

CDP-DAG – cytidine diphosphate diacylglycerol

CFLSA – carboxyfluorescein liposome stability assay

CL – cardiolipin

DOPC – 1,2-dioleoyl-sn-glycero-3-phosphocholine

Glua-DAG – glucuronosyl diacylglycerol

HLDR – high level daptomycin resistance

IPCA – independent principal component analysis

LC-TOF – liquid chromatography- time of light

LOI – lipid of interest

LUV – large unilamellar vesicles

MIC – minimum inhibitory concentration

PA – phosphatidic acid

PC – phosphatidylcholine

PG – phosphatidylglycerol

pgsA2 – phosphatidylglycerol synthase

PI – phosphatidylinositol

SNPs – single nucleotide polymorphisms

SPR – surface plasmon resonance

WT – wild

Acknowledgments

This work is supported in part by awards to G.D. through the Edward Mallinckrodt, Jr. Foundation (Scholar Award), and from the National Institute of General Medical Sciences (NIGMS: http://www.nigms.nih.gov/), the National Institute of Allergy and Infectious Diseases (NIAID: https://www.niaid.nih.gov/), and the Eunice Kennedy Shriver National Institute of Child Health & Human Development (https://www.nichd.nih.gov/) of the National Institutes of Health (NIH) under award numbers R01GM099538, R01AI123394, and R01HD092414, respectively. Mass spectrometric analysis was performed in the Washington University Mass Spectrometry Resource, which is supported by National Institutes of Health grants P41GM103422, P30DK020579, P30DK056341.

Thank you, to the NHHS, WLC, and MCW crew that got me to WashU: Sue Getzel, Anne Xiong, Rob Balza PhD, Jim Henkel PhD, John Werner PhD, Allison Philips PhD, Kevin Glaeske PhD, Jarrod Erbe PhD, Subramaniam Malarkannan PhD, and Nita Salzman PhD.

Thank you, Wandy Beatty and the Molecular Microbiology Imaging Facility, for assistance with transmission electron microscopy of *C. striatum* samples. Thank you, Pratim Biswas and the Jens Molecular and Nanoscale Analysis Laboratory, for assistance in assaying bacterial membrane charges via Zetasizing. Thank you, Dantas lab, for insightful discussions of the results and conclusions.

I would like to thank my thesis committee for their support and guidance as my projects (and bacteria) have evolved through my time as a graduate student.

Thank you, Carey-Ann, for supplying us with an endless supply of bacterial isolates. Thank you for setting my projects in motion and for giving me a chance to see how the research done in the lab has real world applications.

Thank you, Paul, for getting me excited about lipids, for being a great collaborator, mentor, and friend. Thank you for letting me play around with a very expensive machine that shoots a laser through a sapphire and on to a gold-plated glass chip. It was a lot of fun—when it worked—and I learned more than I ever thought I would.

Thank you, Gautam, for being an incredible mentor and friend. You have taught me more than I thought possible. You gave me independence and the freedom to chase my interests and set me on a path to do great things. I am forever grateful.

Thank you, Chris Bulow, for being my lab partner, my sounding and idea board, and most importantly, my friend. None of this would have been possible without your help.

Thank you to my family on both sides for your unwavering support. Thank you for pretending to know what I've been doing these past 4 years and holding me to the highest standards you could.

To Dr. Rajendra Rathore and Dr. Sonja Glisic, you are my science heroes. You inspired me to be a scientist from the very beginning and set me on my path. Both of you are my guiding stars and I am eternally grateful.

Dad and Mom, I love you. Thank you for everything, and I mean everything. I'm so proud to be your son.

Richa, I love you. You stuck with me through good and bad. You edited my applications, papers, and anything really that I have ever written. You are my best friend and I am so happy that I get to spend my life with you.

Nicholas Goldner

Washington University in St. Louis

August 2018

Dedicated to my family, the strong women in my life that pushed me forward (Lisa Goldner and Rajni Nigam), and to Richa Rathore, the love of my life.

ABSTRACT OF THE DISSERTATION

The Mechanism of Hyper Daptomycin Resistance in *Corynebacterium striatum* and Daptomycin's Mechanism of Action

by

Nicholas K. Goldner

Doctor of Philosophy in Biology and Biomedical Sciences

Molecular Cell Biology

Washington University in St. Louis, 2018

Professor Gautam Dantas, Chair

Daptomycin, a last line-of-defense antibiotic for treating Gram-positive infections, is experiencing clinical failure against important infectious agents, including *Corynebacterium striatum*. The recent transition of daptomycin to generic antibiotic status is projected to dramatically increase availability, use, and clinical failure. Despite daptomycin's more than 30-year history as an important antibiotic, four major questions were left unanswered. 1) How do bacteria become hyper-resistant to daptomycin? 2) What is the *in vivo* membrane target of daptomycin? 3) How does daptomycin interact with the membrane? 4) What is daptomycin's mechanism of killing? These four questions have plagued the daptomycin field, and even now conflicting mechanisms have been reported in the literature. This thesis has focused on teasing apart the intricacies of these four questions.

To answer the first two questions, regarding 1) hyper-resistance to daptomycin and 2) the *in vivo* membrane target of daptomycin, we identified the mechanism of high-level daptomycin resistance in *C. striatum*, which helped us to identify phosphatidylglycerol as the *in vivo* target of daptomycin. Here, we confirm the genetic mechanism of high-level daptomycin resistance (HLDR, MIC > 256 μg/mL) in *C. striatum*, which evolved within a patient during daptomycin therapy, a phenotype recapitulated *in vitro*. In all eight independent cases tested, loss of function mutations in phosphatidylglycerol synthase (*pgsA2*) were necessary and sufficient for high-level daptomycin resistance. Through lipidomic and biochemical analysis, we demonstrate that the activity of daptomycin is dependent on membrane phosphatidylglycerol (PG) concentration. Until now, the verification of PG as the *in vivo* target of daptomycin has proven difficult, as tested cell model systems were not viable without membrane PG. *C. striatum* becomes high-level daptomycin resistant by removing PG from the membrane and changing membrane composition to maintain viability. This work demonstrates that a single loss of function mutation in *pgsA2*, and the loss of membrane PG is necessary and sufficient to produce high-level resistance to daptomycin in *C. striatum* and result in daptomycin's clinical failure.

Even though there have been numerous studies looking at daptomycin's interaction with the membranes, several problems with the model systems and methods used have plagued the field, casting doubt and uncertainty on 3) how daptomycin interacts with the membrane, and 4) how daptomycin kills bacteria. Previous studies have used model membranes that are too large (giant unilamellar vesicles that are 100x bigger than bacteria), indirect measurements through fluorescence, unknown PG and acyl tail requirements for model systems, and chemically altered daptomycin that no longer behaves like daptomycin (as indicated by a drastic increase in minimum inhibitory concentration compared to native daptomycin). The data reported here demonstrates a

shift in how we understand the interactions of daptomycin with the bacterial cell. Once daptomycin binds to the membrane, it is stably integrated in a calcium- and PG-dependent manner (~1:1 daptomycin to PG). It then recruits or co-localizes with other daptomycin molecules to form stable pores with an approximate Stokes radius of 8 nm, which is far larger than the previously reported ion channels. The resulting pore allows metabolites, ions and other intracellular components to exit the cell. When enough PG is present in the bacterial membranes, enough daptomycin pores can be formed to release necessary metabolites, ultimately resulting in cell death.

In summary, 1) bacteria become high-level resistant to daptomycin by removing daptomycin's 2) *in vivo* target, phosphatidylglycerol (PG), from the membrane. 3) In the presence of PG, daptomycin binds and integrates into the membrane to form a large pore that 4) disrupts the membrane potential and allows intracellular metabolites, ions and other important molecules to leak out of the cell, ultimately killing the bacteria.

Chapter 1: Introduction to Daptomycin

Antibiotic resistance is an extreme, worsening and long-term burden to human health, and is exacerbated by poor antibiotic stewardship and stalled drug discovery to treat new emerging diseases. Bacteria evolve resistance to antibiotics by acquiring antibiotic resistance genes (horizontal gene transfer) or by genetic changes that result in antibiotic resistance (vertical gene transfer). Additionally, increased antibiotic use over the past century has enabled multiple clinical pathogens to acquire resistance to the best antibiotics available (Krawczyk et al., 2004; Liu et al., 2012; McElvania TeKippe et al., 2014; Michael et al., 2015; Teatero et al., 2015; Teo et al., 2015). This poses a grave clinical concern with no immediately clear answer. Antibiotic resistance is so pervasive in the bacterial community that every major antibiotic drug class currently in use has reports of pathogens with high-level resistance (Baym et al., 2016; Palmer and Kishony, 2013). What bacteria do naturally—evolve to adapt to their environment—costs the United States more than 55 billion dollars a year and kills more than 40 thousand people annually (GELBAND et al., 2015; Prevention, 2013). By 2050, these tiny ubiquitous organisms will have cost the global economy in excess of 100 trillion dollars and erased hundreds of millions of people from the world (12420, 2015; Dynamics, 2015; LLP, 2014; O'Neill, 2014).

Bacterial acquisition of antibiotic resistance to drugs is drastically outstripping our capacity to produce novel antibiotics. Antibiotics that have reportedly very low levels of resistance, such as daptomycin, are starting to fail (Cesar A. Arias et al., 2001; Hines et al., 2017; McElvania TeKippe et al., 2014). Accordingly, elucidating novel mechanisms of antibiotics resistance has extreme clinical relevance, to help extend the lifetimes of important chemotherapeutics (Rizvi et al., 2015) and identify novel druggable targets (Gonzales et al., 2015). This is especially important as antibiotics go off-patent, as the availability of cheaper generic competition dramatically increases.

With increased usage of generic antibiotics comes an increased risk of antibiotic resistance, which leads to dramatically reduced clinical efficacy of the drug, and an associated increase in patient death due to the ineffectiveness of previously successful treatments.

Daptomycin, an antibiotic discovered over thirty years ago, forms a last line-of-defense against deadly pathogens (Lakey and Lea, 1986). As a cyclic-lipopeptide, daptomycin belongs to a unique class of antibiotics and is backed by extensive research and testing efforts that led to approval for use in humans (Baltz, 2009; Taylor and Palmer, 2016). It has been used judiciously and serves an important role in treating antibiotic-resistant, Gram-positive bacterial infections. Although its mechanism of action has remained unclear, daptomycin targets the bacterial membrane, resulting in leakage of large molecules (determined using intracellular dyes) but not complete cell lysis (Cotroneo et al., 2008; Hobbs et al., 2008). Several mechanisms of action have been proposed, including pore formation (Zhang et al., 2014a), increased membrane permeability (Straus and Hancock, 2006), membrane deformation (Chen et al., 2014), division inhibition (Muller et al., 2016) and peptidoglycan targeting (Allen et al., 1987). The first occurrences of clinical resistance to daptomycin in *Staphylococcus aureus* were incremental (Yang et al., 2013; Yang et al., 2010), and easily managed in patients through small daptomycin dose increases (Weis et al., 2008). The lack of resistance to high doses was ascribed to the target of daptomycin being the cell membrane (Alborn et al., 1991; Allen et al., 1991), with several *in vitro* studies identifying phosphatidylglycerol as its specific lipid target (Muraih et al., 2012). It was incorrectly assumed that bacteria would have difficulty making large scale shifts in membrane lipid composition (Hachmann et al., 2011; Hines et al., 2017), and thus would be unable to develop resistance.

In artificial membrane systems, daptomycin preferentially binds phosphatidylglycerol (PG) (Khatib et al., 2016; Kreutzberger et al., 2017; Taylor et al., 2017b; Taylor et al., 2016). The

most likely proposed mechanism of action is that daptomycin forms 1:1 daptomycin:Ca^{2+} micelles (Jung et al., 2008; Jung et al., 2004; Scott et al., 2007), which dissociate in the presence of PG-containing membranes and then bind to the membrane via the hydrophobic 10-C acyl tail of daptomycin. Once bound, daptomycin integrates into the hydrophobic core of the bilayer (Jung et al., 2004; Lakey and Ptak, 1988[Jung, 2008 #8822) at a proposed ~1:1 ratio of PG to daptomycin (Lee et al., 2017). However, determining the PG:daptomycin interaction stoichiometry has proven difficult, with various methods and lipid preparations yielding predicted stoichiometries ranging from 1:1 in bicelles to 2:1 in liposomes (Zhang et al., 2013) (Muraih and Palmer, 2012). Beyond this point, it is unclear how daptomycin kills bacterial cells; however, there is substantial evidence in favor of membrane disruption, eventually resulting in cell death (Laganas et al., 2003; Mascio et al., 2007; Pogliano et al., 2012; Silverman et al., 2003; Taylor et al., 2017a; Zhang et al., 2014a,[Taylor, 2017 #9958). Previous elegant experiments have begun to dissect the binding and conformational changes observed in membrane-associated daptomycin (Jung et al., 2008; Jung et al., 2004; Lee et al., 2017).

As recently as 2014, it was shown that daptomycin permeability was size- and cation-selective (Alborn et al., 1991; Allen et al., 1991; Zhang et al., 2014a). However, two shortcomings of these findings require resolution. First, at physiological concentrations of daptomycin (between the minimum inhibitory concentration (MIC) of 0.064 μg/mL and the peak reported serum concentrations of 100 μg/mL) of daptomycin (Antachopoulos et al., 2012; McElvania TeKippe et al., 2014), the mechanisms of membrane dysregulation were inconclusive. This could be potentially due to the different acyl tail type used in the model lipids for *in vitro* assays. Second,

efforts to confirm ion leakage and pore formation in *vivo* using the *Bacillus subtilis* model (Muller et al., 2016) yielded results contrary to the proposed mechanisms identified *in vitro*. Studying the mechanism of antibacterial action of daptomycin and other antimicrobial peptides will thus require a holistic approach, calling on genomics, transcriptomics, metabolomics and lipidomics, as well as classical biochemical and biophysical techniques.

Recent clinical reports of treatment failures have emerged with target pathogens exhibiting >2000-fold increases in daptomycin resistance (Akins et al., 2015; Garcia-de-la-Maria et al., 2013; McElvania TeKippe et al., 2014), often over rapid time-scales (hours to a few days of treatment), which are beginning to challenge daptomycin's efficacy. These failures are expected to expand as daptomycin transitions to generic status (OptumRx, 2016) , as availability for clinical use increases. Case in point, C. *striatum* is an emerging opportunistic pathogen that colonizes the skin much like *S. aureus*. *C. striatum*'s ability to rapidly transition from susceptible to resistant to daptomycin poses a serious epidemiological threat to our healthcare system (Chatzopoulou et al., 2016). However, these two pathogens evolve daptomycin resistance in mechanistically distinct ways. In *S. aureus*, low-level, step-wise accumulations in resistance phenotypes are responsible for low (Minimum Inhibitory Concentration (MIC): 2-4 µg/ml) and intermediate (MIC: 4-8 µg/ml) daptomycin resistance. The majority of these observations come from pathogenic *S. aureus*, which was the first approved therapeutic target for daptomycin (Sauermann et al., 2008). Accumulation of multiple single nucleotide polymorphisms (SNPs) in the *yycFGHI* operon in *S. aureus* has resulted in 2-6-fold increases in daptomycin resistance through cell wall thickening and alteration of membrane charge (Bayer et al., 2013; Gaupp et al., 2015; Mishra et al., 2014; Quinn et al., 2007; Raad et al., 2007; Reyes et al., 2015). Increases in positively charged membrane phospholipids, which reduces the affinity of the $Ca2^{+}$-conjugated daptomycin for the surface membrane, increased

the MIC. Additionally, mutations that alter lipid translocation, decrease membrane fluidity, and thickening of the cell wall have led to low-level (3-6 fold) increases in daptomycin resistance (Mishra et al., 2014; Mishra et al., 2009). Mutations associated with the above physiological changes in pathogenic *S. aureus* have all led to small stepwise increases (2-6 fold) in resistance over long periods of time (weeks of treatment) and lose resistance to daptomycin when no longer under daptomycin's selection pressure(Li et al., 2017). In contrast, some environmental *Streptomyces* species have been shown to inactivate daptomycin (D'Costa et al., 2012; Vanessa M. D'Costa, 2006) enzymatically; clinical isolates have not used this mechanism to date.

The first report of higher levels (~20-fold over wild-type) of daptomycin resistance come from laboratory adaptive evolution experiments with the non-pathogenic, soil bacterium, *Bacillus subtilis* (Hachmann et al., 2011). Daptomycin resistant *B. subtilis* was found to harbor SNPs in 44 genes, including predicted reduction/loss of function mutations in phosphatidylglycerol synthase A (*pgsA*), an essential enzyme for phosphatidylglycerol (PG) synthesis (Hachmann et al., 2009; Hachmann et al., 2011). Characterization of the lipid membrane revealed a reduction in PG content from 30% in the wild-type to 10% in the resistant mutant. Consistent with the lack of complete ablation of PG in the membrane, attempts to knock out *pgsA* alone genetically were not successful, due to presumed essentiality of PG in *B. subtilis* (Hachmann et al., 2011). Nevertheless, studies of daptomycin's target to date corroborate *in vivo* the importance of PG in daptomycin activity (Hachmann et al., 2009; Hachmann et al., 2011; Hines et al., 2017). Indeed, a recent comparative genomic and lipidomic study of *S. aureus*, *C. striatum*, and *Enterococcus faecalis* indicated mutations in PG synthase and subsequent lack of PG synthesis confers daptomycin resistance(Hines et al., 2017)(Hines et al., 2017)(Hines et al., 2017)(Hines et al., 2017)(Hines et al., 2017)(Hines et al., 2017)(Hines et al., 2017)(Hines et al., 2017)[16, 69] (Hines et al., 2017) .

Over the past few years, there has been a steady increase in reports of even higher-level daptomycin resistance (≥4000 fold increase in resistance) in a number of clinical pathogens, including viridians group *Streptococci* (Akins et al., 2015), *Enterococcus faecium* (Humphries et al., 2012), and C. *striatum* (McElvania TeKippe et al., 2014). This high-level daptomycin resistance (HLDR)—defined here as having a MIC ≥ 256 μg/ml daptomycin—was first observed in *C. striatum*, in a patient with native valve endocarditis in 2012 (Tran et al., 2012). In 2014, a clinical laboratory reported *in vivo* evolution of HLDR *C. striatum* in a patient with an infected left ventricular assist device, during 17 days of daptomycin therapy (McElvania TeKippe et al., 2014). Evolution of HLDR was recapitulated *in vitro* in 100% of tested *C. striatum* isolates (n=50) after 24 hours of daptomycin exposure (McMullen et al., 2017a). *C. striatum* is a Gram-positive bacterium which typically resides as a commensal organism on the skin (Oh et al., 2014). However, it has become a growing threat to hospital systems and patients as an opportunistic pathogen. Indeed, *C. striatum* has been associated with a plethora of infection types over the past 20 years including bacteremia, endocarditis, urinary tract, wound, respiratory, central line, medical device and hardware infections (Gomila et al., 2012; Hahn et al., 2016; Mattos-Guaraldi et al., 2015; McElvania TeKippe et al., 2014; Souza et al., 2015; Wang et al., 2016; Werth et al., 2016; Wong et al., 2010).

In this dissertation, we use a combination of comparative genomics, transcriptomics, lipidomics, metabolomics, electron microscopy and zeta potential to understand daptomycin's effect on wild type and high level daptomycin resistant *C. striatum*. We verify the *in vivo* work biochemically and biophysically *in vitro*, using surface plasmon resonance, carboxyfluorescein liposome stability assays and resistive pore blocking. We demonstrate that loss of function mutations in *pgsA2* results in PG, the primary target of this last-resort drug daptomycin, to be

reduced from ~45% to <1% in the membrane, resulting in HLDR. We further demonstrate that in wild type *C. striatum* and artificial liposomes, daptomycin binds to PG in the membrane, forms large pores (~8 nm Stokes radius) and allows metabolites, ions and other important molecules to leak out of the cell, ultimately killing the bacteria. Our work demonstrates the important considerations needed for designing future lipopeptide antibiotics, that bacterial cells can readily manipulate membrane lipid composition to effectively evade lipid-targeting lipopeptide antibiotics.

1.1 References:

Akins, R. L., Katz, B. D., Monahan, C., & Alexander, D. (2015). Characterization of high-level daptomycin resistance in Viridans group *Streptococci* developed upon in vitro exposure to daptomycin. *Antimicrob Agents Chemother, 59*(4), 2102-2112. doi:10.1128/AAC.04219-14

Alborn, W. E., Jr., Allen, N. E., & Preston, D. A. (1991). Daptomycin disrupts membrane potential in growing *Staphylococcus aureus*. *Antimicrob Agents Chemother, 35*(11), 2282-2287.

Allen, N. E., Alborn, W. E., Jr., & Hobbs, J. N., Jr. (1991). Inhibition of membrane potential-dependent amino acid transport by daptomycin. *Antimicrob Agents Chemother, 35*(12), 2639-2642.

Allen, N. E., Hobbs, J. N., & Alborn, W. E., Jr. (1987). Inhibition of peptidoglycan biosynthesis in gram-positive bacteria by LY146032. *Antimicrob Agents Chemother, 31*(7), 1093-1099.

Antachopoulos, C., Iosifidis, E., Sarafidis, K., Bazoti, F., Gikas, E., Katragkou, A., . . . Roilides, E. (2012). Serum levels of daptomycin in pediatric patients. *Infection, 40*(4), 367-371. doi:10.1007/s15010-011-0240-3

Baltz, R. H. (2009). Daptomycin: mechanisms of action and resistance, and biosynthetic engineering. *Curr Opin Chem Biol, 13*(2), 144-151. doi:10.1016/j.cbpa.2009.02.031

Bayer, A. S., Schneider, T., & Sahl, H. G. (2013). Mechanisms of daptomycin resistance in *Staphylococcus aureus*: role of the cell membrane and cell wall. *Ann N Y Acad Sci, 1277*, 139-158. doi:10.1111/j.1749-6632.2012.06819.x

Baym, M., Stone, L. K., & Kishony, R. (2016). Multidrug evolutionary strategies to reverse antibiotic resistance. *Science, 351*(6268), aad3292. doi:10.1126/science.aad3292

Cesar A. Arias, M. D., Ph.D., Diana Panesso, Ph.D.,, Danielle M. McGrath, P. D., Xiang Qin, Ph.D., Maria F. Mojica, M.Sc., Corwin Miller, B.A., Lorena Diaz, B.Sc., Truc T. Tran, Pharm.D.,, Sandra Rincon, M. S., E. Magda Barbu, Ph.D., Jinnethe Reyes, M.Sc.,, & Jung H. Roh, P. D., Elizabeth Lobos, Ph.D., Erica Sodergren, Ph.D., Renata Pasqualini, Ph.D., Wadih Arap, M.D., Ph.D., John P. Quinn, M.D., Yousif Shamoo, Ph.D., Barbara E. Murray, M.D., and George M. Weinstock, Ph.D. (2001). Genetic Basis for In Vivo Daptomycin Resistance in *Enterococci*. *The New England Journal of Medicine, 365*(10), 892-900.

Chatzopoulou, M., Koufakis, T., Voulgaridi, I., Gabranis, I., & Tsiakalou, M. (2016). A case of fatal sepsis due to multidrug-resistant *Corynebacterium striatum*. *Hippokratia, 20*(1), 67-69.

Chen, Y. F., Sun, T. L., Sun, Y., & Huang, H. W. (2014). Interaction of daptomycin with lipid bilayers: a lipid extracting effect. *Biochemistry, 53*(33), 5384-5392. doi:10.1021/bi500779g

Cotroneo, N., Harris, R., Perlmutter, N., Beveridge, T., & Silverman, J. A. (2008). Daptomycin exerts bactericidal activity without lysis of *Staphylococcus aureus*. *Antimicrob Agents Chemother, 52*(6), 2223-2225. doi:10.1128/AAC.01410-07

D'Costa, V. M., Mukhtar, T. A., Patel, T., Koteva, K., Waglechner, N., Hughes, D. W., . . . De Pascale, G. (2012). Inactivation of the lipopeptide antibiotic daptomycin by hydrolytic mechanisms. *Antimicrob Agents Chemother, 56*(2), 757-764. doi:10.1128/AAC.05441-11

Dynamics, C. f. D. (2015). State of the World's Antibiotics, 2015. *Economics & Policy, CDDEP: Washington, D.C.*

Garcia-de-la-Maria, C., Pericas, J. M., Del Rio, A., Castaneda, X., Vila-Farres, X., Armero, Y., . . . Hospital Clinic Experimental Endocarditis Study, G. (2013). Early in vitro and in vivo development of high-level daptomycin resistance is common in mitis group *Streptococci* after exposure to daptomycin. *Antimicrob Agents Chemother, 57*(5), 2319-2325.

Gomila, M., Renom, F., Gallegos Mdel, C., Garau, M., Guerrero, D., Soriano, J. B., & Lalucat, J. (2012). Identification and diversity of multiresistant *Corynebacterium striatum* clinical isolates by MALDI-TOF mass spectrometry and by a multigene sequencing approach. *BMC Microbiol, 12*, 52. doi:10.1186/1471-2180-12-52

Gonzales, P. R., Pesesky, M. W., Bouley, R., Ballard, A., Biddy, B. A., Suckow, M. A., . . . Dantas, G. (2015). Synergistic, collaterally sensitive beta-lactam combinations suppress resistance in MRSA. *Nat Chem Biol, 11*(11), 855-861. doi:10.1038/nchembio.1911

Hachmann, A. B., Angert, E. R., & Helmann, J. D. (2009). Genetic analysis of factors affecting susceptibility of *Bacillus subtilis* to daptomycin. *Antimicrob Agents Chemother, 53*(4), 1598-1609. doi:10.1128/AAC.01329-08

Hachmann, A. B., Sevim, E., Gaballa, A., Popham, D. L., Antelmann, H., & Helmann, J. D. (2011). Reduction in membrane phosphatidylglycerol content leads to daptomycin resistance in *Bacillus subtilis*. *Antimicrob Agents Chemother, 55*(9), 4326-4337. doi:10.1128/AAC.01819-10

Hahn, W. O., Werth, B. J., Butler-Wu, S. M., & Rakita, R. M. (2016). Multidrug-Resistant *Corynebacterium striatum* Associated with Increased Use of Parenteral Antimicrobial Drugs. *Emerg Infect Dis, 22*(11). doi:10.3201/eid2211.160141

Hines, K. M., Waalkes, A., Penewit, K., Holmes, E. A., Salipante, S. J., Werth, B. J., & Xu, L. (2017). Characterization of the Mechanisms of Daptomycin Resistance among Gram-Positive Bacterial Pathogens by Multidimensional Lipidomics. *mSphere, 2*(6). doi:10.1128/mSphere.00492-17

Hobbs, J. K., Miller, K., O'Neill, A. J., & Chopra, I. (2008). Consequences of daptomycin-mediated membrane damage in *Staphylococcus aureus*. *J Antimicrob Chemother, 62*(5), 1003-1008. doi:10.1093/jac/dkn321

Humphries, R. M., Kelesidis, T., Tewhey, R., Rose, W. E., Schork, N., Nizet, V., & Sakoulas, G. (2012). Genotypic and phenotypic evaluation of the evolution of high-level daptomycin nonsusceptibility in vancomycin-resistant *Enterococcus faecium*. *Antimicrob Agents Chemother, 56*(11), 6051-6053. doi:10.1128/AAC.01318-12

Jung, D., Powers, J. P., Straus, S. K., & Hancock, R. E. (2008). Lipid-specific binding of the calcium-dependent antibiotic daptomycin leads to changes in lipid polymorphism of model membranes. *Chem Phys Lipids, 154*(2), 120-128. doi:10.1016/j.chemphyslip.2008.04.004

Jung, D., Rozek, A., Okon, M., & Hancock, R. E. (2004). Structural transitions as determinants of the action of the calcium-dependent antibiotic daptomycin. *Chem Biol, 11*(7), 949-957. doi:10.1016/j.chembiol.2004.04.020

Khatib, T. O., Stevenson, H., Yeaman, M. R., Bayer, A. S., & Pokorny, A. (2016). Binding of Daptomycin to Anionic Lipid Vesicles Is Reduced in the Presence of Lysyl-Phosphatidylglycerol. *Antimicrob Agents Chemother, 60*(8), 5051-5053. doi:10.1128/AAC.00744-16

Krawczyk, B., Samet, A., Bronk, M., Hellmann, A., & Kur, J. (2004). Emerging linezolid-resistant, vancomycin resistant *Enterococcus faecium* from a patient of a haematological unit in Poland. *Pol J Microbiol, 53*(3), 193-196.

Kreutzberger, M. A., Pokorny, A., & Almeida, P. F. (2017). Daptomycin-Phosphatidylglycerol Domains in Lipid Membranes. *Langmuir, 33*(47), 13669-13679. doi:10.1021/acs.langmuir.7b01841

Laganas, V., Alder, J., & Silverman, J. A. (2003). In vitro bactericidal activities of daptomycin against Staphylococcus aureus and *Enterococcus faecalis* are not mediated by inhibition of lipoteichoic acid biosynthesis. *Antimicrob Agents Chemother, 47*(8), 2682-2684.

Lakey, J. H., & Lea, E. J. (1986). The role of acyl chain character and other determinants on the bilayer activity of A21978C an acidic lipopeptide antibiotic. *Biochim Biophys Acta, 859*(2), 219-226.

Lakey, J. H., & Ptak, M. (1988). Fluorescence indicates a calcium-dependent interaction between the lipopeptide antibiotic LY146032 and phospholipid membranes. *Biochemistry, 27*(13), 4639-4645.

Lee, M. T., Hung, W. C., Hsieh, M. H., Chen, H., Chang, Y. Y., & Huang, H. W. (2017). Molecular State of the Membrane-Active Antibiotic Daptomycin. *Biophys J, 113*(1), 82-90. doi:10.1016/j.bpj.2017.05.025

Li, S., Yin, Y., Chen, H., Wang, Q., Wang, X., & Wang, H. (2017). Fitness Cost of Daptomycin-Resistant *Staphylococcus aureus* Obtained from in Vitro Daptomycin Selection Pressure. *Front Microbiol, 8*, 2199. doi:10.3389/fmicb.2017.02199

Liu, H., Tian, W., Li, B., Wu, G., Ibrahim, M., Tao, Z., . . . Sun, G. (2012). Antifungal effect and mechanism of chitosan against the rice sheath blight pathogen, *Rhizoctonia solani. Biotechnol Lett, 34*(12), 2291-2298. doi:10.1007/s10529-012-1035-z

LLP, K. (2014). The global economic impact of anti-microbial resistance. *www.KPMG.co.uk*.

Mascio, C. T., Alder, J. D., & Silverman, J. A. (2007). Bactericidal action of daptomycin against stationary-phase and nondividing *Staphylococcus aureus* cells. *Antimicrob Agents Chemother, 51*(12), 4255-4260. doi:10.1128/AAC.00824-07

Mattos-Guaraldi, A. L., Guimaraes, L. C., Santos, C. S., Veras, A. A., Carneiro, A. R., Soares, S. C., . . . Ramos, R. T. (2015). Draft Genome Sequence of *Corynebacterium striatum* 1961 BR-RJ/09, a Multidrug-Susceptible Strain Isolated from the Urine of a Hospitalized 37-Year-Old Female Patient. *Genome Announc, 3*(4). doi:10.1128/genomeA.00869-15

McElvania TeKippe, E., Thomas, B. S., Ewald, G. A., Lawrence, S. J., & Burnham, C. A. (2014). Rapid emergence of daptomycin resistance in clinical isolates of *Corynebacterium striatum*... a cautionary tale. *Eur J Clin Microbiol Infect Dis, 33*(12), 2199-2205. doi:10.1007/s10096-014-2188-6

McMullen, A. R., Anderson, N., Wallace, M. A., Shupe, A., & Burnham, C. A. (2017). When Good Bugs Go Bad: Epidemiology and Antimicrobial Resistance Profiles of *Corynebacterium striatum*, an Emerging Multidrug Resistant, Opportunistic Pathogen. *Antimicrob Agents Chemother*. doi:10.1128/AAC.01111-17

Michael, G. B., Freitag, C., Wendlandt, S., Eidam, C., Fessler, A. T., Lopes, G. V., . . . Schwarz, S. (2015). Emerging issues in antimicrobial resistance of bacteria from food-producing animals. *Future Microbiol, 10*, 427-443. doi:10.2217/fmb.14.93

Mishra, N. N., Bayer, A. S., Weidenmaier, C., Grau, T., Wanner, S., Stefani, S., . . . Yang, S. J. (2014). Phenotypic and genotypic characterization of daptomycin-resistant methicillin-resistant *Staphylococcus aureus* strains: relative roles of mprF and dlt operons. *PLoS One, 9*(9), e107426. doi:10.1371/journal.pone.0107426

Mishra, N. N., Yang, S. J., Sawa, A., Rubio, A., Nast, C. C., Yeaman, M. R., & Bayer, A. S. (2009). Analysis of cell membrane characteristics of in vitro-selected daptomycin-resistant strains of methicillin-resistant *Staphylococcus aureus*. *Antimicrob Agents Chemother, 53*(6), 2312-2318. doi:10.1128/AAC.01682-08

Muller, A., Wenzel, M., Strahl, H., Grein, F., Saaki, T. N., Kohl, B., . . . Hamoen, L. W. (2016). Daptomycin inhibits cell envelope synthesis by interfering with fluid membrane microdomains. *Proc Natl Acad Sci U S A*. doi:10.1073/pnas.1611173113

Muraih, J. K., Harris, J., Taylor, S. D., & Palmer, M. (2012). Characterization of daptomycin oligomerization with perylene excimer fluorescence: stoichiometric binding of phosphatidylglycerol triggers oligomer formation. *Biochim Biophys Acta, 1818*(3), 673-678. doi:10.1016/j.bbamem.2011.10.027

Muraih, J. K., & Palmer, M. (2012). Estimation of the subunit stoichiometry of the membrane-associated daptomycin oligomer by FRET. *Biochim Biophys Acta, 1818*(7), 1642-1647. doi:10.1016/j.bbamem.2012.02.019

O'Neill, J. (2014). Antimicrobial Resistance: Tackling a crisis for the health and wealth of nations. *The Review on Antimicrobial Resistance*.

Oh, J., Byrd, A. L., Deming, C., Conlan, S., Program, N. C. S., Kong, H. H., & Segre, J. A. (2014). Biogeography and individuality shape function in the human skin metagenome. *Nature, 514*(7520), 59-64. doi:10.1038/nature13786

OptumRx. (2016). Cubicin (daptomycin) - First-Time Generic.

Palmer, A. C., & Kishony, R. (2013). Understanding, predicting and manipulating the genotypic evolution of antibiotic resistance. *Nat Rev Genet, 14*(4), 243-248. doi:10.1038/nrg3351

Pogliano, J., Pogliano, N., & Silverman, J. A. (2012). Daptomycin-mediated reorganization of membrane architecture causes mislocalization of essential cell division proteins. *J Bacteriol, 194*(17), 4494-4504. doi:10.1128/JB.00011-12

Prevention, U. S. D. o. H. a. H. S. C. f. D. C. a. (2013). Antibiotic Resistance Threats in the United States, 2013. *CDC*.

Quinn, B., Hussain, S., Malik, M., Drlica, K., & Zhao, X. (2007). Daptomycin inoculum effects and mutant prevention concentration with *Staphylococcus aureus*. *J Antimicrob Chemother, 60*(6), 1380-1383. doi:10.1093/jac/dkm375

Raad, I., Hanna, H., Jiang, Y., Dvorak, T., Reitzel, R., Chaiban, G., . . . Hachem, R. (2007). Comparative activities of daptomycin, linezolid, and tigecycline against catheter-related methicillin-resistant *Staphylococcus* bacteremic isolates embedded in biofilm. *Antimicrob Agents Chemother, 51*(5), 1656-1660. doi:10.1128/AAC.00350-06

Reyes, J., Panesso, D., Tran, T. T., Mishra, N. N., Cruz, M. R., Munita, J. M., . . . Arias, C. A. (2015). A liaR deletion restores susceptibility to daptomycin and antimicrobial peptides in multidrug-resistant *Enterococcus faecalis*. *J Infect Dis, 211*(8), 1317-1325. doi:10.1093/infdis/jiu602

Rizvi, M., Ahmad, J., Khan, F., Shukla, I., Malik, A., & Sami, H. (2015). Synergy of drug combinations in treating multidrug-resistant *Pseudomonas aeruginosa*. *Australas Med J, 8*(1), 1-6. doi:10.4066/AMJ.2015.2096

Sauermann, R., Rothenburger, M., Graninger, W., & Joukhadar, C. (2008). Daptomycin: a review 4 years after first approval. *Pharmacology, 81*(2), 79-91. doi:10.1159/000109868

Scott, W. R., Baek, S. B., Jung, D., Hancock, R. E., & Straus, S. K. (2007). NMR structural studies of the antibiotic lipopeptide daptomycin in DHPC micelles. *Biochim Biophys Acta, 1768*(12), 3116-3126. doi:10.1016/j.bbamem.2007.08.034

Silverman, J. A., Perlmutter, N. G., & Shapiro, H. M. (2003). Correlation of daptomycin bactericidal activity and membrane depolarization in *Staphylococcus aureus*. *Antimicrob Agents Chemother, 47*(8), 2538-2544.

Souza, C., Faria, Y. V., Sant'Anna Lde, O., Viana, V. G., Seabra, S. H., Souza, M. C., . . . Mattos-Guaraldi, A. L. (2015). Biofilm production by multiresistant *Corynebacterium striatum* associated with nosocomial outbreak. *Mem Inst Oswaldo Cruz, 110*(2), 242-248. doi:10.1590/0074-02760140373

Straus, S. K., & Hancock, R. E. (2006). Mode of action of the new antibiotic for Gram-positive pathogens daptomycin: comparison with cationic antimicrobial peptides and lipopeptides. *Biochim Biophys Acta, 1758*(9), 1215-1223. doi:10.1016/j.bbamem.2006.02.009

Taylor, R., Beriashvili, D., Taylor, S., & Palmer, M. (2017a). Daptomycin Pore Formation Is Restricted by Lipid Acyl Chain Composition. *ACS Infect Dis*. doi:10.1021/acsinfecdis.7b00138

Taylor, R., Beriashvili, D., Taylor, S., & Palmer, M. (2017b). Daptomycin Pore Formation Is Restricted by Lipid Acyl Chain Composition. *ACS Infect Dis, 3*(11), 797-801. doi:10.1021/acsinfecdis.7b00138

Taylor, R., Butt, K., Scott, B., Zhang, T., Muraih, J. K., Mintzer, E., . . . Palmer, M. (2016). Two successive calcium-dependent transitions mediate membrane binding and oligomerization of daptomycin and the related antibiotic A54145. *Biochim Biophys Acta, 1858*(9), 1999-2005. doi:10.1016/j.bbamem.2016.05.020

Taylor, S. D., & Palmer, M. (2016). The action mechanism of daptomycin. *Bioorg Med Chem, 24*(24), 6253-6268. doi:10.1016/j.bmc.2016.05.052

Teatero, S., McGeer, A., Li, A., Gomes, J., Seah, C., Demczuk, W., . . . Fittipaldi, N. (2015). Population Structure and Antimicrobial Resistance of Invasive Serotype IV Group B *Streptococcus*, Toronto, Ontario, Canada. *Emerg Infect Dis, 21*(4), 585-591. doi:10.3201/eid2014.140759

Teo, J., Lim, T. P., Hsu, L. Y., Tan, T. Y., Sasikala, S., Hon, P. Y., . . . Apisarnthanarak, A. (2015). Extensively drug-resistant *Acinetobacter baumannii* in a Thai hospital: a molecular epidemiologic analysis and identification of bactericidal Polymyxin B-based combinations. *Antimicrob Resist Infect Control, 4*(1), 2. doi:10.1186/s13756-015-0043-x

Tran, T. T., Jaijakul, S., Lewis, C. T., Diaz, L., Panesso, D., Kaplan, H. B., . . . Arias, C. A. (2012). Native valve endocarditis caused by *Corynebacterium striatum* with heterogeneous high-level daptomycin resistance: collateral damage from daptomycin therapy? *Antimicrob Agents Chemother, 56*(6), 3461-3464. doi:10.1128/AAC.00046-12

Vanessa M. D'Costa, K. M. M., Donald W. Hughes, Gerard D. Wright. (2006). Sampling the Antibiotic Resistome. *Science, 311*, 374-377.

Wang, J., Wang, Y., Du, X., Cui, J., Wang, K., Zhang, L., & Han, Y. (2016). Rapid transmission of multidrug-resistant *Corynebacterium striatum* among susceptible patients in a tertiary hospital in China. *J Infect Dev Ctries, 10*(12), 1299-1305. doi:10.3855/jidc.7577

Wang, W., Wei, Z., Lam, T. W., & Wang, J. (2011). Next generation sequencing has lower sequence coverage and poorer SNP-detection capability in the regulatory regions. *Sci Rep, 1*, 55. doi:10.1038/srep00055

Weis, F., Beiras-Fernandez, A., & Schelling, G. (2008). Daptomycin, a lipopeptide antibiotic in clinical practice. *Curr Opin Investig Drugs, 9*(8), 879-884.

Werth, B. J., Hahn, W. O., Butler-Wu, S. M., & Rakita, R. M. (2016). Emergence of High-Level Daptomycin Resistance in *Corynebacterium striatum* in Two Patients with Left Ventricular Assist Device Infections. *Microb Drug Resist, 22*(3), 233-237. doi:10.1089/mdr.2015.0208

Wong, K. Y., Chan, Y. C., & Wong, C. Y. (2010). *Corynebacterium striatum* as an emerging pathogen. *J Hosp Infect, 76*(4), 371-372. doi:10.1016/j.jhin.2010.05.018

Yang, S. J., Mishra, N. N., Rubio, A., & Bayer, A. S. (2013). Causal role of single nucleotide polymorphisms within the mprF gene of *Staphylococcus aureus* in daptomycin resistance. *Antimicrob Agents Chemother, 57*(11), 5658-5664. doi:10.1128/AAC.01184-13

Yang, S. J., Nast, C. C., Mishra, N. N., Yeaman, M. R., Fey, P. D., & Bayer, A. S. (2010). Cell wall thickening is not a universal accompaniment of the daptomycin nonsusceptibility phenotype in *Staphylococcus aureus*: evidence for multiple resistance mechanisms. *Antimicrob Agents Chemother, 54*(8), 3079-3085. doi:10.1128/AAC.00122-10

Zhang, T., Muraih, J. K., MacCormick, B., Silverman, J., & Palmer, M. (2014). Daptomycin forms cation- and size-selective pores in model membranes. *Biochim Biophys Acta, 1838*(10), 2425-2430. doi:10.1016/j.bbamem.2014.05.014

Zhang, T., Muraih, J. K., Mintzer, E., Tishbi, N., Desert, C., Silverman, J., . . . Palmer, M. (2013). Mutual inhibition through hybrid oligomer formation of daptomycin and the semisynthetic lipopeptide antibiotic CB-182,462. *Biochim Biophys Acta, 1828*(2), 302-308. doi:10.1016/j.bbamem.2012.10.008

Chapter 2: Mechanism of High-Level Daptomycin Resistance in *Corynebacterium striatum*

Nicholas K. Goldner[1*], Christopher Bulow[1*], Kevin Cho[2,3], Meghan Wallace[4], Fong-Fu Hsu[5], Gary Patti[2,3], Carey-Ann Burnham[4,6,9], Paul Schlesinger[7], Gautam Dantas[1,4,8,9]

[1]The Edison Family Center for Genome Sciences & Systems Biology, Washington University in St. Louis School of Medicine, St. Louis, MO 63110, USA

[2]Department of Chemistry, Washington University in St. Louis, St. Louis, Missouri 63130, United States

[3]Department of Medicine, Washington University School of Medicine, St. Louis, Missouri 63110, United States

[4]Department of Pathology and Immunology, Division of Laboratory and Genomic Medicine, Washington University School of Medicine, St. Louis, Missouri, USA.

[5]Division of Endocrinology, Metabolism & Lipid Research, Washington University School of Medicine, St. Louis, MO 63110, USA.

[6]Department of Pediatrics, Washington University School of Medicine, St. Louis, Missouri 63110, USA.

[7]Department of Cell Biology and Physiology, Washington University School of Medicine, Saint Louis, United States.

[8]Department of Biomedical Engineering, Washington University, St. Louis, Missouri, USA

[9]Department of Molecular Microbiology, Washington University School of Medicine, St. Louis, Missouri 63110, USA.

2.1 Abstract

Daptomycin, a last line of defense antibiotic for treating Gram positive infections, is experiencing clinical failure against important infectious agents including *Corynebacterium striatum*. The recent transition of daptomycin to generic status is projected to dramatically increase availability, use, and clinical failure. Here we confirm the genetic mechanism of high-level daptomycin resistance (HLDR, MIC > 256 μg/mL) in *C. striatum*, which evolved within a patient during daptomycin therapy, a phenotype recapitulated *in vitro*. In all 8 independent cases tested, loss of function mutations in phosphatidylglycerol synthase (*pgsA2*) were necessary and sufficient for high-level daptomycin resistance. Through lipidomic and biochemical analysis we demonstrate that daptomycin's activity is dependent on membrane phosphatidylglycerol (PG) concentration. Until now, the verification of PG as the *in vivo* target of daptomycin has proven difficult since tested cell model systems were not viable without membrane PG. *C. striatum* becomes high-level daptomycin resistant by removing PG from the membrane and changing membrane composition to maintain viability. This work demonstrates that loss of function mutation in *pgsA2* and the loss of membrane PG is necessary and sufficient to produce high-level resistance to daptomycin in *C. striatum*.

2.2 Introduction

Current trends in increasing antibiotic resistance and decreasing drug development require urgent mitigation (Maragakis et al., 2008; O'Neill, 2014; O'Neill, 2015). Antibiotic resistant infections claim over 700,000 lives globally, and this annual toll is predicted to swell to 10 million deaths a year by 2050 without significant intervention. A growing number of bacterial infections are already resistant to virtually all first-line antibiotics (Dynamics, 2015; O'Neill, 2014). Physicians are forced to use "last-resort", broad-spectrum antibiotics more frequently, and resistance to even these carefully safeguarded drugs has emerged (Srinivasan, 2017; Srinivasan and Davidson, 2017). Daptomycin is one such last-resort non-lytic (Cotroneo et al., 2008) lipopeptide antibiotic, effective against both stationary and log phase Gram-positive bacterial pathogens (Mascio et al., 2007) including *Staphylococcus aureus, Enterococcus faecium,* and *Corynebacterium striatum* (Humphries et al., 2012; Jorgensen et al., 2003; Jorgensen et al., 1987). Daptomycin integrates Ca^{2+} dependently into the bacterial cell membrane, causing membrane dysfunction that leads to K^{+}, Mg^{2+}, and ATP leakage and cell death (Ho et al., 2008; Hobbs et al., 2008). Very low levels of resistance were observed during the early phase of daptomycin's clinical use. Regrettably, recent clinical reports of treatment failures have emerged with target pathogens exhibiting >2000-fold increases in daptomycin resistance (Akins et al., 2015; Garcia-de-la-Maria et al., 2013; McElvania TeKippe et al., 2014), often over rapid time-scales (hours to a few days of treatment), which are beginning to challenge daptomycin's efficacy. These failures are expected to expand as daptomycin use is predicted to increase dramatically because its recent transition to generic status (OptumRx, 2016) will increase its availability for clinical use.

C. striatum is an emerging opportunistic pathogen that colonizes the skin much like *S. aureus*. *C. striatum*'s ability to rapidly transition from susceptible to resistant to the critical antibiotic daptomycin poses a serious epidemiological threat to our healthcare system (Chatzopoulou et al., 2016). This work establishes a genetic, transcriptomic, lipidomic and biochemical understanding of how *C. striatum* rapidly evolves high-level daptomycin resistance which is mechanistically distinct from *S. aureus* and *Streptomyces spp.* In *S. aureus*, low-level, step-wise accumulations in resistance phenotypes are responsible for low (Minimum Inhibitory Concentration, MIC: 2-4 μg/ml) and intermediate (MIC: 4-8 μg/ml) daptomycin resistance. The majority of these observations come from pathogenic *S. aureus*, which was the first approved therapeutic target for daptomycin (Sauermann et al., 2008). Accumulation of multiple single nucleotide polymorphisms (SNPs) in the *yycFGHI* operon in *S. aureus* has resulted in 2-6-fold increases in daptomycin resistance through cell wall thickening and alteration of membrane charge (Bayer et al., 2013; Gaupp et al., 2015; Mishra et al., 2014; Quinn et al., 2007; Raad et al., 2007; Reyes et al., 2015). Increases in positively charged membrane phospholipids, which reduces the affinity of the $Ca2^{+}$-conjugated daptomycin for the surface membrane increased the MIC. Additionally, mutations that alter lipid translocation, decrease membrane fluidity, and thickening of the cell wall have led to low-level (3-6 fold) increases in daptomycin resistance(Mishra et al., 2014; Mishra et al., 2009). Mutations associated with the above physiological changes in pathogenic *S. aureus* have all led to small stepwise increases (2-6 fold) in resistance over long periods of time (weeks of treatment) and lose resistance to daptomycin when no longer under daptomycin's selection pressure(Li et al., 2017). In contrast, some environmental *Streptomyces* species have been shown to inactivate daptomycin (D'Costa et al., 2012; Vanessa M. D'Costa, 2006) enzymatically; clinical isolates have not used this mechanism to date.

The first report of higher levels (~20-fold over wild-type) of daptomycin resistance come from laboratory adaptive evolution experiments with the non-pathogenic, soil bacterium, *Bacillus subtilis* (Hachmann et al., 2011). Daptomycin resistant *B. subtilis* was found to harbor SNPs in 44 genes, including predicted reduction/loss of function mutations in phosphatidylglycerol synthase A (*pgsA*), an essential enzyme for phosphatidylglycerol (PG) synthesis (Hachmann et al., 2009; Hachmann et al., 2011). Characterization of the lipid membrane revealed a reduction in PG content from 30% in the wild-type to 10% in the resistant mutant. Consistent with the lack of complete ablation of PG in the membrane, attempts to knock out *pgsA* alone genetically were not successful due to presumed essentiality of PG in *B. subtilis* (Hachmann et al., 2011). Nevertheless, studies of daptomycin's target to date corroborate *in vivo* the importance of PG in daptomycin activity (Hachmann et al., 2009; Hachmann et al., 2011; Hines et al., 2017). Indeed, a recent comparative genomic and lipidomic study of *S. aureus*, *C. striatum*, and *Enterococcus faecalis* indicated mutations in PG synthase and subsequent lack of PG synthesis confers daptomycin resistance(Hines et al., 2017)(Hines et al., 2017)(Hines et al., 2017)(Hines et al., 2017)(Hines et al., 2017)(Hines et al., 2017)(Hines et al., 2017).

Over the past few years, there has been a steady increase in reports of even higher-level daptomycin resistance (≥4000 fold increase in resistance) in a number of clinical pathogens, including viridians group *Streptococci* (Akins et al., 2015), *Enterococcus faecium* (Humphries et al., 2012), and C. *striatum* (McElvania TeKippe et al., 2014). This high-level daptomycin resistance (HLDR)—defined here as a minimum inhibitory concentration (MIC) ≥ 256 μg/ml

daptomycin—was first observed in *C. striatum*, in a patient with native valve endocarditis in 2012 (Tran et al., 2012). In 2014, a clinical laboratory reported *in vivo* evolution of HLDR *C. striatum* in a patient with an infected left ventricular assist device, during 17 days of daptomycin therapy (McElvania TeKippe et al., 2014). Evolution of HLDR was recapitulated *in vitro* in 100% of tested *C. striatum* isolates (n=50) after 24 hours of daptomycin exposure (McMullen et al., 2017a). *C. striatum* is a Gram-positive bacterium which typically resides as a commensal organism on the skin (Oh et al., 2014). However, it has become a growing threat to hospital systems and patients as an opportunistic pathogen. Indeed, *C. striatum* has been associated with a plethora of infection types over the past 20 years including bacteremia, endocarditis, urinary tract, wound, respiratory, central line, medical device and hardware infections (Gomila et al., 2012; Hahn et al., 2016; Mattos-Guaraldi et al., 2015; McElvania TeKippe et al., 2014; Souza et al., 2015; Wang et al., 2016; Werth et al., 2016; Wong et al., 2010). Here we use a combination of comparative genomics, transcriptomics, lipidomics, electron microscopy, and biochemical lipid and liposome characterization to elucidate the mechanism of HLDR evolved in *C. striatum* both within patients and *in vitro*. We demonstrate that loss of function mutations in *pgsA2* results in PG, the primary target of this last-resort drug, to be reduced from ~45% to <1% in the membrane resulting in HLDR. Our work demonstrates the important consideration for designing future antibiotics that bacterial cells can readily manipulate membrane lipid composition to effectively evade lipid targeted lipopeptides.

2.3 Results

2.3.1 PG synthase mutations in HLDR *C. striatum* strains

All cases of evolved high-level daptomycin resistance (HLDR) in *C. striatum* that were tested (Figure 2.1 and Supplemental Table 2.1) had a predicted loss of function mutation in PG synthase. We performed whole genome sequencing of eight pairs of *in vivo* and *in vitro* evolved HLDR *C. striatum* isolates (n = 16), and found *pgsA2* to be the only gene mutated consistently in all HLDR mutants. The affected gene encodes PG synthase, responsible for converting CDP-DAG to PG (Figure 2.1A). The mutations observed include coding changes at universally conserved sites (Figure 2.1B), the dimer interface (Figure 2.1C), the active site (Figure 2.1D), and those leading to premature stop codons (Figure 2.1E). Each of these mutations is predicted by snpEFF (Cingolani et al., 2012a; Cingolani et al., 2012b) and PHYREII (Kelley et al., 2015; Kelley and Sternberg, 2009) homology modeling to result in loss of PG synthase activity.

We found no additional SNPs in the *C. striatum* genomes predicted to alter cellular biosynthetic processes in potential compensation for PG synthase loss of function. In *B. subtilis*, loss of just *pgsA*2 (PG synthase) was lethal and compensatory mutations were necessary for cell survival (Hachmann et al., 2011) leading us to consider whether additional mutations may also be required for HLDR in *C. striatum*. A total of 8 additional non-synonymous SNPs in biosynthetic pathways were detected in the *in vivo* evolved isolate (Supplemental Figure 2.1). Aside from the *pgsA2* mutation, no SNPs in biosynthetic pathways were detected in the *in vitro* evolved HLDR isolates. This is consistent with the longer time between susceptible and resistant isolate collection *in vivo* (17 days) versus *in vitro* (24 hours). The remaining SNPs in genes not related to biosynthesis did not cluster in similar pathways (Raw data file, All SNPs tab). No consistent genetic change besides the loss of function mutation in *pgsA* is predicted to result in compensatory changes that would contribute to membrane viability or HLDR in *C. striatum*.

Each of the parent daptomycin susceptible *C. striatum* isolates were derived from different patients, and the *in vivo* and *in vitro* HLDR phenotypes were evolved independently (Supplemental Table 2.1). This breadth of evolution events in *C. striatum* isolates obtained from infected patients provides a robust, clinically relevant cohort for assessing mutations necessary to daptomycin resistance. Accordingly, comparative genomics indicates that loss of function SNPs in *pgsA2* encoding PG synthase are the only genomic change necessary for HLDR and no additional mutations are required to maintain resistant cell viability (Figure 2.1A-E). In a recent report of evolved xenobiotic resistance in Corynebacterineae (the suborder which includes *Corynebacterium*) minimal genetic mutations were observed between susceptible and resistant pairs, but large-scale transcriptomic changes were found to explain the change in phenotype (Hines et al., 2017; Yoneda et al., 2016). Accordingly, we tested whether whole cell transcriptional changes were potentially responsible for compensating the loss of PG synthase function and stabilization of the membrane in HLDR *C. striatum*.

2.3.2 Minimal transcriptional changes in HLDR *C. striatum*

No significant transcriptional changes were detected in biosynthetically linked genes in clinically evolved HLDR in *C. striatum* (Figure 2.2C, Supplemental Figure 2.2B and Raw Data: Transcriptomics). We compared the transcriptomes of the WP1a (index, daptomycin susceptible) and RP1b (HLDR evolved in the patient) strains grown in cation-adjusted Mueller-Hinton broth (CAMHB) to exponential phase in biological triplicate. Even the largest magnitude transcriptional changes did not exceed +/- 85%, much smaller than transcriptomic changes typically associated with phenotypic alteration (Yoneda et al., 2016). Expression changes in genes related to

phospholipid biosynthesis were small in magnitude (less than 25%) and not significant (Figure 2.2C and Supplemental Figure 2.2). Furthermore, most transcriptomic changes observed occurred in transposase genes and hypothetical proteins of viral origin. The most notable biosynthetically linked change was the LGFP repeat protein transcript detected at levels 1.302-fold (~30%) greater in the HLDR strain. *PgsA*2 expression levels changed by only 0.981-fold (not significant) in the HLDR strain, further indicating that the HLDR phenotypic consequence of the predicted PG synthase loss-of-function binding pocket mutation in the RP1b strain is due to loss of activity rather than expression. Lack of transcriptional alterations prompted us to interrogate the membrane composition of daptomycin susceptible and HLDR *C. striatum* strains using a comparative lipidomics approach. We hypothesized that the HLDR phenotype resulted from the disruption of PG synthase activity, which effectively removes PG from the membrane (Figure 2.2A).

2.3.3 Lipidomics reveals loss of phosphatidylglycerol in the membrane

We found that loss of PG synthase function leads to removal or at least a > 360-fold reduction of membrane phosphatidylglycerol (PG) content in HLDR *C. striatum* isolates. Analysis by mass spectrometry of whole-cell membrane lipid content of four pairs of daptomycin susceptible and HLDR isolates, which represent each of the four types of predicted loss-of-function *pgsA2* mutations (Figure 2.2 B-E and Supplemental Table 2.1) reveals loss of PG. In each isolate pair, PG detection was 369-1990-fold ($p \leq 0.0001$) lower in the evolved HLDR isolates than in the daptomycin susceptible ancestor (Figure 2.3A), levels in the HLDR isolates which are indicative of complete removal of PG in the membrane, resulting in the HLDR phenotype. In addition to PG, cardiolipin (CL, a derivative of PG) was the other lipid absent in the HLDR isolates (Figure 2.3A,

C). However, CL was also absent in the daptomycin susceptible WP1a isolate, and because of subsequent *in vitro* data, we posit it is not the primary target of daptomycin. We also found no lipidomic evidence that the sn-1/sn-2 fatty acyl groups in PG is being modified to shield it from daptomycin binding hypothesized in low-level resistant *S. aureus* isolates (Ernst et al., 2009; Mishra and Bayer, 2013; Peschel and Collins, 2001; Staubitz et al., 2004). Conversion of PG to CL, a proposed mechanism of daptomycin resistance (Zhang et al., 2014b), also does not contribute to the *C. striatum* HLDR mechanism, since CL is absent in the HLDR strains ($p \leq 0.0001$) (Figure 2.3C). PG synthase converts CDP-Dag, a biosynthetic precursor of PG, into phosphatidyl glycerol (Figure 2.2A). In the absence of PG synthase, we expected CDP-Dag to either be utilized in a secondary lipid synthesis pathway or to accumulate in the cell. In support of the latter hypothesis, we found that CDP-Dag levels are significantly (543-5946-fold; $p \leq 0.0001$) higher in HLDR isolates over their WT counterparts (Figure 2.2A and Figure 2.3B). PG synthase in HLDR strains across mutation types is nonfunctional (Figure 2.1B-E and Figure 2.2A) and no transcriptional compensatory changes are being made in the PG biosynthesis pathway (Figure 2.2A-C, Supplemental Figure 2), enabling high-level CDP-Dag accumulation (Fig. 2a and Fig. 3).

Until recently, determining the *in vivo* target of daptomycin had been challenging because it was biologically untenable to remove PG from the membrane of model Gram-positive bacteria without cell death (Garcia-de-la-Maria et al., 2013; Rubio et al., 2012). A recent study (Hines et al., 2017) corroborates that *C. striatum* appears to uniquely compensate for the complete removal of PG in its membrane by increasing the proportion of two other lipids in the membrane: PI (Figure 2.3E and Supplemental Figure 2.2A,B) and glucuronosyl diacylglycerol (Glua-Dag) (Figure 2.3D). PI is 1.6-5.3-fold higher ($p \leq 0.0001$ and $p \leq 0.001$) in HLDR over WT (Figure 2.3E and Supplemental Figure 2.3A) and Glua-Dag is 5.5-23.0-fold higher ($p \leq 0.0001$ and $p \leq 0.01$) in HLDR over WT

(Figure 2.3D). We demonstrate that the previously proposed mechanisms of daptomycin resistance which include altering membrane fluidity, leaflet organization, and morphology do not contribute to HLDR in *C. striatum*, as the lipid membrane composition changes in the HLDR isolates do not visibly alter the membrane (by transmission electron microscopy, Supplemental Figure 2.4A) or charge (by zeta potential, Supplemental Figure 2.4B) compared to daptomycin susceptible counterparts. These data affirm that PG is the *in vivo* target of daptomycin and loss of PG due to non-functional PG-synthase is necessary and sufficient for the HLDR phenotype.

2.3.4 Surface plasmon resonance indicates PG is the preferred target of daptomycin

In support of our genomic and lipidomic conclusions, we performed a structure-function analysis of PG, which we show is the target of daptomycin and is necessary and sufficient for daptomycin activity *in vitro.* By combining Surface Plasmon Resonance (SPR), which measures binding. and carboxyfluorescein liposome stability assays (CFLSA) studies, which measure activity, we are able to understand the structural interactions of daptomycin with PG. We use 200 nm artificial liposomes of relevant membrane lipid compositions to determine these relationships. Four lipid species—PG, CL, phosphatidic acid (PA) and phosphatidylcholine (PC) (Supplemental Figure 2.3 and Figure 2.4F)—were tested for daptomycin binding affinity. PI and Glua-Dag are both found in WT and HLDR isolates, and we did not test them in the next set of experiments because our lipidomics analysis indicated they are not the *in vivo* targets of daptomycin. Three types of liposomes of defined composition were assembled, comprised of PG, CL, and PA combined at a 1:1 molar ratio with PC, and compared with homogeneous PC-only liposomes. Daptomycin showed a significantly higher affinity to PG liposomes ($p \leq 0.0001$ and $p \leq 0.001$) than any of the

other lipids tested (Figure 2.4). PG has been hypothesized to be an *in vitro* target of daptomycin due to its charged phosphate, however, the lack of binding to PC and minimal binding to PA (Figure 2.4E) indicate that the negatively charged phosphate plays a subordinate role in daptomycin binding. Additionally, when the fatty acyl groups are restricted to the bilayer surface plane, as they are in CL, daptomycin binds with much lower affinity (Figure 2.4A-E). When the phosphatidyl-sn-glycerol-3-phosphate glycerol head group is accessible, as it is with PG, the daptomycin binds more efficiently (Figure 2.4A-E). Also, the daptomycin binding to the 1:1 PG liposomes appears to saturate with daptomycin above 20 μg/ml indicating that PG is acting as a binding site for the daptomycin (Figure 4E). Accordingly, we would expect daptomycin activity to correlate with the binding of PG, CL, PA, and PC, and we tested this through a carboxyfluorescein liposome stability assay (CLFSA).

2.3.5 CFLSA indicates PG is necessary and sufficient for daptomycin activity

We found that presence of PG in the bacterial membrane correlates with daptomycin's bactericidal activity. Carboxyfluorescein liposome stability assays (CLFSA) confirmed PG's role in daptomycin activity *in vitro*. Liposomes were generated as above in the presence of self-quenching carboxyfluorescein. Daptomycin is added and interacts with the liposome membrane, releasing and diluting the carboxyfluorescein, which is then unquenched in the buffer producing dramatically increased fluorescence (Saito et al., 2000a). Daptomycin had higher activity against PG containing membranes in all cases (Figure 2.5A-F) and acts in a concentration dependent manner against both PG and PA (Figure 2.5F). Even though PA had lower binding affinity to daptomycin than CL (Figure 2.4E), daptomycin was more active against PA than it was against

liposomes containing CL where there are no available glycerol-3-phosphates extending from the membrane surface for daptomycin binding (Figure 2.5A, D). This is consistent with the observed PG to CL daptomycin activity relationship. Furthermore, this suggests to us that the larger (4 alkane chain CL) suppresses daptomycin's integration with membrane structure that is necessary for increased permeability in the CFLSA assay inhibiting daptomycin activity. We observed a reduction in daptomycin activity in liposomes that contain CL even though they have a higher binding affinity than PA and PC (Figure 2.4E and Figure 2.5A-F). These findings indicate that the conversion of PG to CL can reduce activity of daptomycin in membranes providing low-level resistance against daptomycin *in vivo*.

2.3.6 CFLSA indicates PG concentration predicts daptomycin activity *in vivo*

We found that daptomycin bactericidal activity is correlated with the percent composition of PG in the membrane. Liposomes with 0%-50% PG were generated as above and daptomycin's activity against those liposomes were tested at a consistent 35 μg /ml daptomycin. At or above 20% PG composition, daptomycin did not show a significant change in activity (Figure 2.5G). This observation directly maps to daptomycin's *in vivo* bactericidal activity as measured by MIC across a number of bacterial species. *B. subtilis*, *C. striatum,* and *S. aureus* strains with 30-50% membrane PG (Hachmann et al., 2011; McMullen et al., 2017b; Randall et al., 2013) content have MICs ≤ 1 μg/ml daptomycin. Below 20% PG content, daptomycin's activity drops precipitously, both *in vitro and in vivo.* Daptomycin resistant *B. subtilis* with a PG content of 10% showed a 27-fold increase in MIC (Hachmann et al., 2011). This is recapitulated with our artificial liposomes where equivalent daptomycin reduction results in 3.66-fold decrease in carboxyfluorescein-based

fluorescence (Figure 2.5G), indicative of a loss in daptomycin activity. When membrane PG composition is ≤ 5%, daptomycin's activity is indistinguishable from complete absence of PG in the artificial liposome. In HLDR *C. striatum,* which has 0% PG in its membrane we see a ≥4000 increase in MIC (McElvania TeKippe et al., 2014; McMullen et al., 2017b) and our data shows a 13.5-fold decrease in carboxyfluorescein fluorescence when the liposomes have < 5% PG. Thus, the percentage composition of PG relative to other membrane lipids is predictive of daptomycin susceptibility and activity both *in vivo* and *in vitro*. It also suggests that the CFLSA *in vitro* model is an effective method of studying daptomycin's interactions with membranes.

2.4 Conclusions

C. striatum is an emerging, commensal opportunistic pathogen that has the potential to cause widespread harm in our hospital systems. The rapid adaptive evolution of loss of function *pgsA2* (PG synthase) mutations which result in the significant loss or removal of membrane PG are necessary and sufficient for high-level daptomycin resistance in *C. striatum*, which lead to catastrophic daptomycin treatment failure in patients. No additional genomic or transcriptomic compensation mechanisms are evident for the evolved HLDR phenotype. The HLDR mutants also have no changes in cell wall thickness, cell surface charge, conversion of PG to cardiolipin, or membrane shape, which are all mechanisms previously implicated in lower-level daptomycin resistance (Bayer et al., 2015; Bayer et al., 2016; Bayer et al., 2014; Bayer et al., 2013; D'Costa et al., 2012; Gaupp et al., 2015; Mishra et al., 2015; Mishra et al., 2009; Quinn et al., 2007; Raad et al., 2007; Reyes et al., 2015; Vanessa M. D'Costa, 2006; Zhang et al., 2014b). Rebalancing of membrane composition to include more PI in the absence of PG as observed by lipidomic profiling likely results in membrane stability. *C. striatum*'s ability to completely remove PG from its

membrane, with simple loss-of-function point mutations in PG synthase, further demonstrates that PG is the *in vivo* and *in vitro* target of daptomycin. The remarkable ability of *C. striatum* to remove a previously presumed necessary membrane phospholipid could make *C. striatum* an ideal model for developing new Gram-positive antibiotics like daptomycin and studying the potential for resistance to develop.

2.5 Methods

2.5.1 Whole genome sequencing and comparison

We sequenced 8 sets of *C. striatum* strains before and after emergence of high-level resistance to daptomycin. Isolates were sequenced using the Illumina Hi Seq 2500 platform, generating 101bp paired-end reads. One case of resistance emergence occurred in a patient bloodstream while the remaining strains evolved resistance during *in vitro* selection. We used the original susceptible patient isolate as our reference strain and assembled this genome de novo using SPADES (Bankevich et al., 2012). This reference genome was annotated using the Prokka v1.12 and the Pfam database. (Seemann, 2014) We assembled the remaining 15 genomes by mapping to this reference using bowtie2 (Langmead and Salzberg). We identified Single Nucleotide Polymorphisms (SNPs) between the resistant strains and their respective susceptible controls using Pilon. (Walker et al.) The effects of these mutations were predicted using SNPeff. (Cingolani et al.) All of the genes annotated in the reference genome were clustered by predicted metabolic function using Blast2Go(Conesa et al., 2005). Genes with predicted loss of function mutation were annotated on this metabolic map. *pgsA2* was the only gene with biosynthetic function predicted to contain loss of function mutations in more than one case of HLDR (in fact, *pgsA2* loss of function mutations were found in all cases of resistance). 33 other non-synonymous SNPs were detected

across all 8 strain pairs. Only 8 of these SNPs were in genes predicted to affect biosynthetic processes. After clustering by Gene Ontology (GO), *pgsa2* altering phospholipid biosynthesis was the only metabolic alteration predicted in more than one case of resistance. Phyre2 homology modeling(Kelley et al., 2015)supported predictions that the *pgsA2* mutation in every resistant strain was loss of function.

2.5.2 Transcriptomic methods

We performed transcriptomic profiling of the susceptible and the *in vivo* evolved resistant isolate from the original patient in triplicate. Frozen culture was streaked onto CAMHB plus blood plates and grown overnight for single colony selection and then and inoculated into 50 ml CAMHB broth and grown overnight. The following day, the cultures were diluted to 0.5 McFarland standard and split into three 100 ml cultures per condition. The diluted cultures were incubated at 37 °C with shaking for 1 hour. The cells were collected by centrifugation at 200 g for 15 minutes. The pellets were resuspended in RNAlater (76104 Qiagen) and frozen at -80 until analysis.

We used bead beating and SDS treatment to disrupt the sample cells, phenol: chloroform extraction to remove proteins, and alcohol precipitation followed by DNAase treatment to isolate RNA from the frozen samples. Ribosomal RNA was removed with Ribo-Zero rRNA Removal Kit (Epicentre). cDNA libraries were generated from the isolated RNA and amplified as described in Yoneda, Henson *et al*., 2016. The double stranded cDNA libraries were sequenced using the Nextera (Baym et al., 2015) platform to generate at least 7 million 75bp reads from each sample.

Reads from the triplicate susceptible and HLDR samples were aligned to the reference genome constructed from the index susceptible isolate using cufflinks. (Trapnell et al.) Differences in expression between susceptible and HLDR strains were calculated using cuffdiff. (Trapnell et al.,

2013) Fold change was calculated as resistant expression level divided by susceptible expression level. Expression levels of the control housekeeping genes *rpoA* and *gyrA* remained constant in resistant versus susceptible samples (Fold change 1.02 and 1.00). Significance of changes was calculated using the beta negative binomial distribution previously described in Trapnell *et al*.(Trapnell et al., 2013) using a significance level of $p < 0.05$.

2.5.3 Zeta potential measurement methods

We performed surface charge measurement of the susceptible and HLDR resistant strains using zeta potential. (Kaisersberger Vincek et al., 2017) Frozen culture was streaked onto CAMHB plus blood plates and grown overnight for single colony selection and then and inoculated into 50 ml CAMHB broth and grown overnight. The following day, the cultures were diluted to 0.5 McFarland standard and one 4 ml culture was grown per condition. The diluted cultures were incubated at 37 °C with shaking for 1 hour. One (1) ml of the culture was placed in a Malvern zeta-sizing cuvette. Zeta potential (surface charge) was measured using a Zetasizer Nano ZS (ZEN3600) Dynamic Light Scattering System (Malvern Instruments) and compared between susceptible and HLDR paired strains. Expression levels of genes related to lipid biosynthesis are found in Figure 2 and Supplemental Figure 3. Additionally, genes with greatest fold changes are found in the Supplemental spreadsheet.

2.5.4 Lipidomic methods

We performed comparative lipidomics across all four mutation types. WT and HLDR matched isolates were grown overnight and diluted to an OD of 1 in 2.5 ml liquid culture in quintuplicate. Liquid cultures were spun down to the cell pellet and whole cell lipids were extracted using the Bligh-Dyer method (Bligh and Dyer, 1959). Samples were then stored at -20 until the lipids could be analyzed via liquid chromatography/mass spectrometry (LC/MS). The peak intensities

were normalized to 100 for each lipid with WT or HLDR being the normalizing lipid. The WT lipid was chosen as the normalizing lipid for PG, and Cardiolipin because they were most abundant in WT compared to the HLDR isolate. The HLDR lipid was chosen as the normalizing lipid for CDP-DAG, Glua-DAG and PI because they were most abundant in HLDR compared to the WT isolate. Statistical analysis was performed with 1-way anova and every column was means compared $p \leq 0.05$ (*), $p \leq 0.01$ (**), $p \leq 0.001$ (***), $p \leq 0.0001$ (****).

2.5.5 Carboxyfluorescein liposome stability assay

We performed a liposome disruption assay (Jimah et al., 2017) in triplicate to assess the activity of daptomycin on varying compositions of liposomes. Equimolar ratios of PG:PC, CL:PC and PA:PC with a PC only liposome control were created using the reverse phase method containing carboxyfluorescein (Szoka and Papahadjopoulos, 1978). Liposomes were then suspended in a buffer solution and subjected to varying concentrations of daptomycin from 3.125μg/ml-1000μg/ml. Fluorescence increase due to daptomycin as a result of carboxyfluorescein release was measured using a Varian Eclipse Spectrophotometer with an excitation wavelength of 492 and an emission wavelength of 512. Daptomycin activity was measured as a function of normalization to 100% release by triton x-100. Additionally, to assess PG% on daptomycin activity, PG:PC liposomes were created in triplicate with varying mole fraction ratios converted to PG% (50%, 40%, 20%, 15%, 10%, 5% and 0%) and subjected 35μg/ml daptomycin. Statistical analysis was performed with 1-way anova and every column was means compared $p \leq 0.05$ (*), $p \leq 0.01$ (**), $p \leq 0.001$ (***), $p \leq 0.0001$ (****).

2.5.6 Surface plasmon resonance

We performed surface plasmon resonance(Kinouchi et al., 2013) in triplicate to assess the binding of daptomycin on varying compositions of liposomes. In equimolar ratios (1:1) of PG:PC, CL:PC and PA:PC with a PC only liposome control were created using the reverse phase method (Szoka and Papahadjopoulos, 1978). Liposomes were bound to carboxymethyl dextran hydrogel surface sensor chip that was treated with sphingosine and subjected to varying concentrations of daptomycin from 3.125μg/ml-35μg/ml. Baseline, stable liposome and peak daptomycin binding readings were collected. Daptomycin binding was normalized to liposome binding and presented as daptomycin/lipid unit. Statistical analysis was performed with 1-way anova and every column was means compared $p \leq 0.05$ (*), $p \leq 0.01$ (**), $p \leq 0.001$ (***), $p \leq 0.0001$ (****).

2.6 Main Text Figures

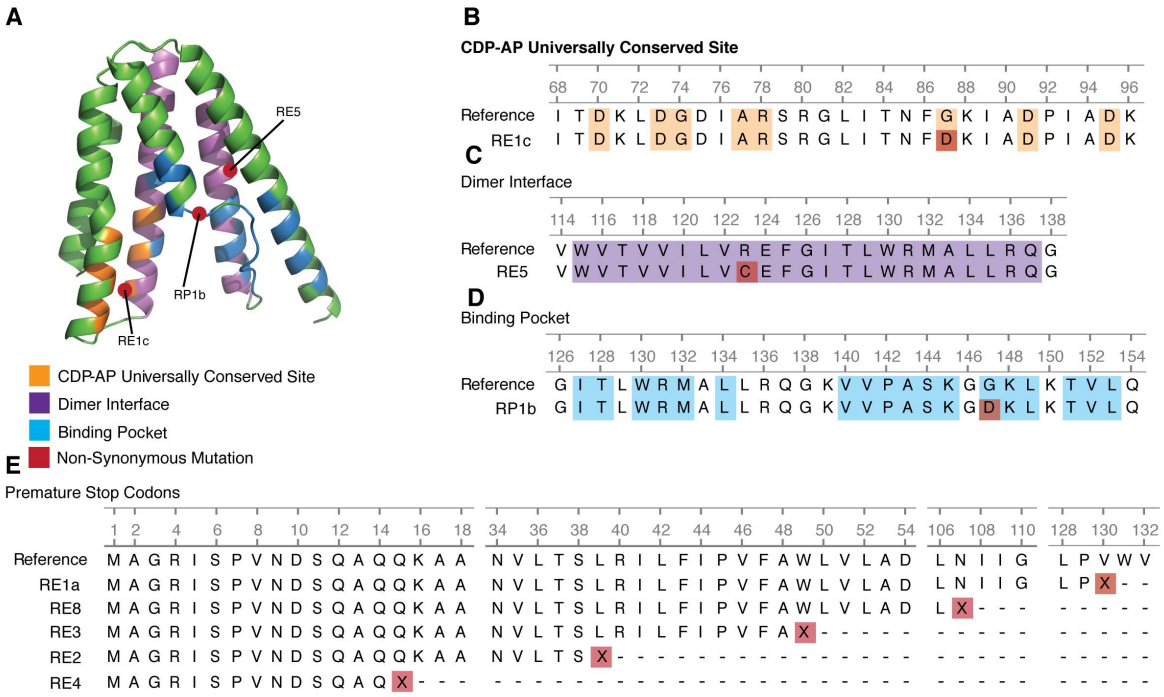

Figure 2.1: All HLDR isolates have predicted nonfunctional mutations in pgsA2

A, Structure of PG synthase monomer with mutations in conserved sites overlaid. **B**, mutation in CDP alcohol phosphatidyl transferase active site conserved across species. **C**, mutation in the dimer interface domain. **D**, mutation in substrate binding pocket. **E**, premature stop mutations predicted to produce truncated products.

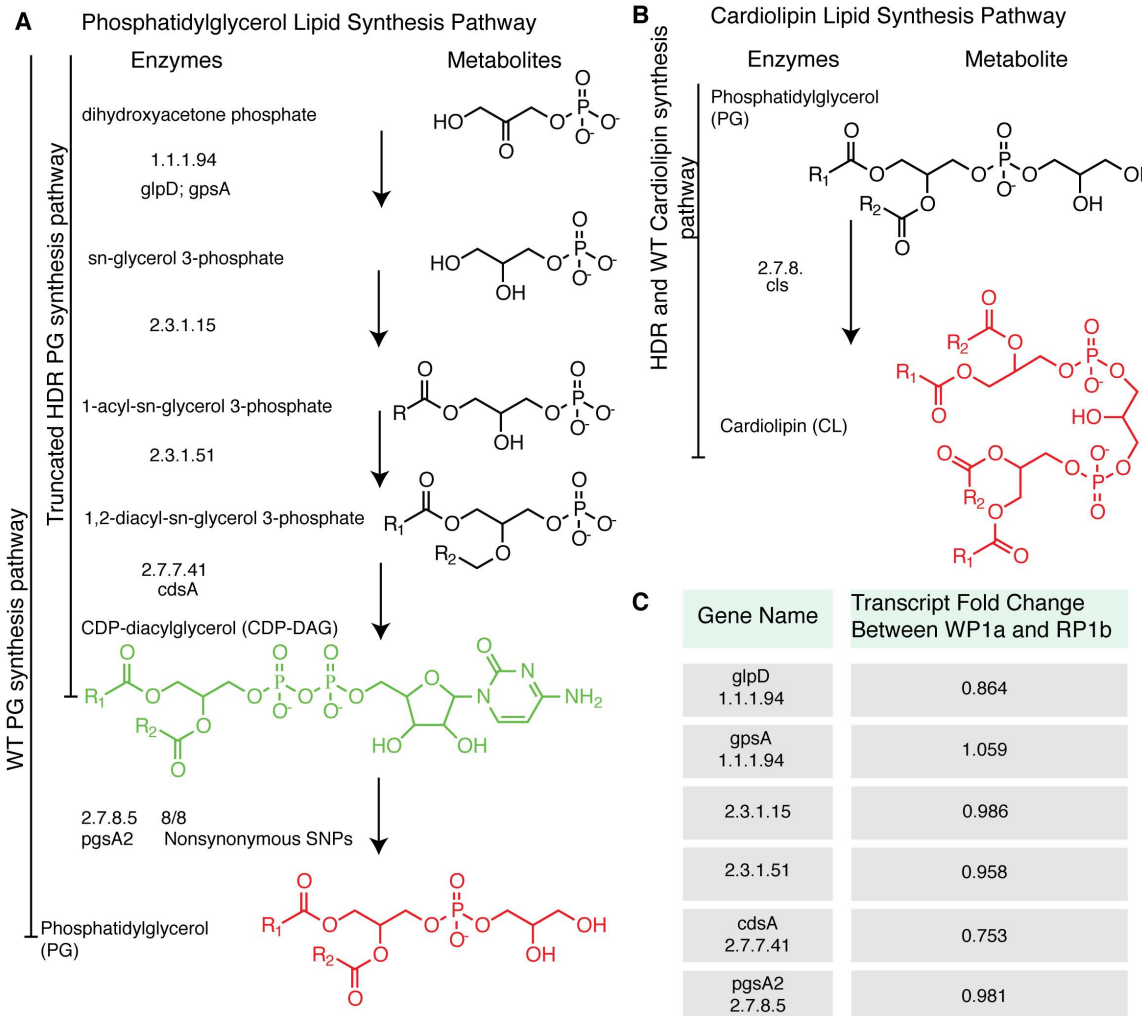

Gene Name	Transcript Fold Change Between WP1a and RP1b
glpD 1.1.1.94	0.864
gpsA 1.1.1.94	1.059
2.3.1.15	0.986
2.3.1.51	0.958
cdsA 2.7.7.41	0.753
pgsA2 2.7.8.5	0.981
cls 2.7.8	0.902
rpoA	1.021

Figure 2.2: Lipid metabolism pathway of Phosphatidylglycerol, observed SNPs and relative abundance changes of key lipids between WT and HLDR isolates

The PG **A**, and CL **B,** lipid synthesis pathways were constructed with KEGG. 8 WT and HLDR isolate paired genomes were compared and nonsynonymous single nucleotide polymorphisms identified. The metabolites names and structures are on the left, with key lipids colored in red and green. R1 represents the 16:0 carbon chain and R2 represents the 18:1 carbon chain. The enzyme nomenclature for each enzymatic step and their corresponding genes are located next to the

appropriate synthesis arrow. SNP mutations for each enzyme/gene unit are to the far right with the number of mutations out of the 8 HLDR isolates, unless no mutations were present in any of the isolates. Except for *pgsA2*, none of the lipid synthesis genes for PG have SNPS. On the left side, black bars indicate the functional completeness of the PG synthesis pathway. WT proceeds through the entire synthesis pathway producing PG, while HLDR ends at the production of CDP-DAG. The green color of the lipid CDP-Dag indicates a 543-5946-fold buildup of that metabolite in the HLDR isolates compared to WT. The Red color of PG and cardiolipin indicates a reduction of that metabolite in the HLDR isolates compared to WT with a 369-1990-fold reduction in PG. **C,** Expression levels of genes involved in lipid synthesis pathways were not significantly altered in HLDR ($p>0.05$). Expression levels of the housekeeping genes *rpoA* and *gyrA* were also not significantly altered ($p>0.05$).

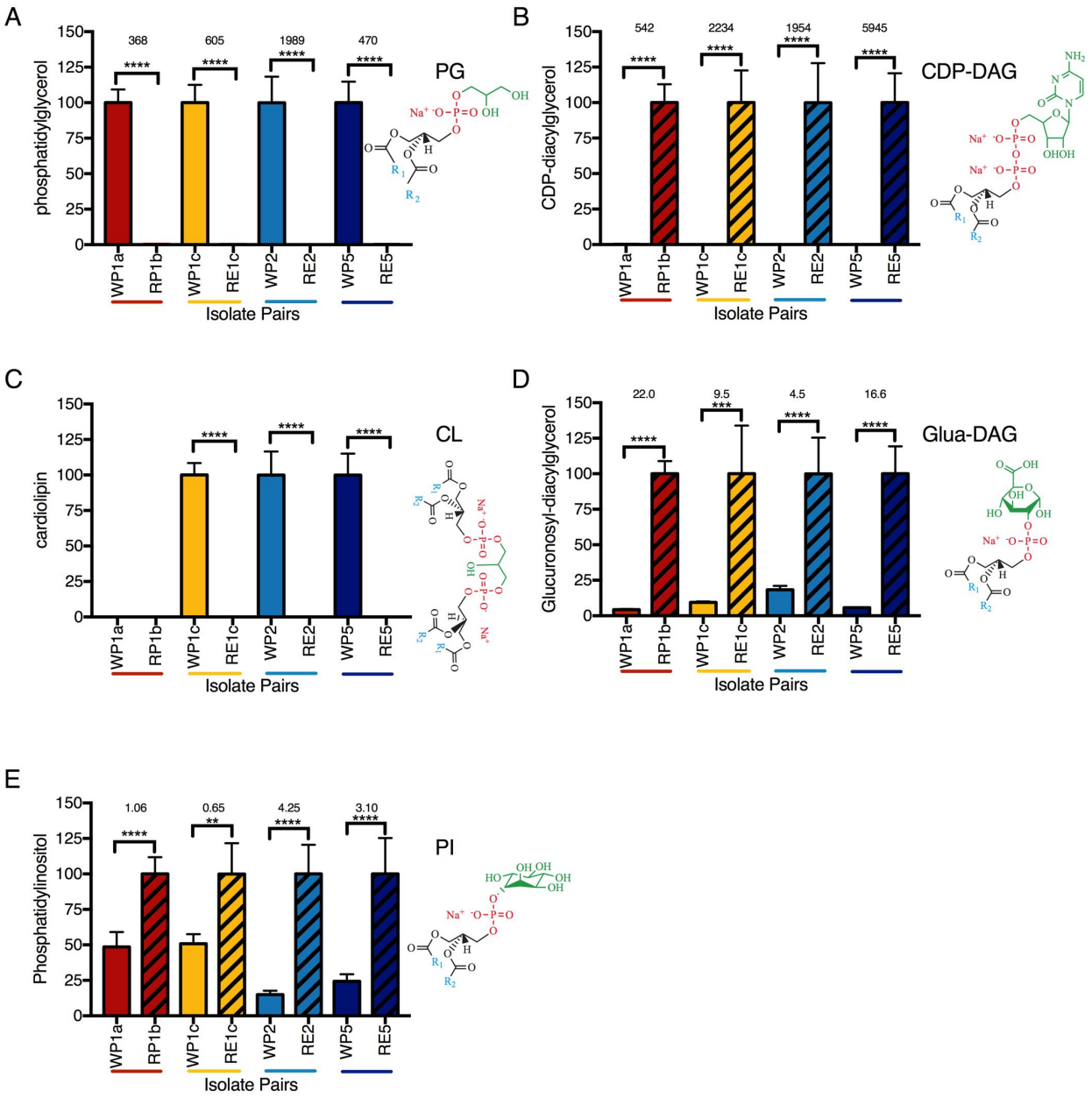

Figure 2.3: Lipidomic comparison of WT and resistant paired isolates across mutation types

A-E The y-axis represents the relative abundance of the important phospholipid between the WT and HLDR isolates. WT-HLDR pairs are associated by color with WT represented by solid block colors and HLDR represented by black striped colors. The lipid that is most abundant in the WT or HLDR isolate has been normalized to 100. Fold changes, where calculable, are listed above the WT and HLDR comparisons; fold change was calculated using (b-a)/a, where 'b' is the largest value and

'a' is the smallest to maintain a positive number. The structures of the lipid are directly to the right of the graph with R_1 = 16:0 carbon chain and R_2 = 18:1 carbon chain. Statistical analysis was performed with 1-way anova and every column was means compared $p \leq 0.05$ (*), $p \leq 0.01$ (**), $p \leq 0.001$ (***), $p \leq 0.0001$ (****).

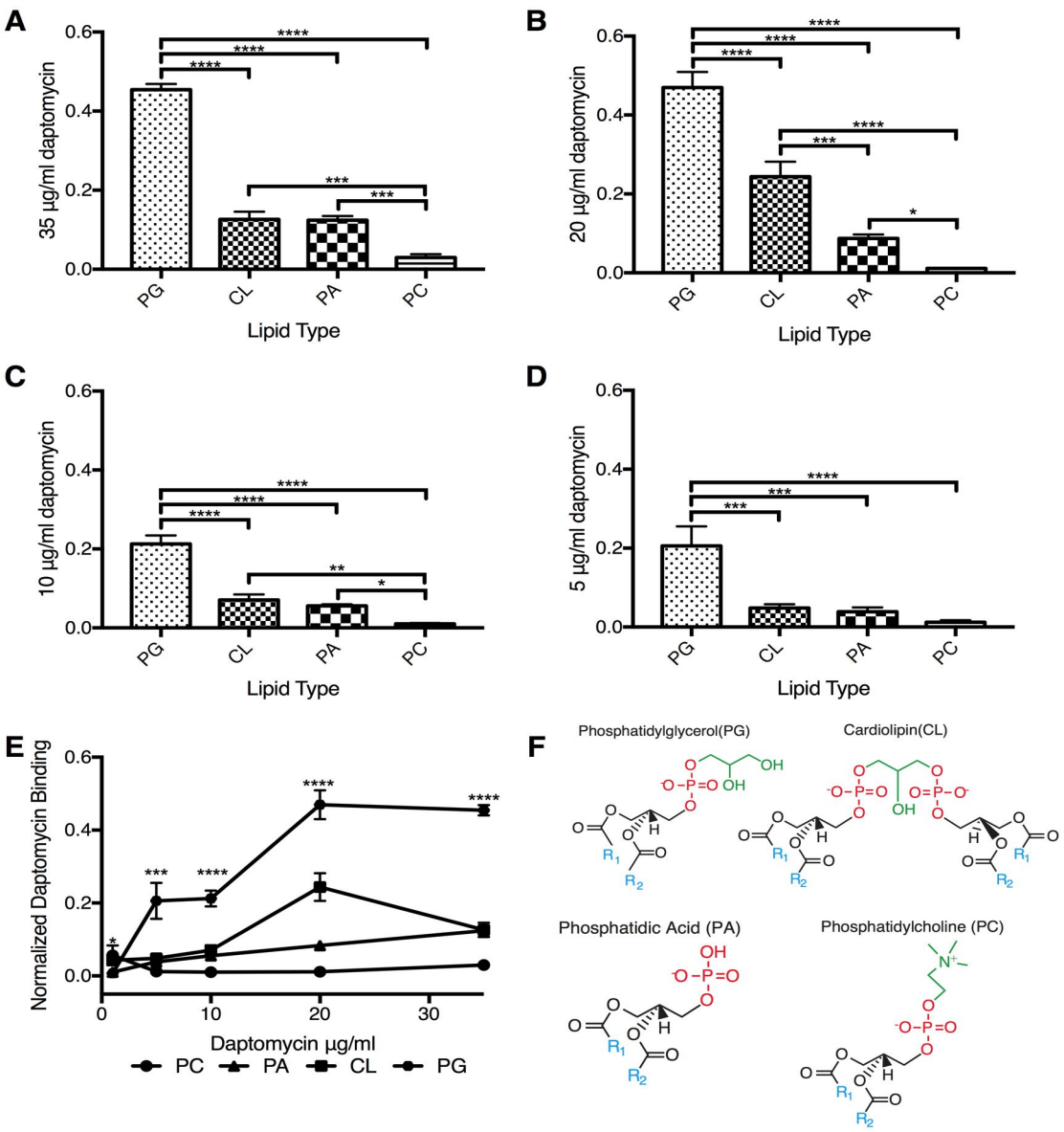

Figure 2.4: Daptomycin binding across concentrations and liposome content

A-E, The y-axis plots the normalized binding of daptomycin at varying concentration ratios to liposomes. The x-axis shows the type of liposomes tested, which include 1:1 equimolar ratios of PG, PA or CL to PC and a control liposome made entirely of PC. **E**, demonstrates stepwise increases in daptomycin binding to PG. **F,** structures of our lipid of interest. Statistical analysis was performed with 1-way anova and every column was means compared, $p \leq 0.05$ (*), $p \leq 0.01$ (**), $p \leq 0.001$ (***), $p \leq 0.0001$ (****).

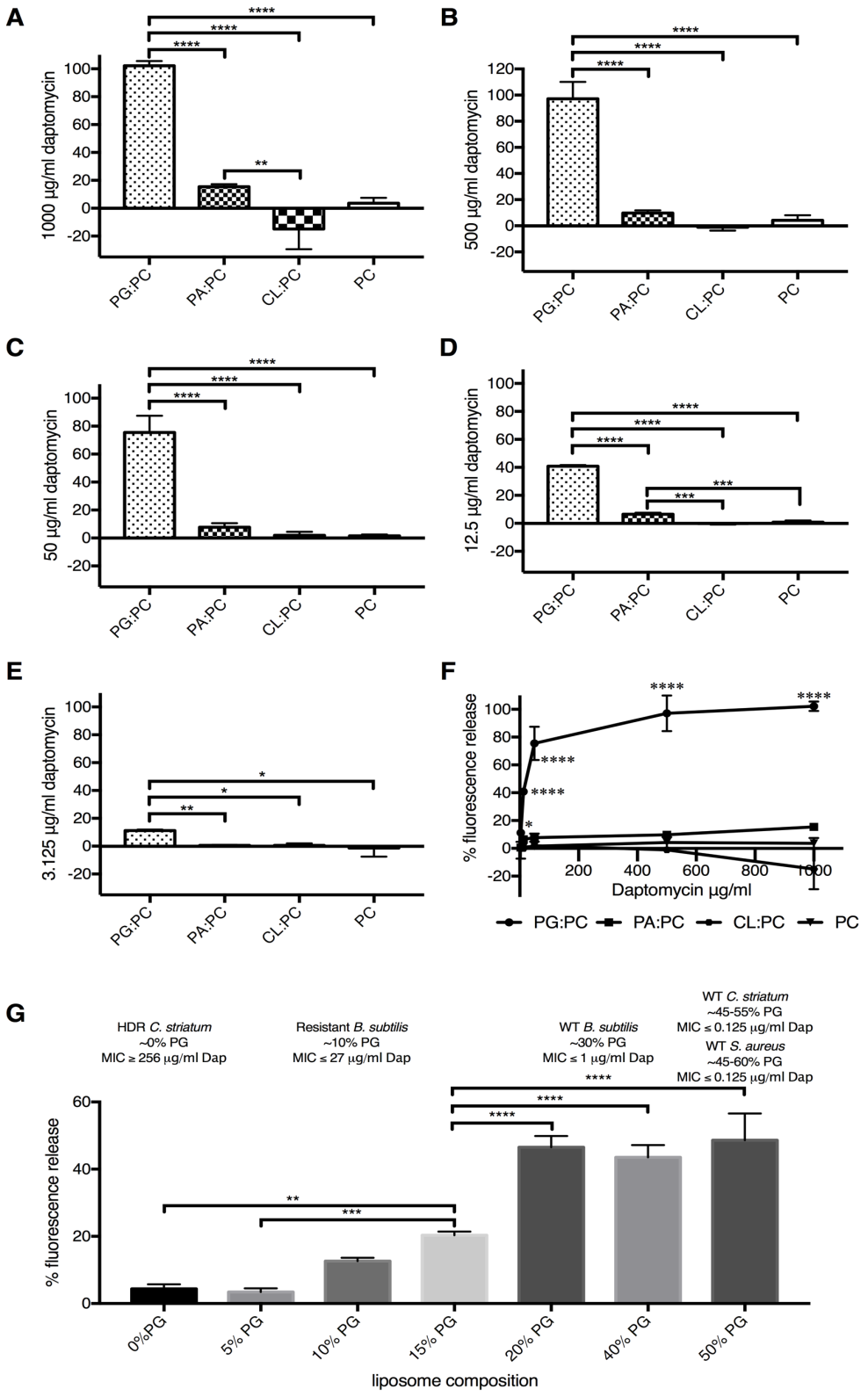

Figure 2.5: Daptomycin activity across concentrations and liposome content

A-F, The y-axis plots the % activity of varying concentrations of daptomycin based on absolute fluorescence that is normalized to the fluorescence achieved by the addition of triton X-100. **A-E**, The x-axis shows the type of liposomes tested, which include 1:1 equimolar ratios of PG, PA, or CL to PC and a control liposome made entirely of PC. **F**, the x axis indicates the concentration of daptomycin added to the different liposome compositions. **G**, Relation of % activity of 35 μg/ml of daptomycin based on absolute fluorescence that is normalized to the fluorescence achieved by the addition of triton X-100 (y-axis) to the % PG content of the liposome tested with PC contributing the remainder of the required lipid to reach 100% composition (x-axis). Daptomycin activity against liposomes is correlated with MIC values for WT and daptomycin resistant bacterial isolates where the % PG content is known. Statistical analysis was performed with 1-way anova and every column was means compared, $p \leq 0.05$ (*), $p \leq 0.01$ (**), $p \leq 0.001$ (***), $p \leq 0.0001$ (****).

2.7 Supplemental Figures

Isolate Name	Isolate Source	MIC μg/ml	Mutation Type in pgsA2	Paired in vitro Evolved Isolate	MIC μg/ml	Mutation Type in pgsA2	Genomics	Transcriptomics	Lipidomics
WP1a	Heart	0.125	Wild Type	RE1a	>256	W130X Stop Codon	WP1a:RE1a	WP1a:RP1b	WP1a:RP1b
RP1b	Blood	>256	G147D Binding Pocket	RE1b	>256	G147D Binding Pocket	RP1b:WP1a		
WP1c	Blood	0.125	Wild Type	RE1c	>256	G87D Conserved Site	WP1a:RE1c		WP1c:RE1c
WP2	Bone	0.064	Wild Type	RE2	>256	L39X Stop Codon	WP1a:RE2		WP2:RE2
WP3	Bone	0.125	Wild Type	RE3	>256	W49X Stop Codon	WP1a:RE3		
WP4	Bone	0.064	Wild Type	RE4	>256	Q15X Stop Codon	WP1a:RE4		
WP5	Blood	0.125	Wild Type	RE5	>256	R123C Dimer Interface	WP1a:RE5		WP5:RE5
WP6	Blood	0.125	Wild Type	RE8	>256	N107X Stop Codon	WP1a:RE8		

Hyper Daptomycin Resistant Isolate Daptomycin Susceptible Isolate in vivo Evolved Patient Isolates

Supplemental Table 2. 1: Available C. striatum isolates

Isolate naming convention: W = WT, R = Resistant, P = Isolated from a patient, E = Evolved from a patient isolate in culture under daptomycin selection, # = Different isolate source, (a,b,c) = Isolate from same patient collected at different time points. All isolates' genomes were sequenced. WP1a was used as the reference genome. All other genomes were mapped to this genome and SNPs found in the resistant and not the susceptible isolate from each pair were analyzed further. Transcriptomics was performed on WPIa and RP1b. Lipidomics was performed on the WT and resistant matched pairs of: WP1a:RP1b, WP1c:RE1c, WP2:RE2, WP5:RE5.

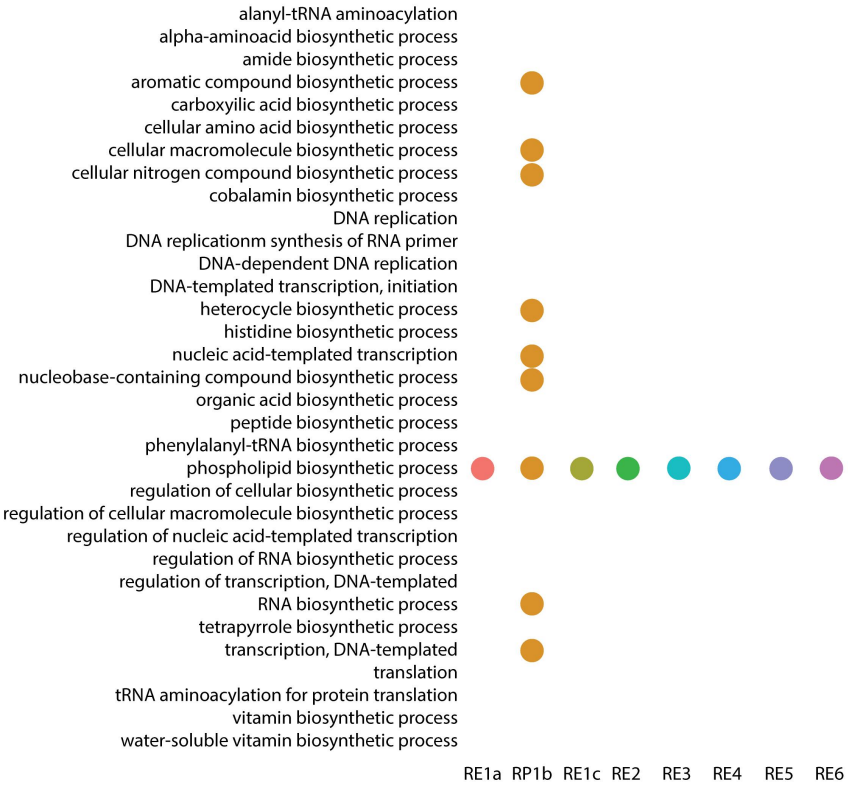

Supplemental Figure 2.1: Nonsynonymous mutations in biosynthetic pathways

SNPs were clustered by functional category (using gene ontology). We found that *pgsA2* was the only gene related to cellular biosynthetic function mutated with the exception of 8 additional mutations observed only in the *in vivo* evolved isolate. These mutations are consistent with the longer evolutionary time (17 days) experienced by the isolate between susceptible and resistant states, in contrast to the only 24 hours of *in vitro* evolution.

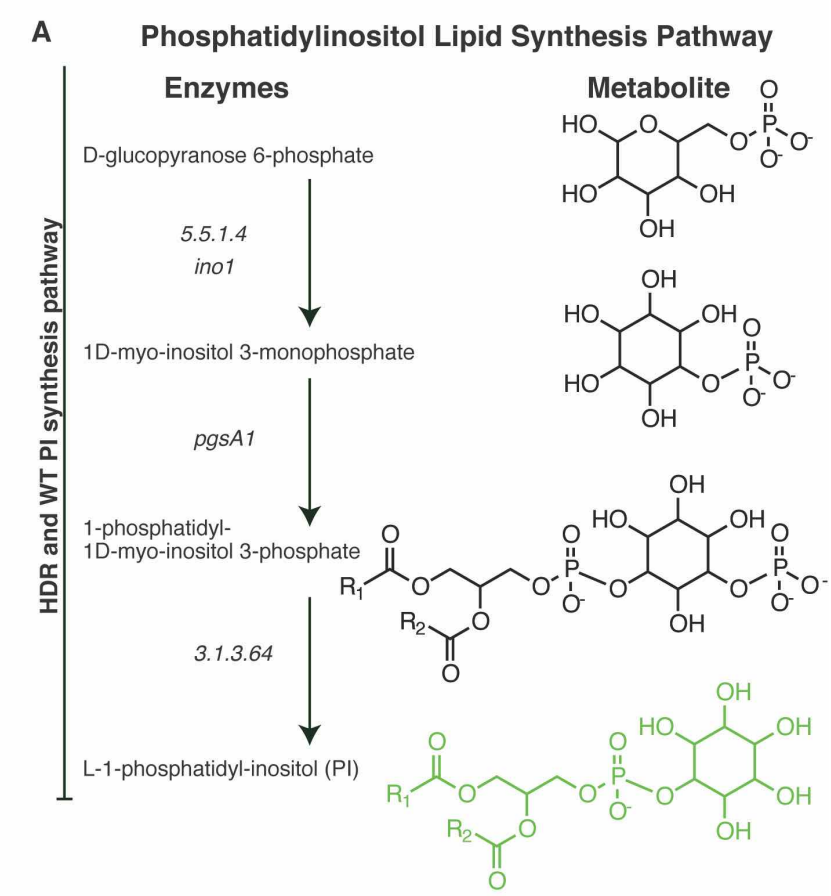

B

Gene Name	Transcript Fold Change Between WP1a and RP1b
pgsA1	1.075
rpoA	1.021

Supplemental Figure 2.2: Phosphatidylinositol lipid biosynthesis pathways

The lipid synthesis pathways were constructed with KEGG. 8 WT and HLDR isolate paired genomes were compared and nonsynonymous single nucleotide polymorphisms identified. The metabolites names and structures are on the left, with key lipids colored in green. R1 represents the 16:0 carbon chain and R2 represents the 18:1 carbon chain. The enzyme nomenclature for each enzymatic step and their corresponding genes are located next to the appropriate synthesis arrow. SNP mutations for each enzyme/gene unit are to the far right with the number of mutations out of the 8 HLDR isolate, unless no mutations were present in any of the isolates. On the left side, black

bars indicate the functional completeness of the PI synthesis pathway. WT and HLDR proceed through the entire synthesis pathway producing PI. The green color of the lipid PI indicates a 0.65-4.25-fold buildup of that metabolite in the HLDR isolates compared to WT. Fold change was calculated using (b-a)/a, where ‘b’ is the largest value and ‘a’ is the smallest to maintain a positive number.

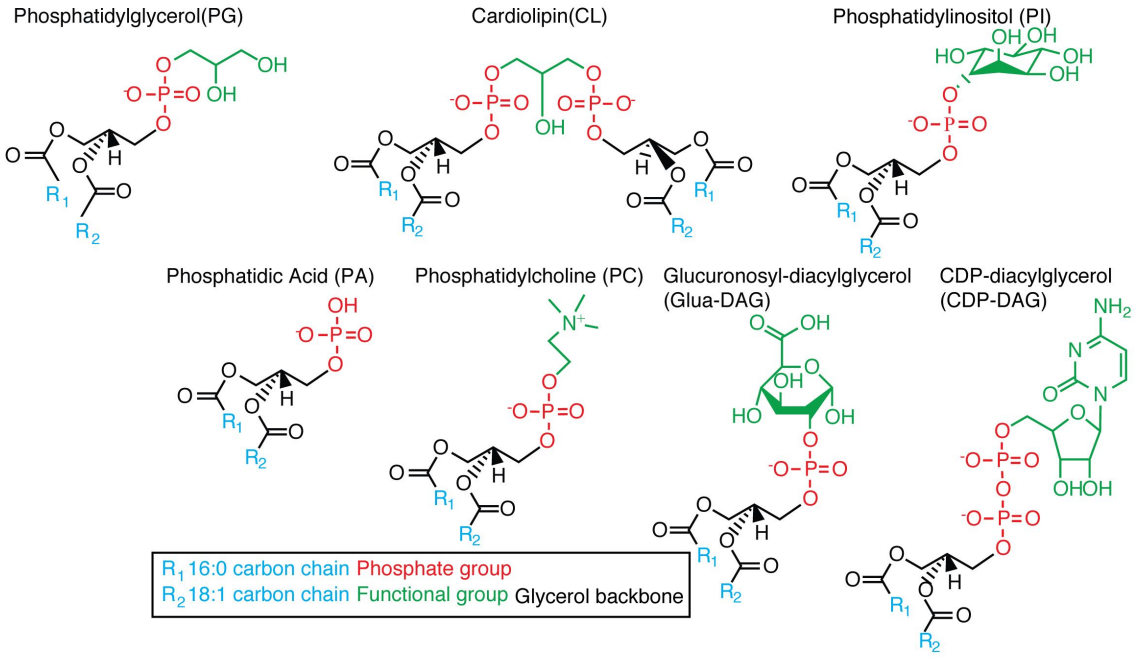

Supplemental Figure 2.3: Structures of the key phospholipids

These lipids are critical to bacterial membrane composition. R_1 = 16:0 carbon chain and R_2 = 18:1 carbon chain, black indicates the glycerol backbone, red indicates the phosphate group and green represents the functional group.

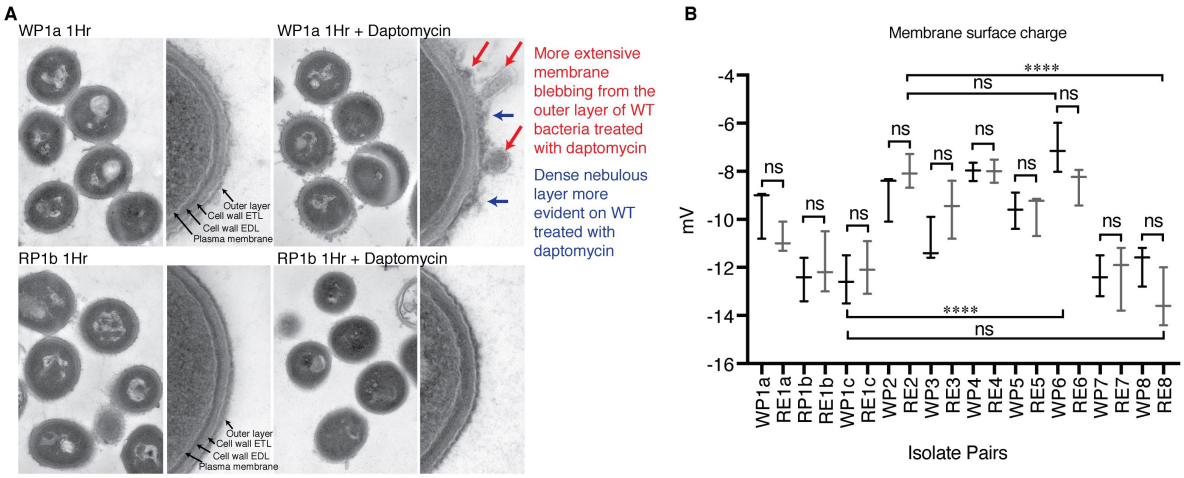

Supplemental Figure 2.4: Comparison of HLDR and WT lipid membranes and surface charge

a, WP1a and RP1b isolates were imaged with transmission electron microscopy after 1 hour with or without the addition of 10μg/ml daptomycin. WP1a without daptomycin and RP1b with and without daptomycin show no membrane irregularities, while WP1a with daptomycin shows membrane blebbing and disruption. **b**, all available WT and HLDR isolate pairs were checked for surface membrane charge changes. Charge was not indicative of HLDR and the range of surface charge between the most and least negative WT and HLDR isolates were not significant, while there was significant variability in charge for both WT and HLDR when compared within MIC group.

Statistical analysis was performed with 1-way anova and paired means analysis, $p \geq 0.05$ (ns), $p \leq 0.05$ (*), $p \leq 0.01$ (**), $p \leq 0.001$ (***), $p \leq 0.0001$ (****).

2.8 References:

Akins, R.L., B.D. Katz, C. Monahan, and D. Alexander. 2015. Characterization of high-level daptomycin resistance in Viridans group *Streptococci* developed upon in vitro exposure to daptomycin. *Antimicrob Agents Chemother*. 59:2102-2112.

Bankevich, A., S. Nurk, D. Antipov, A.A. Gurevich, M. Dvorkin, A.S. Kulikov, V.M. Lesin, S.I. Nikolenko, S. Pham, A.D. Prjibelski, A.V. Pyshkin, A.V. Sirotkin, N. Vyahhi, G. Tesler, M.A. Alekseyev, and P.A. Pevzner. 2012. SPAdes: a new genome assembly algorithm and its applications to single-cell sequencing. *J Comput Biol*. 19:455-477.

Bayer, A.S., N.N. Mishra, L. Chen, B.N. Kreiswirth, A. Rubio, and S.J. Yang. 2015. Frequency and Distribution of Single-Nucleotide Polymorphisms within mprF in Methicillin-Resistant Staphylococcus aureus Clinical Isolates and Their Role in Cross-Resistance to Daptomycin and Host Defense Antimicrobial Peptides. *Antimicrob Agents Chemother*. 59:4930-4937.

Bayer, A.S., N.N. Mishra, A.L. Cheung, A. Rubio, and S.J. Yang. 2016. Dysregulation of mprF and dltABCD expression among daptomycin-non-susceptible MRSA clinical isolates. *J Antimicrob Chemother*. 71:2100-2104.

Bayer, A.S., N.N. Mishra, G. Sakoulas, P. Nonejuie, C.C. Nast, J. Pogliano, K.T. Chen, S.N. Ellison, M.R. Yeaman, and S.J. Yang. 2014. Heterogeneity of mprF sequences in methicillin-resistant *Staphylococcus aureus* clinical isolates: role in cross-resistance between daptomycin and host defense antimicrobial peptides. *Antimicrob Agents Chemother*. 58:7462-7467.

Bayer, A.S., T. Schneider, and H.G. Sahl. 2013. Mechanisms of daptomycin resistance in *Staphylococcus aureus*: role of the cell membrane and cell wall. *Ann N Y Acad Sci*. 1277:139-158.

Baym, M., S. Kryazhimskiy, T.D. Lieberman, H. Chung, M.M. Desai, and R. Kishony. 2015. Inexpensive multiplexed library preparation for megabase-sized genomes. *PLoS One*. 10:e0128036.

Bligh, E.G., and W.J. Dyer. 1959. A rapid method of total lipid extraction and purification. *Can J Biochem Physiol*. 37:911-917.

Chatzopoulou, M., T. Koufakis, I. Voulgaridi, I. Gabranis, and M. Tsiakalou. 2016. A case of fatal sepsis due to multidrug-resistant *Corynebacterium striatum*. *Hippokratia*. 20:67-69.

Cingolani, P., V.M. Patel, M. Coon, T. Nguyen, S.J. Land, D.M. Ruden, and X. Lu. 2012a. Using Drosophila melanogaster as a Model for Genotoxic Chemical Mutational Studies with a New Program, SnpSift. *Front Genet*. 3:35.

Cingolani, P., A. Platts, L. Wang le, M. Coon, T. Nguyen, L. Wang, S.J. Land, X. Lu, and D.M. Ruden. 2012b. A program for annotating and predicting the effects of single nucleotide polymorphisms, SnpEff: SNPs in the genome of *Drosophila* melanogaster strain w1118; iso-2; iso-3. *Fly (Austin)*. 6:80-92.

Conesa, A., S. Gotz, J.M. Garcia-Gomez, J. Terol, M. Talon, and M. Robles. 2005. Blast2GO: a universal tool for annotation, visualization and analysis in functional genomics research. *Bioinformatics*. 21:3674-3676.

Cotroneo, N., R. Harris, N. Perlmutter, T. Beveridge, and J.A. Silverman. 2008. Daptomycin exerts bactericidal activity without lysis of *Staphylococcus aureus*. *Antimicrob Agents Chemother*. 52:2223-2225.

D'Costa, V.M., T.A. Mukhtar, T. Patel, K. Koteva, N. Waglechner, D.W. Hughes, G.D. Wright, and G. De Pascale. 2012. Inactivation of the lipopeptide antibiotic daptomycin by hydrolytic mechanisms. *Antimicrob Agents Chemother*. 56:757-764.

Dynamics, C.f.D. 2015. State of the World's Antibiotics, 2015. *Economics & Policy*. CDDEP: Washington, D.C.

Ernst, C.M., P. Staubitz, N.N. Mishra, S.J. Yang, G. Hornig, H. Kalbacher, A.S. Bayer, D. Kraus, and A. Peschel. 2009. The bacterial defensin resistance protein MprF consists of separable domains for lipid lysinylation and antimicrobial peptide repulsion. *PLoS Pathog*. 5:e1000660.

Forsberg, K.J., S. Patel, M.K. Gibson, C.L. Lauber, R. Knight, N. Fierer, and G. Dantas. 2014. Bacterial phylogeny structures soil resistomes across habitats. *Nature*. 509:612-616.

Garcia-de-la-Maria, C., J.M. Pericas, A. Del Rio, X. Castaneda, X. Vila-Farres, Y. Armero, P.A. Espinal, C. Cervera, D. Soy, C. Falces, S. Ninot, M. Almela, C.A. Mestres, J.M. Gatell, J. Vila, A. Moreno, F. Marco, J.M. Miro, and G. Hospital Clinic Experimental Endocarditis Study. 2013. Early in vitro and in vivo development of high-level daptomycin resistance is common in mitis group *Streptococci* after exposure to daptomycin. *Antimicrob Agents Chemother*. 57:2319-2325.

Gaupp, R., S. Lei, J.M. Reed, H. Peisker, S. Boyle-Vavra, A.S. Bayer, M. Bischoff, M. Herrmann, R.S. Daum, R. Powers, and G.A. Somerville. 2015. *Staphylococcus aureus* metabolic adaptations during the transition from a daptomycin susceptibility phenotype to a daptomycin nonsusceptibility phenotype. *Antimicrob Agents Chemother*. 59:4226-4238.

Gomila, M., F. Renom, C. Gallegos Mdel, M. Garau, D. Guerrero, J.B. Soriano, and J. Lalucat. 2012. Identification and diversity of multiresistant *Corynebacterium striatum* clinical isolates by MALDI-TOF mass spectrometry and by a multigene sequencing approach. *BMC Microbiol*. 12:52.

Hachmann, A.B., E.R. Angert, and J.D. Helmann. 2009. Genetic analysis of factors affecting susceptibility of Bacillus subtilis to daptomycin. *Antimicrob Agents Chemother*. 53:1598-1609.

Hachmann, A.B., E. Sevim, A. Gaballa, D.L. Popham, H. Antelmann, and J.D. Helmann. 2011. Reduction in membrane phosphatidylglycerol content leads to daptomycin resistance in Bacillus subtilis. *Antimicrob Agents Chemother*. 55:4326-4337.

Hahn, W.O., B.J. Werth, S.M. Butler-Wu, and R.M. Rakita. 2016. Multidrug-Resistant *Corynebacterium striatum* Associated with Increased Use of Parenteral Antimicrobial Drugs. *Emerg Infect Dis*. 22.

Hines, K.M., A. Waalkes, K. Penewit, E.A. Holmes, S.J. Salipante, B.J. Werth, and L. Xu. 2017. Characterization of the Mechanisms of Daptomycin Resistance among Gram-Positive Bacterial Pathogens by Multidimensional Lipidomics. *mSphere*. 2.

Ho, S.W., D. Jung, J.R. Calhoun, J.D. Lear, M. Okon, W.R. Scott, R.E. Hancock, and S.K. Straus. 2008. Effect of divalent cations on the structure of the antibiotic daptomycin. *Eur Biophys J*. 37:421-433.

Hobbs, J.K., K. Miller, A.J. O'Neill, and I. Chopra. 2008. Consequences of daptomycin-mediated membrane damage in *Staphylococcus aureus*. *J Antimicrob Chemother*. 62:1003-1008.

Humphries, R.M., T. Kelesidis, R. Tewhey, W.E. Rose, N. Schork, V. Nizet, and G. Sakoulas. 2012. Genotypic and phenotypic evaluation of the evolution of high-level daptomycin nonsusceptibility in vancomycin-resistant *Enterococcus faecium*. *Antimicrob Agents Chemother*. 56:6051-6053.

Jimah, J.R., P.H. Schlesinger, and N.H. Tolia. 2017. Liposome Disruption Assay to Examine Lytic Properties of Biomolecules. *Bio Protoc*. 7.

Jorgensen, J.H., S.A. Crawford, C.C. Kelly, and J.E. Patterson. 2003. In vitro activity of daptomycin against vancomycin-resistant *enterococci* of various Van types and comparison of susceptibility testing methods. *Antimicrob Agents Chemother*. 47:3760-3763.

Jorgensen, J.H., L.A. Maher, and J.S. Redding. 1987. In vitro activity of LY146032 (daptomycin) against selected aerobic bacteria. *Eur J Clin Microbiol*. 6:91-96.

Kaisersberger Vincek, M., A. Mor, S. Gorgieva, and V. Kokol. 2017. Antibacterial activity and cytotoxycity of gelatine-conjugated lysine-based peptides. *J Biomed Mater Res A*. 105:3110-3126.

Kelley, L.A., S. Mezulis, C.M. Yates, M.N. Wass, and M.J. Sternberg. 2015. The Phyre2 web portal for protein modeling, prediction and analysis. *Nat Protoc*. 10:845-858.

Kelley, L.A., and M.J. Sternberg. 2009. Protein structure prediction on the Web: a case study using the Phyre server. *Nat Protoc*. 4:363-371.

Kinouchi, H., M. Onishi, and H. Kamimori. 2013. Lipid membrane-binding properties of daptomycin using surface plasmon resonance. *Anal Sci*. 29:297-301.

Langmead, B., and S.L. Salzberg. 2012. Fast gapped-read alignment with Bowtie 2. *Nat Methods*. 9:357-359.

Li, S., Y. Yin, H. Chen, Q. Wang, X. Wang, and H. Wang. 2017. Fitness Cost of Daptomycin-Resistant *Staphylococcus aureus* Obtained from in Vitro Daptomycin Selection Pressure. *Front Microbiol*. 8:2199.

Maragakis, L.L., E.N. Perencevich, and S.E. Cosgrove. 2008. Clinical and economic burden of antimicrobial resistance. *Expert Rev Anti Infect Ther*. 6:751-763.

Mascio, C.T., J.D. Alder, and J.A. Silverman. 2007. Bactericidal action of daptomycin against stationary-phase and nondividing *Staphylococcus aureus* cells. *Antimicrob Agents Chemother*. 51:4255-4260.

Mattos-Guaraldi, A.L., L.C. Guimaraes, C.S. Santos, A.A. Veras, A.R. Carneiro, S.C. Soares, J.N. Ramos, C. Souza, V.V. Vieira, R. Hirata, Jr., V. Azevedo, L.G. Pacheco, A. Silva, and R.T. Ramos. 2015. Draft Genome Sequence of *Corynebacterium striatum* 1961 BR-RJ/09, a Multidrug-Susceptible Strain Isolated from the Urine of a Hospitalized 37-Year-Old Female Patient. *Genome Announc*. 3.

McElvania TeKippe, E., B.S. Thomas, G.A. Ewald, S.J. Lawrence, and C.A. Burnham. 2014. Rapid emergence of daptomycin resistance in clinical isolates of *Corynebacterium striatum*... a cautionary tale. *Eur J Clin Microbiol Infect Dis*. 33:2199-2205.

McMullen, A.R., N. Anderson, M.A. Wallace, A. Shupe, and C.A. Burnham. 2017a. When Good Bugs Go Bad: Epidemiology and Antimicrobial Resistance Profiles of *Corynebacterium striatum*, an Emerging Multidrug Resistant, Opportunistic Pathogen. *Antimicrob Agents Chemother*.

McMullen, A.R., N. Anderson, M.A. Wallace, A. Shupe, and C.A. Burnham. 2017b. When Good Bugs Go Bad: Epidemiology and Antimicrobial Resistance Profiles of *Corynebacterium striatum*, an Emerging Multidrug-Resistant, Opportunistic Pathogen. *Antimicrob Agents Chemother*. 61.

Mishra, B., T. Lushnikova, and G. Wang. 2015. Small lipopeptides possess anti-biofilm capability comparable to daptomycin and vancomycin. *RSC Adv*. 5:59758-59769.

Mishra, N.N., and A.S. Bayer. 2013. Correlation of cell membrane lipid profiles with daptomycin resistance in methicillin-resistant *Staphylococcus aureus*. *Antimicrob Agents Chemother*. 57:1082-1085.

Mishra, N.N., A.S. Bayer, C. Weidenmaier, T. Grau, S. Wanner, S. Stefani, V. Cafiso, T. Bertuccio, M.R. Yeaman, C.C. Nast, and S.J. Yang. 2014. Phenotypic and genotypic characterization of daptomycin-resistant methicillin-resistant *Staphylococcus aureus* strains: relative roles of mprF and dlt operons. *PLoS One*. 9:e107426.

Mishra, N.N., S.J. Yang, A. Sawa, A. Rubio, C.C. Nast, M.R. Yeaman, and A.S. Bayer. 2009. Analysis of cell membrane characteristics of in vitro-selected daptomycin-resistant strains of methicillin-resistant *Staphylococcus aureus*. *Antimicrob Agents Chemother*. 53:2312-2318.

O'Neill, J. 2014. Antimicrobial Resistance: Tackling a crisis for the health and wealth of nations. *The Review on Antimicrobial Resistance*.

O'Neill, J. 2015. Antimicrobials in Agriculture and Environment: Reducing Unnecessary use and Waste. *Review on Antimicrobial Resistance*.

Oh, J., A.L. Byrd, C. Deming, S. Conlan, N.C.S. Program, H.H. Kong, and J.A. Segre. 2014. Biogeography and individuality shape function in the human skin metagenome. *Nature*. 514:59-64.

OptumRx. 2016. Cubicin (daptomycin) - First-Time Generic. Vol. 2017. OptumRx Clinical Services Department, https://professionals.optumrx.com/content/dam/optum3/professional-optumrx/news/rxnews/new-generics/newgenerics_cubicin_2016-0915.pdf.

Peschel, A., and L.V. Collins. 2001. *Staphylococcal* resistance to antimicrobial peptides of mammalian and bacterial origin. *Peptides*. 22:1651-1659.

Quinn, B., S. Hussain, M. Malik, K. Drlica, and X. Zhao. 2007. Daptomycin inoculum effects and mutant prevention concentration with *Staphylococcus aureus*. *J Antimicrob Chemother*. 60:1380-1383.

Raad, I., H. Hanna, Y. Jiang, T. Dvorak, R. Reitzel, G. Chaiban, R. Sherertz, and R. Hachem. 2007. Comparative activities of daptomycin, linezolid, and tigecycline against catheter-related methicillin-resistant *Staphylococcus* bacteremic isolates embedded in biofilm. *Antimicrob Agents Chemother*. 51:1656-1660.

Randall, C.P., K.R. Mariner, I. Chopra, and A.J. O'Neill. 2013. The target of daptomycin is absent from *Escherichia coli* and other gram-negative pathogens. *Antimicrob Agents Chemother*. 57:637-639.

Reyes, J., D. Panesso, T.T. Tran, N.N. Mishra, M.R. Cruz, J.M. Munita, K.V. Singh, M.R. Yeaman, B.E. Murray, Y. Shamoo, D. Garsin, A.S. Bayer, and C.A. Arias. 2015. A liaR deletion restores susceptibility to daptomycin and antimicrobial peptides in multidrug-resistant *Enterococcus faecalis*. *J Infect Dis*. 211:1317-1325.

Rubio, A., J. Moore, M. Varoglu, M. Conrad, M. Chu, W. Shaw, and J.A. Silverman. 2012. LC-MS/MS characterization of phospholipid content in daptomycin-susceptible and -resistant isolates of *Staphylococcus aureus* with mutations in mprF. *Mol Membr Biol*. 29:1-8.

Saito, M., S.J. Korsmeyer, and P.H. Schlesinger. 2000. BAX-dependent transport of cytochrome c reconstituted in pure liposomes. *Nat Cell Biol*. 2:553-555.

Sauermann, R., M. Rothenburger, W. Graninger, and C. Joukhadar. 2008. Daptomycin: a review 4 years after first approval. *Pharmacology*. 81:79-91.

Seemann, T. 2014. Prokka: rapid prokaryotic genome annotation. *Bioinformatics*. 30:2068-2069.

Souza, C., Y.V. Faria, O. Sant'Anna Lde, V.G. Viana, S.H. Seabra, M.C. Souza, V.V. Vieira, R. Hirata Junior, O. Moreira Lde, and A.L. Mattos-Guaraldi. 2015. Biofilm production by multiresistant *Corynebacterium striatum* associated with nosocomial outbreak. *Mem Inst Oswaldo Cruz*. 110:242-248.

Srinivasan, A. 2017. Antibiotic stewardship: Why we must, how we can. *Cleve Clin J Med*. 84:673-679.

Srinivasan, A., and L.E. Davidson. 2017. Improving Patient Safety Through Antibiotic Stewardship: The Veterans Health Administration Leads the Way, Again. *Infect Control Hosp Epidemiol*. 38:521-523.

Staubitz, P., H. Neumann, T. Schneider, I. Wiedemann, and A. Peschel. 2004. MprF-mediated biosynthesis of lysylphosphatidylglycerol, an important determinant in *staphylococcal* defensin resistance. *FEMS Microbiol Lett*. 231:67-71.

Szoka, F., Jr., and D. Papahadjopoulos. 1978. Procedure for preparation of liposomes with large internal aqueous space and high capture by reverse-phase evaporation. *Proc Natl Acad Sci U S A*. 75:4194-4198.

Tran, T.T., S. Jaijakul, C.T. Lewis, L. Diaz, D. Panesso, H.B. Kaplan, B.E. Murray, A. Wanger, and C.A. Arias. 2012. Native valve endocarditis caused by *Corynebacterium striatum* with heterogeneous high-level daptomycin resistance: collateral damage from daptomycin therapy? *Antimicrob Agents Chemother*. 56:3461-3464.

Trapnell, C., D.G. Hendrickson, M. Sauvageau, L. Goff, J.L. Rinn, and L. Pachter. 2013. Differential analysis of gene regulation at transcript resolution with RNA-seq. *Nat Biotechnol*. 31:46-53.

Trapnell, C., B.A. Williams, G. Pertea, A. Mortazavi, G. Kwan, M.J. van Baren, S.L. Salzberg, B.J. Wold, and L. Pachter. 2010. Transcript assembly and quantification by RNA-Seq reveals unannotated transcripts and isoform switching during cell differentiation. *Nat Biotechnol*. 28:511-515.

Vanessa M. D'Costa, K.M.M., Donald W. Hughes, Gerard D. Wright. 2006. Sampling the Antibiotic Resistome. *Science*. 311:374-377.

Walker, B.J., T. Abeel, T. Shea, M. Priest, A. Abouelliel, S. Sakthikumar, C.A. Cuomo, Q. Zeng, J. Wortman, S.K. Young, and A.M. Earl. 2014. Pilon: an integrated tool for comprehensive microbial variant detection and genome assembly improvement. *PLoS One*. 9:e112963.

Wang, J., Y. Wang, X. Du, J. Cui, K. Wang, L. Zhang, and Y. Han. 2016. Rapid transmission of multidrug-resistant *Corynebacterium striatum* among susceptible patients in a tertiary hospital in China. *J Infect Dev Ctries*. 10:1299-1305.

Wang, W., Z. Wei, T.W. Lam, and J. Wang. 2011. Next generation sequencing has lower sequence coverage and poorer SNP-detection capability in the regulatory regions. *Sci Rep*. 1:55.

Werth, B.J., W.O. Hahn, S.M. Butler-Wu, and R.M. Rakita. 2016. Emergence of High-Level Daptomycin Resistance in *Corynebacterium striatum* in Two Patients with Left Ventricular Assist Device Infections. *Microb Drug Resist*. 22:233-237.

Wong, K.Y., Y.C. Chan, and C.Y. Wong. 2010. *Corynebacterium striatum* as an emerging pathogen. *J Hosp Infect*. 76:371-372.

Yoneda, A., W.R. Henson, N.K. Goldner, K.J. Park, K.J. Forsberg, S.J. Kim, M.W. Pesesky, M. Foston, G. Dantas, and T.S. Moon. 2016. Comparative transcriptomics elucidates adaptive phenol tolerance and utilization in lipid-accumulating *Rhodococcus opacus* PD630. *Nucleic Acids Res*. 44:2240-2254.

Zhang, T., J.K. Muraih, N. Tishbi, J. Herskowitz, R.L. Victor, J. Silverman, S. Uwumarenogie, S.D. Taylor, M. Palmer, and E. Mintzer. 2014. Cardiolipin prevents membrane translocation and permeabilization by daptomycin. *J Biol Chem*. 289:11584-11591.

Chapter 3: Daptomycin forms pores in phosphatidylglycerol-containing membranes *in vitro* and in *Corynebacterium striatum*.

Nicholas K. Goldner[1], John Robinson[2,3], Maximilian Lyon[4], Carey-Ann Burnham[5,6,7], Jeffrey P. Henderson[2,3], Gautam Dantas[1,5,7,9,*], Paul Schlesinger[8,*]

[1]The Edison Family Center for Genome Sciences & Systems Biology, Washington University in St. Louis School of Medicine, Saint Louis, Missouri 63110, USA

[2]Division of Infectious Diseases, Department of Medicine, Washington University School of Medicine, St. Louis, Missouri 63110, United States

[3]Center for Women's Infectious Diseases Research, Washington University School of Medicine, St. Louis, Missouri 63110, United States

[4]Department of Anatomy and Neurobiology, Washington University School of Medicine, St. Louis, Missouri 63110

[5]Department of Pathology and Immunology, Washington University in St. Louis School of Medicine, Saint Louis, Missouri 63110, USA.

[6]Department of Pediatrics, Washington University in St. Louis School of Medicine, Saint Louis, Missouri 63110, USA.

[7]Department of Molecular Microbiology, Washington University in St. Louis School of Medicine, Saint Louis, Missouri 63110, USA.

[8]Department of Cell Biology and Physiology, Washington University in St. Louis School of Medicine, Saint Louis, Missouri 63110, USA.

[9]Department of Biomedical Engineering, Washington University in St. Louis, Saint Louis, Missouri 63130, USA.

3.1 Abstract

Daptomycin, a last line-of-defense antibiotic for treating Gram-positive infections, is experiencing clinical failure against important infectious agents. While daptomycin has been studied for over 30 years, conflicting proposed mechanisms of action have left two important questions unanswered; (1) how daptomycin interacts with the membrane of bacterial cells, and (2) how daptomycin causes cell death in bacteria. The data reported here demonstrates a shift in how we understand the complexity of the interactions between daptomycin and the bacterial cell and aims to answer these two critical questions. We show that when daptomycin binds to the cell membrane, it is stably integrated into the membrane in a calcium- and phosphatidylglycerol (PG)-dependent manner, in a defined ~1:1 ratio of PG to daptomycin. It then recruits or co-localizes with other daptomycin molecules to form stable pores with an approximate Stokes radius of 8 nm, resulting in an expulsion of metabolites, ions and other intracellular components from the cell. When a high enough concentration of PG is present in bacterial membranes, enough daptomycin pores can be formed to release biologically necessary metabolites, ultimately resulting in cell death.

3.2 Introduction

Daptomycin, an antibiotic discovered over thirty years ago, forms a last line-of-defense against deadly pathogens (Lakey and Lea, 1986). As a cyclic-lipopeptide, daptomycin belongs to a unique class of antibiotics and is backed by extensive research and testing efforts that led to approval for use in humans (Baltz, 2009; Taylor and Palmer, 2016). It has been used judiciously and serves an important role in treating antibiotic-resistant, Gram-positive bacterial infections. Although its mechanism of action has remained unclear, daptomycin targets the bacterial membrane, resulting in leakage of large molecules (determined using intracellular dyes) but not complete cell lysis (Cotroneo et al., 2008; Hobbs et al., 2008). Several mechanisms of action have been proposed, including pore formation (Zhang et al., 2014a), increased membrane permeability (Straus and Hancock, 2006), membrane deformation (Chen et al., 2014), division inhibition (Muller et al., 2016) and peptidoglycan targeting (Allen et al., 1987). The first occurrences of clinical resistance to daptomycin in *Staphylococcus aureus* were incremental (Yang et al., 2013; Yang et al., 2010), and easily managed in patients through small daptomycin dose increases (Weis et al., 2008). The lack of resistance to high doses was ascribed to the target of daptomycin being the cell membrane (Alborn et al., 1991; Allen et al., 1991), with several *in vitro* studies identifying phosphatidylglycerol as its specific lipid target (Muraih et al., 2012). It was incorrectly assumed that bacteria would have difficulty making large scale shifts in membrane lipid composition (Hachmann et al., 2011; Hines et al., 2017), and thus would be unable to develop resistance. *Corynebacterium striatum* a Gram-positive opportunistic pathogen, has a unique ability to transition from being daptomycin susceptible (MIC = 0.064 μg/ml) to high level daptomycin resistant (MIC > 256 μg/ml) in 24 hours under daptomycin selective conditions. Its membrane is

well defined and is a biologically relevant pathogen, which allows us to employ it as an effective model for understanding daptomycin *in vivo*.

In artificial membrane systems, daptomycin preferentially binds phosphatidylglycerol (PG) (Khatib et al., 2016; Kreutzberger et al., 2017; Taylor et al., 2017b; Taylor et al., 2016). The most likely proposed mechanism of action is that daptomycin forms 1:1 daptomycin:Ca^{2+} micelles (Jung et al., 2008; Jung et al., 2004; Scott et al., 2007), which dissociate in the presence of PG-containing membranes and then bind to the membrane via the hydrophobic 10-C acyl tail of daptomycin. Once bound, daptomycin integrates into the hydrophobic core of the bilayer (Jung et al., 2004; Lakey and Ptak, 1988[Jung, 2008 #8822) at a proposed ~1:1 ratio of PG to daptomycin (Lee et al., 2017). However, determining the PG:daptomycin interaction stoichiometry has proven difficult, with various methods and lipid preparations yielding predicted stoichiometries ranging from 1:1 in bicelles to 2:1 in liposomes (Zhang et al., 2013) (Muraih and Palmer, 2012). Beyond this point, it is unclear how daptomycin kills bacterial cells; however, there is substantial evidence in favor of membrane disruption, eventually resulting in cell death (Laganas et al., 2003; Mascio et al., 2007; Pogliano et al., 2012; Silverman et al., 2003; Taylor et al., 2017a; Zhang et al., 2014a,[Taylor, 2017 #9958). Previous elegant experiments have begun to dissect the binding and conformational changes observed in membrane-associated daptomycin (Jung et al., 2008; Jung et al., 2004; Lee et al., 2017).

As recently as 2014, it was shown that daptomycin permeability was size- and cation-selective (Alborn et al., 1991; Allen et al., 1991; Zhang et al., 2014a). However, two shortcomings of these findings require resolution. First, at physiological concentrations of daptomycin (between the

minimum inhibitory concentration (MIC) of 0.064 μg/mL and the peak reported serum concentrations of 100 μg/mL) of daptomycin (Antachopoulos et al., 2012; McElvania TeKippe et al., 2014), the mechanisms of membrane dysregulation were inconclusive. This could be potentially due to the different acyl tail type used in the model lipids for *in vitro* assays. Second, efforts to confirm ion leakage and pore formation *in vivo* using the *Bacillus subtilis* model (Muller et al., 2016) yielded results contrary to the proposed mechanisms identified *in vitro*. Studying the mechanism of antibacterial action of daptomycin and other antimicrobial peptides will thus require a holistic approach, calling on genomics, transcriptomics, metabolomics and lipidomics, as well as classical biochemical and biophysical techniques.

In this work, we address both outstanding issues regarding daptomycin's mechanism; first, characterizing *in vitro* lipid:daptomycin interactions under physiologically relevant conditions, and then determining whether daptomycin is able to produce a pore of finite size and stable structure in both liposomes and bacterial cells themselves. We use planar lipid bilayers to differentiate the mechanism of action of daptomycin from that of valinomycin, an ionophore with a proposed mechanism similar to daptomycin. We employ a number of techniques that we first introduced in our studies of the Bax protein (Saito et al., 2000b) and the malaria protein CELTOS (Jimah et al., 2016) to identify and characterize the existence of a daptomycin-dependent pore. Surface plasmon resonance is used to directly quantitate daptomycin binding and subsequent integration into surface-supported liposomes, which allows us to directly measure the stoichiometry of the daptomycin-bilayer-PG interaction. We then extended these studies to measure the kinetics of daptomycin binding and release. Using large unilamellar vesicles (LUVs) of defined lipid composition, we first demonstrate that carboxyfluorescein is released by daptomycin and measure the properties of the pore via "resistive blocking" with dextran. Finally,

we use mass spectrometry to detect cellular components released from wild type *Corynebacterium striatum* by daptomycin treatment.

3.3 Results

3.3.1 Daptomycin disrupts membranes through a different mechanism than valinomycin.

We first tested whether the mechanism of action of daptomycin can be explained solely by its interactions with the lipid bilayer. In order to determine how native daptomycin and lipid bilayers interact under physiological conditions, we turned to the planar lipid bilayer technique. We constructed planar lipid bilayers using a ratio of 1,2-dioleoyl-sn-glycero-3-phosphocholine (DOPC) to PG of 80:20, comparable to the ratio observed in susceptible bacteria (Hayami et al., 1979). The salt concentrations on either side of the formed membrane were varied considerably, but we found that by having 145 mM NaCl and 5 mM KCl on each side of the membrane, we could directly compare valinomycin and daptomycin in the same salt solution. Triplicate trials were conducted using either daptomycin (0 to 64 μg/mL) or valinomycin (0 to 0.11 μg/mL). At sub-micromolar concentrations and at their respective minimal inhibitory concentrations (MICs) (3.4 μg/mL and 0.625 μg/mL for daptomycin and valinomycin respectively), both antibiotics reduced resistance by increasing membrane permeability and disrupting the required ion gradients of Na+ and K+ (Figure 3.1A). Removing the PG from membranes reduced daptomycin-induced permeability but had no effect on valinomycin. Plotting normalized membrane resistance (conductance^{-1}) against antibiotic concentration also showed clearly different dose response curves (Figure 3.1B). Finally, we routinely observe large, voltage-dependent current spikes at slightly higher daptomycin concentrations (12.8 μg/mL) (Figure 3.1C). These current spikes are consistent with a pore or channel, and the magnitude of these spikes suggests that the observed pore or channel is larger than an ion channel.

3.3.2 Daptomycin binds and stably integrates into PG-containing membranes.

We employed surface plasmon resonance (SPR) to further define the daptomycin-PG interaction. Daptomycin preferentially bound to PG-containing membranes (Figure 3.2A and E) and remained stably integrated into the membrane for over 4 hours (Figure 3.2 – Supplement 1A). PG:phosphatidylcholine (PC) liposomes retained 87.78% of total daptomycin at 10 minutes, and 82.59% at 25 minutes, indicating that the daptomycin integrated into the membrane. Daptomycin bound cardiolipin (CL) membranes transiently but only minimally integrated into the membranes, with only 35.43% and 24.68% retention at 10 and 25 minutes respectively (Figure 3.2A and D). Daptomycin bound to phosphatidic acid (PA)-containing membranes transiently and to approximately the same magnitude as CL but was retained even more poorly, with only 11.55% remaining after 10 minutes. The PC-only control liposomes showed the least initial binding and retention of all three lipids, with only 7.75% retention after 10 minutes, even in the presence of a negatively charged phosphate group (similar to PG). The stability of daptomycin in PG-containing membranes likely contributes to the non-lytic nature of daptomycin and makes the determination of the time of bacterial cell death problematic, since all measurements of cell death are taken 24 hours later, after viability testing by growth plate (Murillo et al., 2009; Rybak et al., 2000). We employed SPR to determine the ratio of PG:daptomycin to better understand the relationship between daptomycin activity, as quantified by MIC, and the PG composition of bacterial membranes.

3.3.3 Daptomycin binds to PG at a 1:1 ratio.

Using SPR, we determined the relationship between daptomycin and PG in order to understand the concentration-dependent nature of daptomycin activity (Batrakov and Bergelson, 1978; Hachmann et al., 2009; Hachmann et al., 2011). Artificial LUVs (200 nM of defined composition

liposomes) which contain equimolar PG:PC and PA:PC lipid compositions were treated with 20 or 35 μg/mL daptomycin. Using the signal change between the baseline and the liposome binding steady state, we were able to determine the signal specific to our lipids of interest (LOI: PG and PA) by multiplying by the mass fraction of 1:1 LOI:PC (Figure 3.3C). The LOI binding measurement was then plotted against daptomycin binding units and analyzed by linear regression, with the slope of the line corresponding to the daptomycin:LOI ratio. PG was found to bind daptomycin at a ~1:1 ratio (Figure 3.3A and D) while the PA to daptomycin binding ratio was ~4.4:1, suggesting a significant decrease in the amount of daptomycin that can bind and integrate into PA-containing liposomes (Figure 3.2C). These data were corroborated by Lee et al., 2017, using small angle X-ray scattering to determine the daptomycin:PG stoichiometry (Lee et al., 2017), indicating that SPR may be a valid method of determining antimicrobial peptide:lipid ratios in the future.

3.3.4 Daptomycin binds and integrates rapidly into phosphatidylglycerol containing membranes.

Daptomycin was injected at a fixed 35 μg/ml concentration over 1:20 PG:PC-containing liposomes for 15, 30 and 60 seconds. Daptomycin bound and integrated into the membrane in less than 15 seconds, with mean retention of 78.14% after 10 minutes (Figure 3.4D and Figure 3.4 – Supplement 1). At 30 seconds, daptomycin binding had a slightly higher binding peak (Figure 3.4A and C) than at 15 seconds, but after shedding unintegrated daptomycin, the mean retention of daptomycin was 75.85% at 10 minutes (Figure 3.4C, Figure 3.4 – Supplement 1), and was not statistically different from the 15 second injection, indicating the presence of a saturation point. The 60 second injection of daptomycin overwhelmed the liposomes; daptomycin bound the 1:20 PG:PC liposomes transiently, saturating the PG in the membrane. Unpaired daptomycin was then

washed off the membrane, (Figure 3.4A, B and E) and liposomes showed 54.17% daptomycin retention at 10 min.

3.3.5 Daptomycin forms pores large enough to be inhibited by 148.2 kDa dextran which has a Stokes radius of ~8 nm.

Daptomycin forms pores at both 10 and 35 μg/mL (Figure 3.5A and B) in the presence of 20 μM dextran, ranging in size from 5-2000 kDa (66.9 kDa ~5.8 nm Stokes radius, 148.2 kDa ~8 nm Stokes radius, 500 kDa ~14.7 nm Stokes radius, and 2000 kDa ~27 nm Stokes radius) (Armstrong et al., 2004; Jimah et al., 2016; Saito et al., 2000b; Y Tang, 2016). At both 10 and 35 μg/mL, daptomycin pores were only blocked by 148.2 kDa dextran (Figure 3.5A and C) which resulted in 56.3% and 41.4% reductions in carboxyfluorescein release, respectively (Figure 3.5D). The remaining dextran sizes were either too small or too large to block the pore, although there was a trend towards pore blockage as we increase the dextran size from 3 kDa to 148.2 kDa. The trenched nature of the fluorescence decrease is indicative of pore blockage, and the decrease independent of daptomycin concentration indicates that the pores are uniform in size (Stokes radius of ~8 nm) and may require a minimum amount of PG coupled to daptomycin to form.

3.3.6 Daptomycin-treated C. striatum releases metabolites after treatment in a manner consistent with pore formation.

C. striatum cultures were treated with daptomycin or vehicle control, and supernatants were collected at varying times thereafter. Analyzing these supernatants by mass spectrometry yielded relative intensities of 2960 molecular features present in at least one sample. Selecting only those features that were present in more than two samples containing *C. striatum*, and absent from media

alone, resulted in a final list of 111 features (Figure 3.6 – Supplement 1A). The distribution of feature intensities was strongly left-skewed, so intensities were $\log_{10}$-transformed to make them more normally distributed (Figure 3.6 – Supplement 1B and C).

Independent Principal Component Analysis (IPCA) was utilized to identify features that differed in the supernatants from cells exposed to daptomycin compared to untreated cells. Using two principal components separated the treated and untreated culture supernatants at all five time points (Figure 3.6A). Of the 111 features used in the IPCA, 17 were assigned negative weights on principal component #1, suggesting that they were found in higher concentrations in supernatants from daptomycin-treated cells. Plotting these intensities over time showed this to be the case for many of the above features (Figure 3.6C). The masses of these features ranged from 188 to over 600 Da, but the distribution of feature masses was not significantly different from the distribution of all feature masses detected in the experiment (Figure 3.6 – Supplement 1E) indicating that the method uniformly identified peaks in both the treated and untreated bacteria. The increase of feature appearance by principal component analysis in the daptomycin-treated cells suggests to us that a pore in the bacterial membrane could be the cause for feature release. However, these data prevent an estimation of an upper limit on the daptomycin pore size.

3.4 Discussion

The mechanistic details of the bactericidal action of daptomycin have remained vague due to conflicting reports, using multiple model systems that each have their own drawbacks. (Boudjemaa et al., 2016; Kreutzberger et al., 2017; Muller et al., 2016; Muraih and Palmer, 2012; Muraih et al., 2011; Pogliano et al., 2012; Tran et al., 2013; Zhang et al., 2013). The activity of daptomycin

is directly related to its ability to make conformation shifts in its peptide core to interact with the cell membrane (Taylor et al., 2016; Zhang et al., 2014b). The simple substitution of Ca^{2+} to Mg^{2+} (or another divalent cation) (Ho et al., 2008), or removal of Ca^{2+} from solution is enough to increase the MIC of daptomycin from 1 μg/mL to > 32 μg/mL MIC (a > 32-fold increase) and the MIC of valinomycin from 0.625 μg/mL to > 64 ug/mL MIC (a > 102-fold increase) (Jung et al., 2004), showing that a single atom has the potential to drastically affect the activity of daptomycin *in vivo*. The addition of Bodipy, Alexa, or NBD to daptomycin results in small molecule conjugation to daptomycin at points of interaction with bacterial cell membranes, which reduces its efficacy and potentially changes its target, which is reflected in its MIC (Taylor and Palmer, 2016); this increased MIC could be as a result of altering the ability of daptomycin to bind and integrate into membranes and later associate to form pores. Additionally, it is postulated that a lack in uniformity of the acyl chains of the LOIs—dimyristoyl lipids, palmitoleyl lipids, dioleyl lipids—contributes to these conflicting results (Taylor et al., 2017b). It is certainly possible that the acyl chain of daptomycin plays a role in efficacy as well; to address this, we used palmitoleyl lipids, 16:0-18:1, that represent the dominant acyl chain in wild type bacteria as well as daptomycin-susceptible *Corynebacterium striatum*, which is more biologically relevant. Based on studies to date, there are multiple and often conflicting proposed mechanism of how daptomycin interacts with the membrane and the cell. In this paper, we used clinically available daptomycin, and the SPR and carboxyfluorescein liposome stability assay (CFLSA) assays were performed on bacterially-relevant size domain (200 nm) liposomes and wild type and daptomycin susceptible *Corynebacterium striatum* (MIC = 0.064 μg/ml), to ensure biological relevance (McElvania TeKippe et al., 2014). Some of these findings have been alluded to in previous publications; however, a direct observation and measurement of these interactions with unaltered daptomycin

or PG has not yet been published. Furthermore, our data indicates that daptomycin kills susceptible bacteria by stably binding to membrane phosphatidylglycerol in a 1:1 ratio, integrating into the membrane to form large, stable, non-lytic pores, and releasing cytosolic metabolites and ions into the extracellular space.

By starting our examination of daptomycin and valinomycin on planar lipid bilayers, we were able to directly observe membrane effects, in contrast to other methods that rely on indirect measures that may be subject to cellular interference. Previous work with ion-specific electrodes suggests that daptomycin at effective concentrations results in K^+ loss, with depolarization occurring synchronously with cell death (Alborn et al., 1991; Allen et al., 1991). In membranes composed of phosphatidylcholine (PC) or PC-cholesterol mixtures, daptomycin increased permeability (Lakey and Lea, 1986), but the observed increase was judged insufficient to be toxic. Therefore, we decided to revisit the planar lipid bilayer experiments to determine if daptomycin has a sufficient effect on ion permeability to kill bacterial cells when presented with the right combination of lipids. The result is that while valinomycin is ion-specific, daptomycin appears to be ion-agnostic. At the center of the dose response curve, the fitted line has a slope that is proportional to the number of molecules that are required for transport across the membrane. Because the resistance is normalized, we cannot calculate the actual quantity of molecules required, but the slope for daptomycin is much larger than the slope for valinomycin, which corroborates daptomycin's non-selective nature and hints at a larger pore structure than has previously been suggested.

Daptomycin binding was originally cited as being potentially attracted to PG, based on the positively charged Ca^{2+} ion interacting with the acidic and negatively charged phosphate (Epand et al., 2008; Jung et al., 2008). We tested the binding across 4 different liposomes (PG:PC, PA:PC,

CL:PC and PC alone), focusing on the ability of daptomycin to integrate into the membrane after transient binding. The choline group in PC shields the phosphate from daptomycin and indicated that phosphate binding is secondary to the structure of the R-group atop the phosphate for initial binding and recruitment (Figure 3.2E). However, when the phosphate is unshielded (as in the PA liposomes) (Figure 3.2C) or has an amenable R-group (PG or CL liposomes) (Figure 3.2B and D), the phosphate plays an integral role in initial binding and recruitment of daptomycin to the membrane, but plays almost no role in the transition of daptomycin from its bound to integrated state (Figure 3.2A). The glycerol R-group of PG and CL has the structural characteristics that are optimal for daptomycin binding (Figure 3.2 – Supplement 1B). CL is unique here, in that it has the same R-groups as PG, but the glycerol is bound to another triacyl glycerol, such that the structure has a sequential triacyl glycerol – phosphate – glycerol – phosphate – triacyl glycerol (Figure 3.2 – Supplement 1B). This fundamentally limits the movement of the glycerol R-group, such that when daptomycin binds, it cannot interact with PG in a way that allows for robust and rapid integration into the membrane. This leads to initial transient binding but limited long-term integration. It has been reported that CL inhibits the progression of daptomycin from the outer leaflet to inner leaflet of the membrane (Zhang et al., 2014b); in conjunction with our SPR data, this indicates that CL reduces the amount of daptomycin that can physically pack into the membrane to form a pore, which also increases the dissociation of daptomycin from the membrane. PG is unencumbered, which allows the glycerol R-group to conform appropriately to daptomycin and integrate into the membrane, indicating that both the phosphate and the glycerol groups are crucial for the binding and recruitment of daptomycin to the membrane, and the subsequent integration of daptomycin for pore formation (Figure 3.2A and B, and Figure 3.2 – Supplement 1A and B).

Reduced PG content in the membranes of bacterial isolates has been associated with daptomycin resistance (increased MIC) (Hines et al., 2017) (Hachmann et al., 2011). Wild type *C. striatum* and *Staphylococcus aureus* have low daptomycin MICs, 0.032 – 0.125 μg/mL (McMullen et al., 2017a) and 0.064-0.38 μg/mL (Kaur et al., 2012) respectively, which can be in a large part due to the abundance of PG (~40%) (Hayami, 1979; Hines et al., 2017) in the membrane of each species. We used SPR to understand the relationship between PG and daptomycin and were able to elucidate that the stoichiometric ratio between the two is indeed ~1:1 (Figure 3.3A and D). Daptomycin activity is therefore constrained by the amount of PG present in the membrane. The result is that as membrane PG content decreases, daptomycin has a harder time locating PG and integrating into the membrane. To overcome the odds of locating a PG binding partner, more daptomycin is needed to ensure enough binding and membrane integration to form a pore (Hachmann et al., 2011). This hints at the possibility that there is a threshold amount of daptomycin that needs to be in the membrane to result in bacterial cell death; concentrations lower than this will allow bacteria to survive, suggesting that there is a minimum number of pores required for cell death.

Daptomycin binding and subsequent integration or dissociation happens on the order of seconds (Figure 3.4D), so when daptomycin-susceptible *C. striatum* or *S. aureus* are exposed to daptomycin, the high PG content of both membranes allows daptomycin to locate, bind and integrate into the membrane extremely quickly. When PG is reduced from 4:10 lipids to 1:20 lipids, we still see daptomycin binding very quickly when an overabundance of daptomycin is present (Figure 3.4). However, if we overload the system and oversaturate the PG content of the liposomes with daptomycin, almost all excess daptomycin dissociates (Figure 3.4B). When binding occurs but integration does not, as in the case with PA:PC liposomes, on average 81.5% ± 7.7% of all daptomycin releases from the membrane after 60 seconds (Figure 3.2C). The

combination of the 1:1 interaction, rapid binding and integration or dissociation helps explain why a reduction in PG results in an increased MIC.

The planar lipid bilayer studies indicate that daptomycin forms a large pore that increases all ion permeability, not just potassium ion permeability. Potassium permeability was previously considered a mechanism of killing (Hobbs et al., 2008; Silverman et al., 2003; Zhang et al., 2014a) and while it still may contribute to cell death, it seems to be one of many factors. Using a carboxyfluorescein liposome stability assay coupled with dextran blocking, we were able to determine what daptomycin does after membrane integration (Jimah et al., 2016). If daptomycin formed an ion channel, very small pore, or no pore at all, then none of the dextran tested would block the pore. Our CFLSA studies indicate that daptomycin is forming a pore that is blocked by a 148.2 kDa dextran, with the same Stokes radius as the pore of ~8 nm across multiple daptomycin concentrations. This indicates that the pore size is stable and consistent across daptomycin doses (Figure 3.5). We further interrogated the pore by assessing mass of metabolites leaking through using *C. striatum* as an *in vivo* system.

If daptomycin creates pores in model membranes, then it should behave similarly in bacterial membranes, causing intracellular metabolites to leak into the culture supernatant. Supernatants from *C. striatum* cultures treated with daptomycin were compared with supernatants from untreated cultures using liquid chromatography/time-of-flight (LC-TOF) mass spectrometry. As expected, this method detected daptomycin in all samples to which it was added (Figure 3.6 – Supplement 1D). To avoid ambiguity regarding the origin of the features, we selected only those features that were present in more than two samples and absent from media alone. IPCA analysis of the remaining features clearly separated treated from untreated supernatants (Figure 3.6A). Notably, the daptomycin-treated supernatant collected after 3 minutes was more similar to the

untreated time points than the other daptomycin-treated supernatants, suggesting that the bactericidal effects of daptomycin manifest between 3 and 5 minutes post-treatment (Figure 3.6B). This was supported by the intensities of individual features identified by IPCA as associated with daptomycin treatment. The 4 most heavily-weighted features were all undetectable after 3 minutes in daptomycin, but increased substantially after 5 minutes, trends highly suggestive of metabolites leaking from daptomycin-treated cells (Figure 3.6C). In addition, several other features either began at high levels or peaked and then declined by 30 minutes post-daptomycin treatment. These trajectories are consistent with metabolites rapidly leaking out of cells and subsequently degrading. The masses of these features ranged from 188 to over 600 Da, suggesting that daptomycin-generated pores are at least that large, but there is insufficient data to place an upper limit on the pore size (Figure 3.6 – Supplement 1E). Leakage of metabolites so shortly after the addition of daptomycin is consistent with rapid pore formation and recapitulates the *in vitro* data. Further work will be needed to characterize the structure and formation of the pore *in vivo*, and to establish an upper limit on the size of expelled metabolites.

This data represents a shift in our understanding of how daptomycin interacts with the bacterial cell membrane, and how bacterial cell death results from daptomycin treatment. Once daptomycin binds to the membrane and integrates in a calcium- and PG-dependent manner, it is stably integrated. It then recruits or co-localizes with other daptomycin molecules to form stable pores with an approximate Stokes radius of 8 nm. The resulting pore allows metabolites, ions and other intracellular components to be released from the cell. When sufficient PG is present in the bacterial membranes, enough daptomycin pores can be formed to ultimately result in cell death.

3.5 Materials and Methods

3.5.1 Planar lipid bilayer data collection and analysis

Planar lipid bilayers were prepared by applying 40 μg of DOPC:PG or other lipids in n-decane to the 0.25 mm orifice of a polystyrene cuvette (Warner Instrument LLC, Hamden, CT). This orifice communicates between the cis and trans solutions of the bilayer chamber. These chambers were electrically connected by Ag/AgCl electrodes and 3 M KCl–3% agar bridges and currents monitored by a BCA-525-c bilayer clamp and headstage (Warner Instrument Corp.). The data were digitized using Axon software and a Digidata 1200 board (Axon Instruments, Foster City CA). Records were archived on video tape using a Neurocorder DR-484 (Neuro Data Instrument Corp., Water Town Gap, Hz). Data were filtered at 1000 Hz, and digitization was at 1.67x103 points/s. Analysis of the data was done using Axon, Excel and Origin software, OriginLab Corporation, MA. Prior to studies, membranes were allowed to thin to a capacitance of 400 nano-farads and had a leak current of ≤2 pA at 100 mV of applied potential. The daptomycin and valinomycin were added to the 1.0 mL cis chamber with stirring, and currents and voltages referenced to the trans chamber.

3.5.2 Surface plasmon resonance data collection and analysis

We performed surface plasmon resonance ***(Kinouchi et al., 2013)*** in triplicate on a Reichert SR7000 DC with an auto sampler, using a Carboxymethyl Dextran Hydrogel Surface Sensor Chip (#13206066). SPR Autolink Software version 1.1.8-0 was used to read and export data to Microsoft Excel. SPR was used to assess the stability of daptomycin binding, how daptomycin integrated into the membrane, rate of daptomycin integration into the membrane and ratio of daptomycin to lipid of interest (LOI) on varying compositions of liposomes. Four lipid types were

used: PC (1-palmitoyl-2-oleoyl-sn-glycero-3-phosphocholine 16:0-18:1, Avanti Polar Lipids 850457C), PG (1-palmitoyl-2-oleoyl-sn-glycero-3-phospho-(1'-rac-glycerol) (sodium salt) 16:0-18:1, Avanti Polar Lipids 840457C), PA (1-palmitoyl-2-oleoyl-sn-glycero-3-phosphate (sodium salt) 16:0-18:1, Avanti Polar Lipids 840857C), and CL (1',3'-bis[1,2-dioleoyl-sn-glycero-3-phospho]-sn-glycerol (sodium salt) 18:1, Avanti Polar Lipids 710335C). Stable daptomycin binding and integration was performed on equimolar ratios (1:1) of PG:PC, CL:PC and PA:PC with a PC-only liposome control. Daptomycin-to-lipid ratio was performed on equimolar ratios (1:1) of PG:PC and PA:PC liposomes. Rate of daptomycin binding and integration or dissociation was calculated with 1:20 PG:PC liposomes. All liposomes were created using the reverse phase method, 200 nm in size ***(Szoka and Papahadjopoulos, 1978)***, in the presence of elution buffer containing 100 mM KCl, 10 mM HEPES at pH 7.0, and 2 nM Ca^{2+}. Liposomes were bound to a carboxymethyl dextran hydrogel surface sensor chip (#13206066) that was derivatized by treating the chip with a 1:1 mixture of 0.4 M EDC and 0.1 M NHS, then treated with 0.4 mM Sphingosine in DMSO. Reaction was quenched by 0.2 M Ethanolamine at pH 8.5. Bound liposomes were subjected to two concentrations of daptomycin (20 μg/mL and 35 μg/mL). Baseline, stable liposome and peak daptomycin binding readings were collected. Data was exported as a CSV and analyzed in Excel. 3 values are used during analysis to determine the daptomycin unit to lipid unit ratio: no lipid baseline, lipid peak, daptomycin peak. For daptomycin retention analysis, liposomes were completely loaded, and the plateaued value was aggregated and averaged up to the addition of daptomycin. The peak value of daptomycin was identified, and the range of values were aggregated and averaged. The delta of the peak daptomycin and lipid was divided by the delta of the daptomycin and lipid after the liposomes were washed with buffer (PG and CL at 25 minutes or 1500 seconds, and PC and PA at 10 minutes or 600 seconds, due to plateauing of daptomycin

retention). For binding V integration analysis, the preceding 60 data points before daptomycin injection were examined for the lowest lipid unit value. The lowest lipid unit value was then subtracted from the daptomycin unit value to normalize and align all daptomycin peaks in triplicate and at the daptomycin injection time. All graphs and statistical significance were generated using a one-way ANOVA, and individual data columns compared for significance using the Tukey's multiple comparisons test. XY data were analyzed by linear regression and the equation and slope with standard deviation are reported. $p \leq 0.05$ (*), $p \leq 0.01$ (**), $p \leq 0.001$ (***), $p \leq 0.0001$ (****).

3.5.3 Carboxyfluorescein liposome stability assay data collection and analysis

We performed a liposome disruption assay (Jimah et al., 2017) in triplicate to determine the size of the pore created by daptomycin in equimolar ratios of PG:PC liposomes. Liposomes were created using the reverse phase method containing carboxyfluorescein (Szoka and Papahadjopoulos, 1978) buffer, containing 100 mM KCl, 10 mM HEPES at pH 7.0, 2 nM Ca^{2+} and 10 mM carboxyfluorescein. Extrasomal carboxyfluorescein was removed from the liposomes using a G25 Sephadex sizing column with one volume of elution buffer. Liposomes were then suspended in a buffer solution in triplicate, containing 20 μM dextran at a size of 5 kDa, 9 kDa, 39 kDa, 66.9 kDa, 148.2 kDa, 500 kDa, and 2000 kDa and subjected to two concentrations of daptomycin (10 μg/mL or 35 μg/mL). Fluorescence increase due to daptomycin as a result of carboxyfluorescein release was measured using a Varian Eclipse Spectrophotometer with an excitation wavelength of 492 nm and an emission wavelength of 512 nm. Daptomycin activity was measured as a function of normalization to 100% release by Triton X-100. Statistical analysis was generated using a one-way Anova and every column was means compared and multiple hypothesis corrected for significance using the Tukey's multiple comparisons test. $p \leq 0.05$ (*), $p \leq 0.01$ (**), $p \leq 0.001$ (***), $p \leq 0.0001$ (****).

3.5.4 *In vivo* daptomycin pore formation data collection and analysis

Time course of daptomycin treatment

Wild-type *C. striatum* was grown overnight at 37°C in cation-adjusted Mueller-Hinton Broth (CA-MHB) and then diluted to an OD of 1.0 using fresh CA-MHB. 5 mL of this culture was then treated with 1 µL of 50 mg/mL daptomycin in water for a final concentration of 10 µg/mL. A control culture was grown in media without daptomycin and a blank was prepared by adding daptomycin to 5 mL of CA-MHB without cells. At 3, 5, 10, 15, and 30 minutes after daptomycin addition, 750 µL of each culture was spun down at 3800×*g* for 6 minutes at 4°C. The supernatant was then removed and immediately frozen for storage at -20°C.

Culture supernatant analysis by LC-QTOF

A 100 µL aliquot of each culture supernatant was diluted in 300 µL MilliQ H_2O and clarified using a 0.45 µm PVDF syringe filter. A 2 µL aliquot of each sample was then injected into an Agilent 1290 Infinity UPHLC system fitted with a Waters Acquity UPLC HSS T3 column (2.1mm x 150mm, 1.8 µm beads). Metabolites were separated using a linear gradient starting by holding 98% solvent A (0.1% formic acid in water) for 2 minutes. Solvent B (0.1% formic acid in acetonitrile) was increased to 98% in 9 minutes, held at 98% Solvent B for 6 minutes, and returned to 98% Solvent A over 1 minute. The column was allowed to re-equilibrate for 4 minutes between runs. Metabolites eluting from the UPLC were detected using an Agilent 6550 Jet Stream qTOF high resolution tandem mass spectrometer. The qTOF was set to 350 for sheath gas temperature, 12 L/min for sheath gas flow, 250 for drying gas temperature, 11 L/min for drying gas flow, 35 psi for nebulizer pressure, and 3500 V for capillary voltage. The fragmentor voltage was set to 135 V. Data was collected in positive-ion mode.

Sample chromatograms were aligned, and molecular features extracted using MassHunter Profinder and Mass Profiler Professional (Agilent). Features detected in the media blanks or present in ≤ 2 samples were discarded, leaving 111 features. Independent Principal Component Analysis (IPCA) was performed on the $\log_{10}$-transformed feature intensities using the mixOmics package for the R statistical language (Liquet et al., 2012; Yao et al., 2012).

3.6 Figures

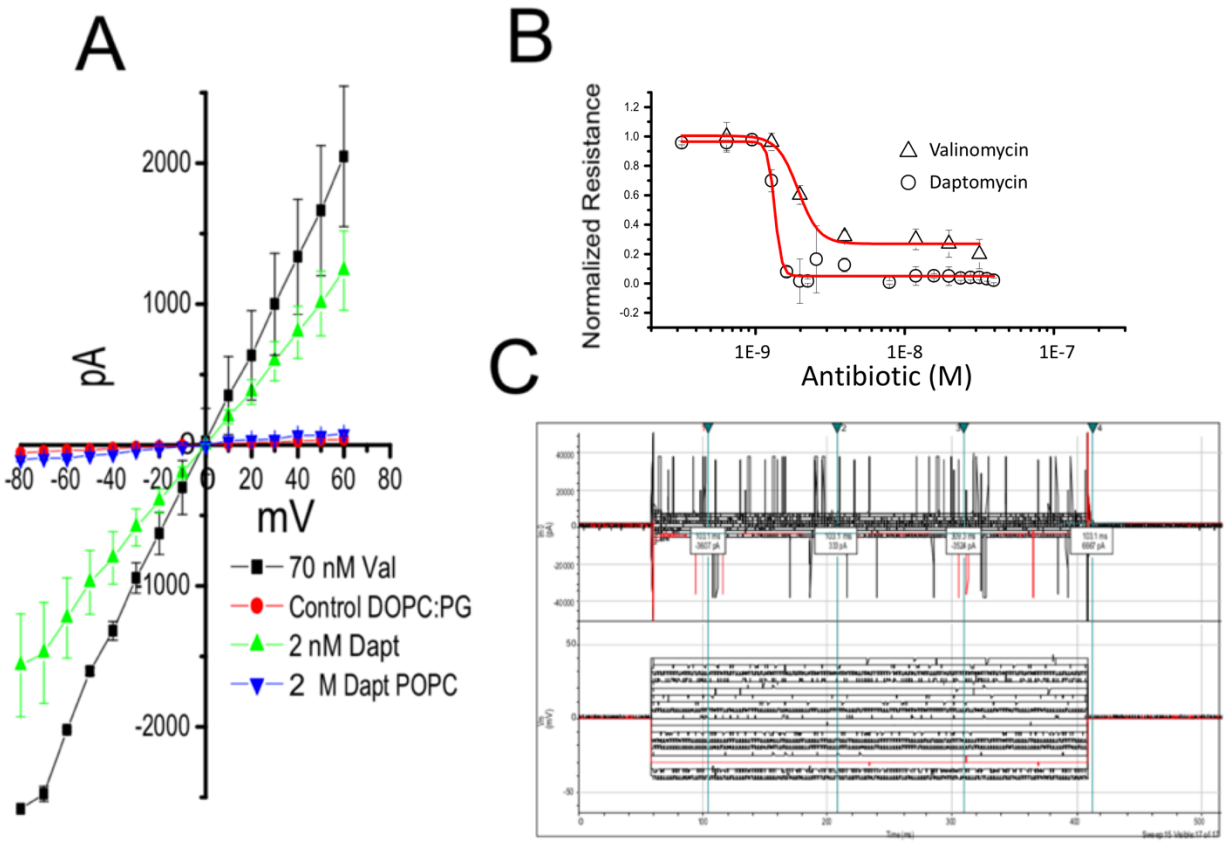

Figure 3.1: Daptomycin disrupts membranes through a different mechanism than valinomycin.

Planar lipid bilayers were constructed as described in Methods from DOPC:PG (80:20) or DOPC as indicated. (A) Valinomycin (in DMSO) or daptomycin (water) was diluted to the indicated concentration in 145 mM NaCl, 5 mM KCl and 10 mM HEPES at pH 7 (solution composition in both cis and trans chambers). Starting with no daptomycin or valinomycin present, a current-voltage relationship was developed for each membrane by pulsing the membrane. Daptomycin was added with stirring and a minute allowed for complete mixing, with 2 mM $CaCl_2$ present in the buffer. The conductance of each membrane was determined by pulsing at -80 to +80 mV (in 10 mV steps) for 500 msec. The current produced was averaged over three trials and each

concentration of daptomycin or valinomycin was tested in triplicate. The stable current in each pulse was used to averaged and used to construct a current-voltage profile for each membrane with valinomycin or daptomycin. (B) From the slope of each current voltage profile, the membrane resistance was calculated and normalized to 1 gigohm for native bilayer membranes. This is presented as a sigmoid fitted plot. (C) A complete I-V trial is shown with the record of voltage pulses on the bottom and the current response on top. The large rapid current pulses produced at constant voltage stimulus were seen when the daptomycin concentration exceeded ~4.4 μM and membrane voltage greater than ± 40 mV.

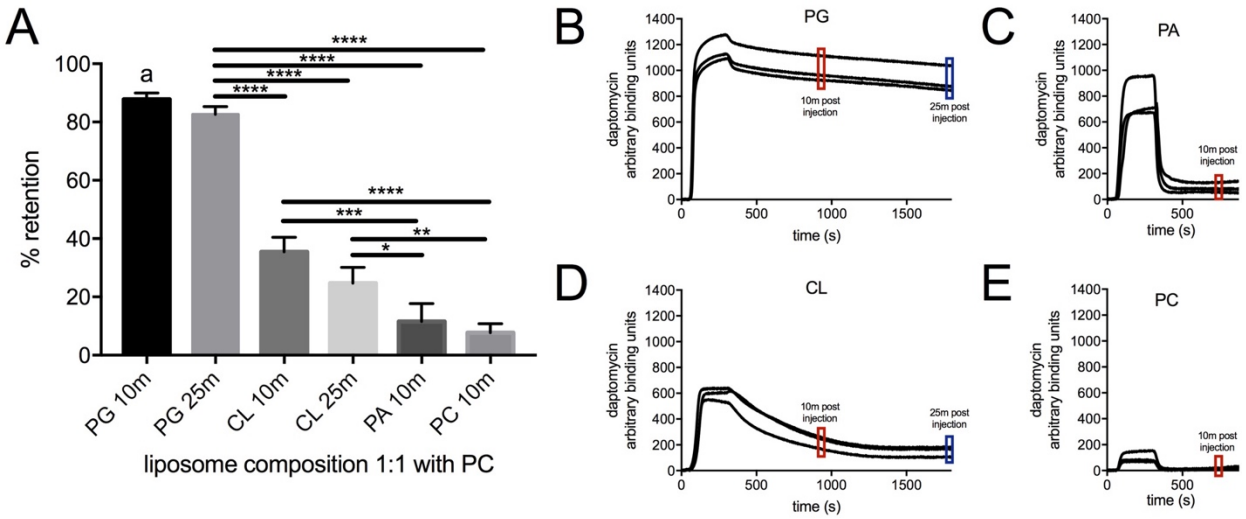

Figure 3.2. Daptomycin stably binds and integrates into PG-containing membranes. (A) Percent retention of daptomycin to the 1:1 PG:PC, PA:PC, CL:PC and PC-only liposomes at 10 and 25 minutes (PG and CL) or 10 minutes only (PC and PA) due to plateaued daptomycin retention. PG 10m (a) and PG 25m are not statistically different from each other and have the same statistically significant difference with CL 10m, CL 25m, PA 10m and PC 10m. Statistical analysis was performed with one-way Anova and every column was means compared using a Tukey HSD test with $p \leq 0.05$ (*), $p \leq 0.01$ (**), $p \leq 0.001$ (***), $p \leq 0.0001$ (****). Triplicate SPR tracings of daptomycin binding to artificial liposomes and release of daptomycin is observed over 10-25 minutes (**B**) for PG (**C**) for PA (**D**) for CL (**E**) and for PC. PA and PC had only transient binding but no integration (**C** and **E**). PG and CL had sustained binding, but complete integration into the membrane was only observed in PG containing membranes (**B** and **D**).

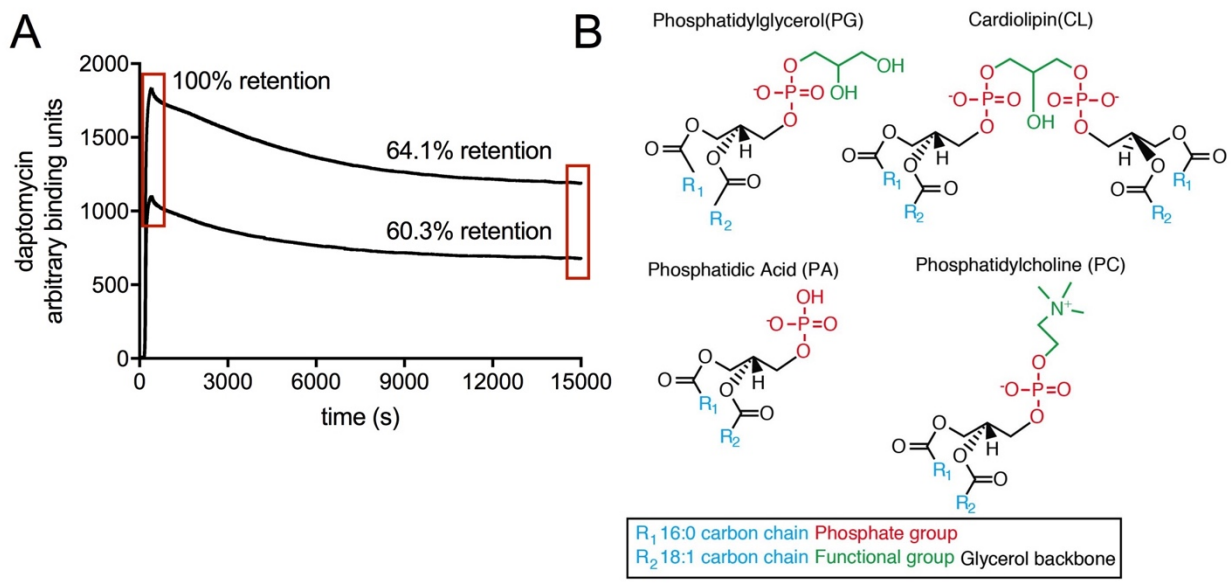

Figure 3.2 – Supplement 1: Long term daptomycin binding and lipid of interest structures. (**A**) Daptomycin binds PG stably over time. SPR tracings run in duplicate for 4.5 hours with daptomycin bound to equimolar PG:PC liposomes. Daptomycin retention at 4.5 hours is between 60.3-64.1%. (**B**) Liposomes were made using PG, CL, PA and PC; the 16:0 18:1 R-group fatty acid tails are in blue, the glycerol backbone is in black, the phosphate is in red and the functional group is in green.

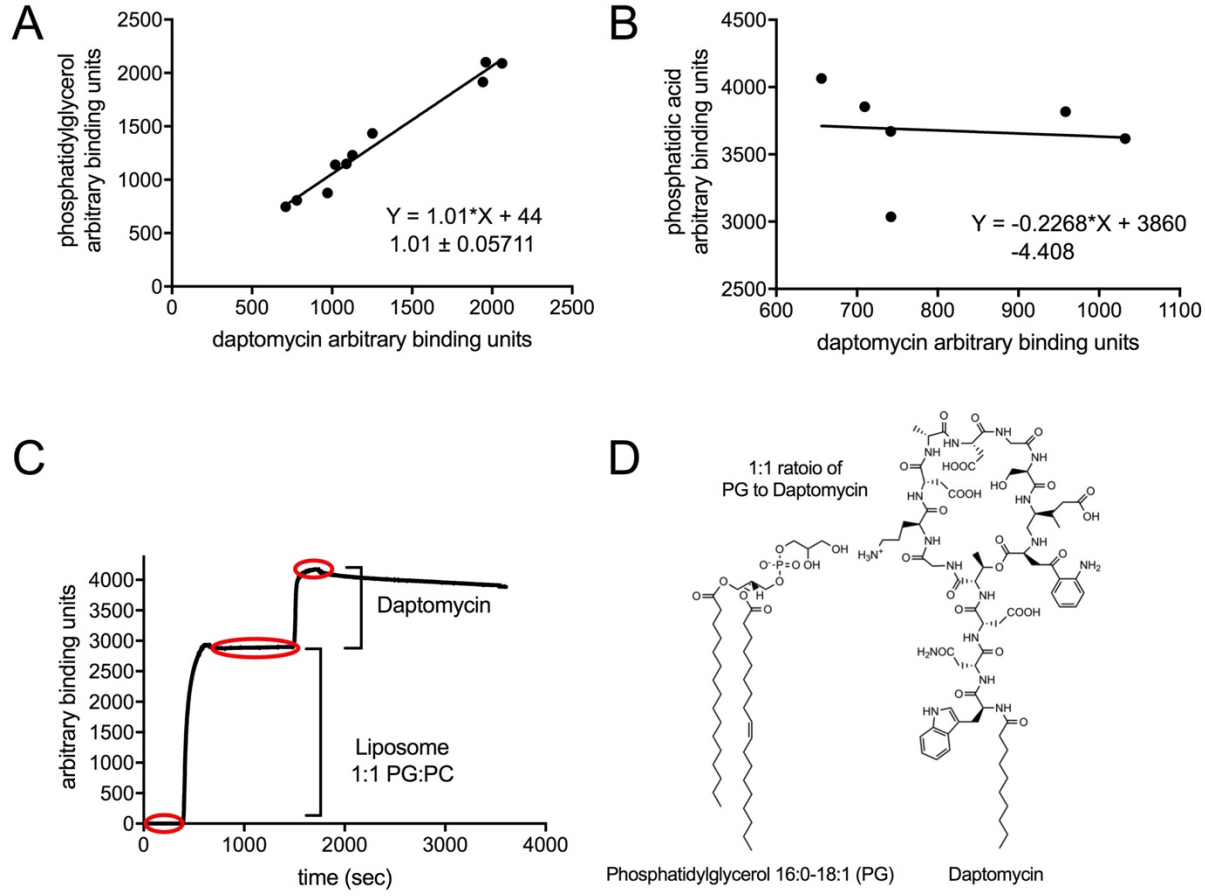

Figure 3.3: The phosphatidylglycerol to daptomycin stoichiometric ratio is ~1:1.

20 and 35 µg/mL daptomycin was bound to equimolar (**A**) PG:PC (n=9) or (**B**) PA:PC (n=6) liposomes. Linear regression was applied to the data points and the equation and slope with standard deviation are reported. The slope of the line represents the lipid-to-daptomycin stoichiometry, (**A**) 1.01 for PG:daptomycin and (**B**) 0.2268 for daptomycin:PA or 4.41 for PA:daptomycin. (**C**) The arbitrary binding units for the LOI and daptomycin are normalized and each n is plotted on the XY graph (**A, B**). (**D**) The structure of daptomycin and PG in a representative but not a spatially accurate 1:1 ratio.

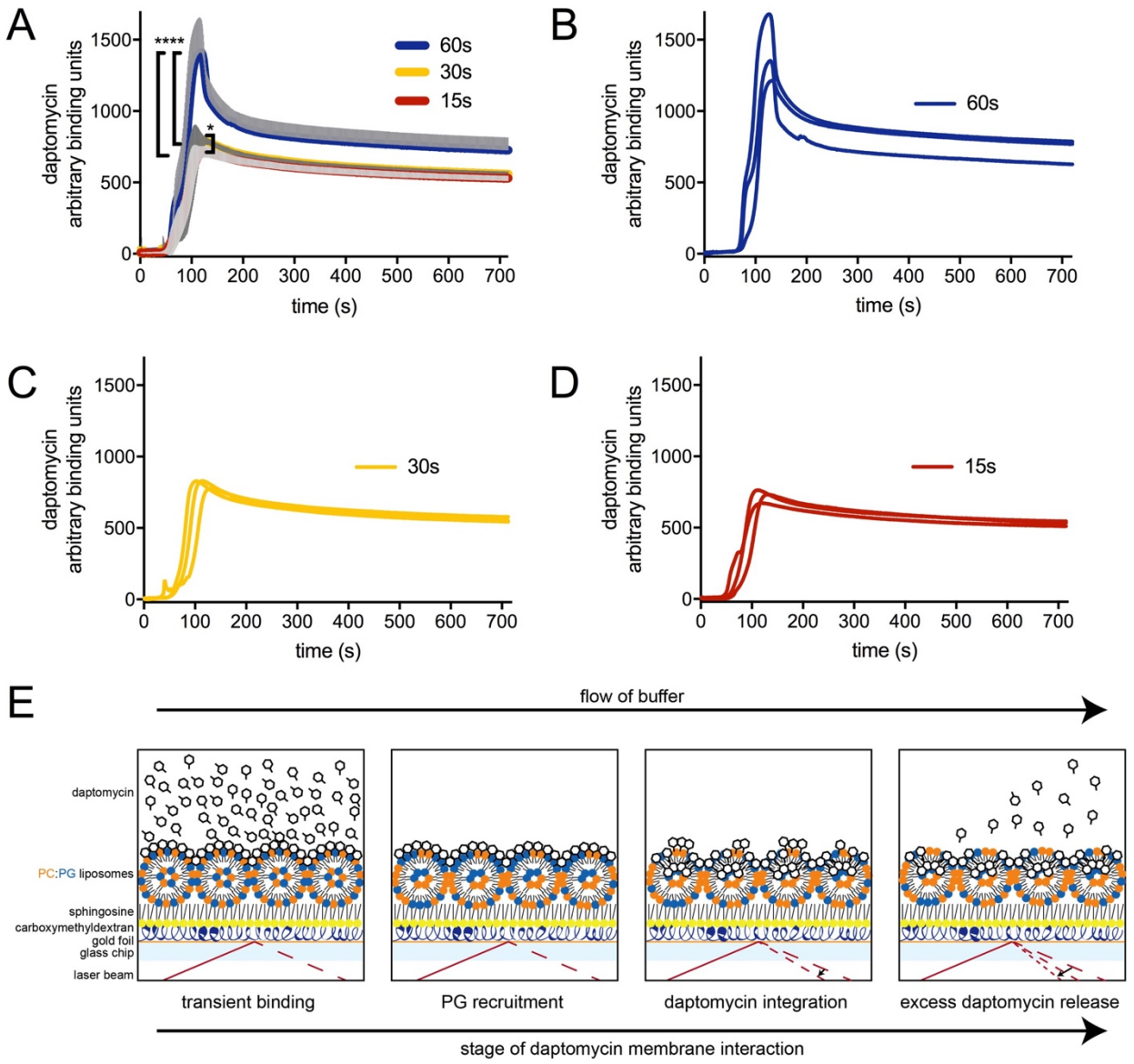

Figure 3.4: Daptomycin binds and integrates into phosphatidylglycerol-containing membranes rapidly and can saturate membranes with low phosphatidylglycerol content.

(**A**) 35 μg/mL daptomycin flowed over 1:20 PG:PC artificial liposomes in triplicate at injection times of 15 seconds, 30 seconds, and 60 seconds. The individual normalized SPR tracings (**D**) 15s

and (**C**) 30s injections indicate similar binding and integration of daptomycin with the (**B**) 60s injections experiencing high transient binding of daptomycin, subsequent integration of daptomycin and a release of all non-integrated daptomycin. Statistical analysis was performed with one-way Anova and every triplicate tracing was means compared using a Tukey HSD test, with $p \leq 0.05$ (*), $p \leq 0.01$ (**), $p \leq 0.001$ (***), $p \leq 0.0001$ (****). (**B, E**) At 5% PG, there is not adequate PG in the membrane for all available daptomycin to bind and maintain the ~1:1 binding ratio of PG to daptomycin, which results in nonintegrated daptomycin releasing from the membrane during washing, such that only integrated daptomycin remains.

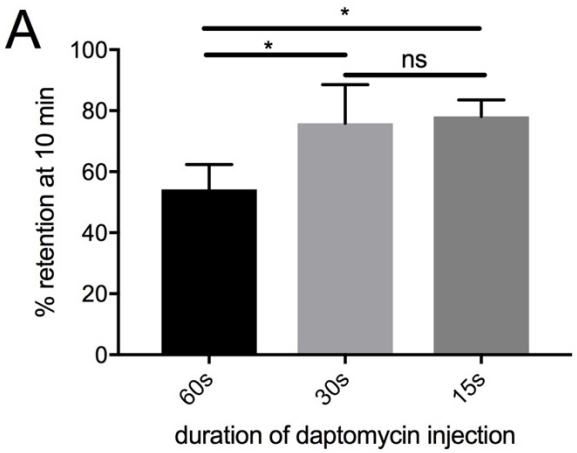

Figure 3.4 – Supplement 1: Daptomycin retention after 15, 30 and 60 second injections.

(**A**) Percent retention of daptomycin in 1:20 PG:PC liposomes after 60 seconds, 30 seconds and 15 seconds. The 60 seconds injection saw a significant drop in retention, indicating saturation of daptomycin to PG and a rapid dissociation of daptomycin from the membrane. Statistical analysis was performed with one-way Anova and every triplicate point was means compared using a Tukey HSD test with $p \leq 0.05$ (*).

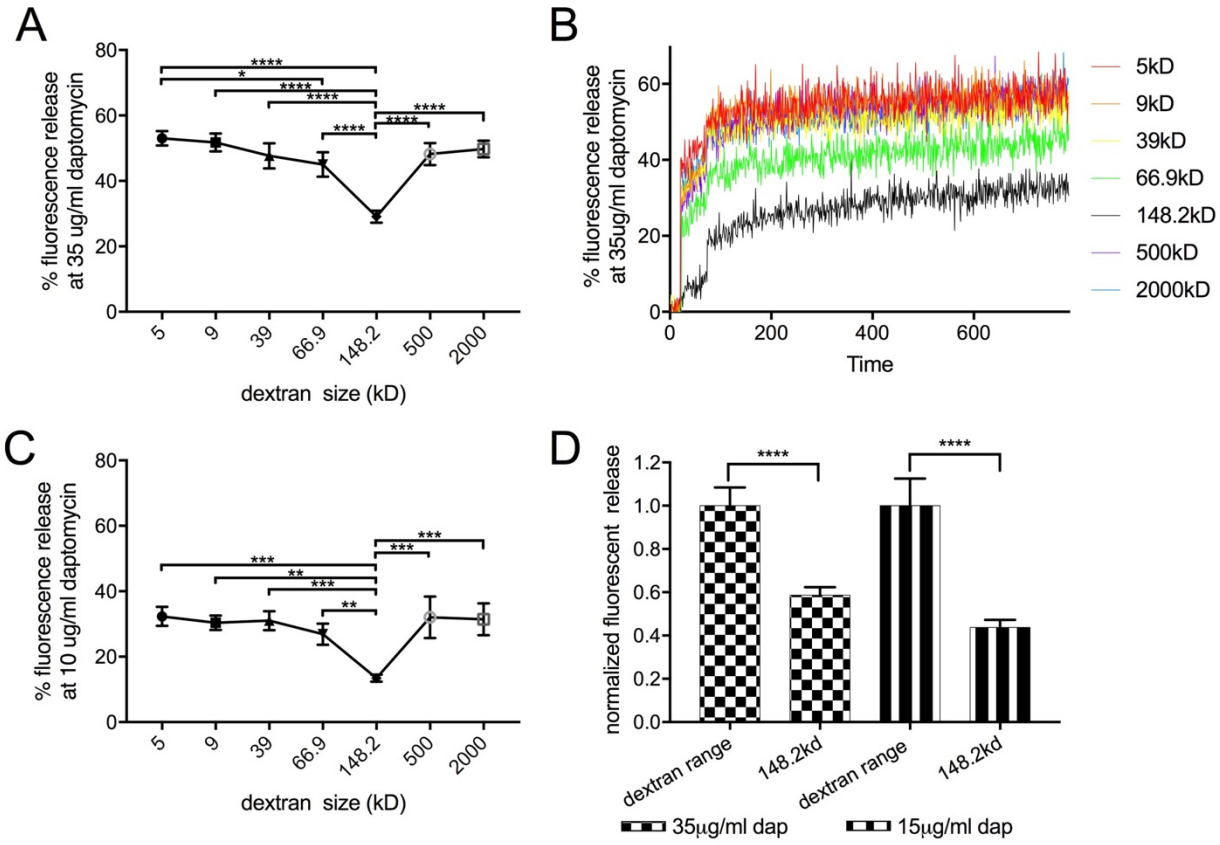

Figure 3.5: Daptomycin forms pores in PG-containing artificial membranes.

Equimolar PG:PC liposomes were treated with daptomycin in the presence of various kDa dextran ranging in size from 5-2000 kDa in triplicate. (**B**) Daptomycin activity is time-dependent with a rapid release of carboxyfluorescein from the liposomes followed by a steady increase in florescence. Liposomes in 148.2 kDa dextran buffer treated with (**A**) 35 μg/mL or (**C**) 10 μg/mL of daptomycin saw a (**D**) 41%-56% decrease in normalized fluorescence, indicating that 148.2 kDa dextran blocks daptomycin pores. It also indicates that the size of the pore is consistent across daptomycin concentrations. Statistical analysis was performed with one-way Anova and means compared using a Tukey HSD test with $p \leq 0.05$ (*), $p \leq 0.01$ (**), $p \leq 0.001$ (***), $p \leq 0.0001$ (****).

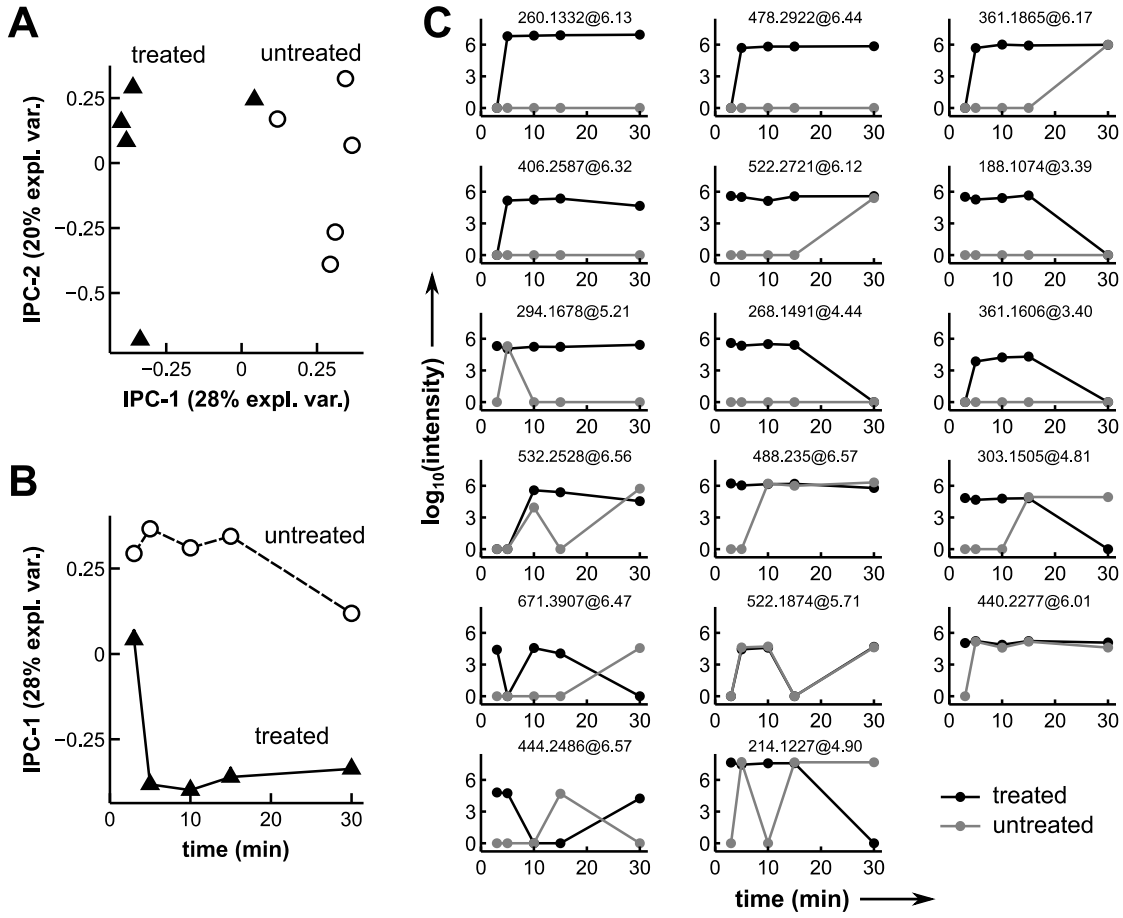

Figure 3.6: Mass spectrometry detects molecular features increased in culture supernatants by daptomycin treatment.

(**A**) Plot of IPCA scores for untreated cell supernatants (white circles) and daptomycin-treated cell supernatants (black triangles). (**B**) Plot of IPCA scores on component #1 versus time, showing that the composition of the cell supernatants from treated and untreated cultures diverges sharply between 3 and 5 minutes post-treatment. (**C**) Plots of feature intensities versus time for each molecular feature assigned a negative weight in IPCA component #1. Features are sorted by weight, with the most strongly-weighted features in the top row. The neutral mass in Daltons and retention time in minutes are listed above each feature plot.

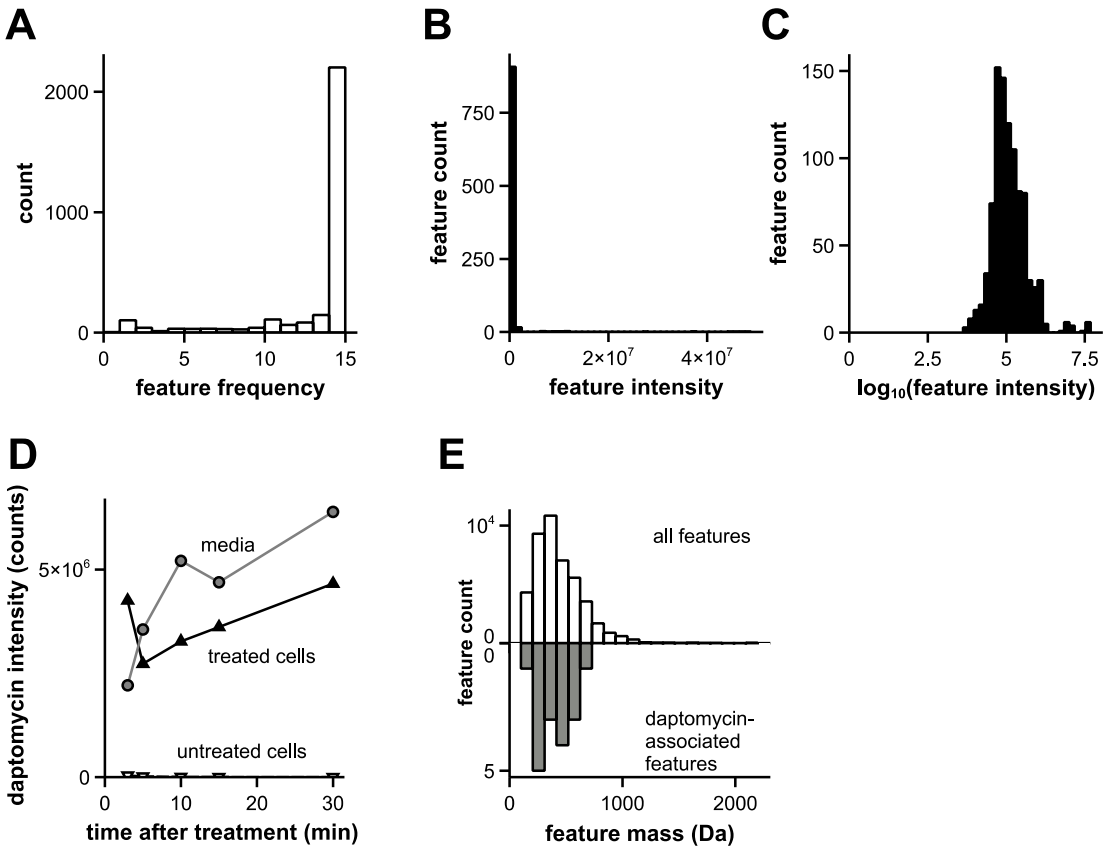

Figure 3.6 – Supplement 1: Treated and untreated supernatant features and distributions.

(**A**) Frequencies with which each chemical feature was detected across all 15 samples. (**B**) Histogram of raw feature intensities showing that the distribution is extremely left-skewed. (**C**) Applying the $\log_{10}(n+1)$ transformation to the intensities gives a histogram that is much closer to a normal distribution. (**D**) Intensity of the daptomycin signal in each culture supernatant. As expected, daptomycin was only detected in samples to which it was added. (**E**) Comparing the detection frequencies for all features (top) to the daptomycin-associated features alone (bottom) does not provide an upper limit on pore size.

3.7 References

Akins, R.L., B.D. Katz, C. Monahan, and D. Alexander. 2015. Characterization of high-level daptomycin resistance in Viridans group Streptococci developed upon in vitro exposure to daptomycin. *Antimicrob Agents Chemother*. 59:2102-2112.

Alborn, W.E., Jr., N.E. Allen, and D.A. Preston. 1991. Daptomycin disrupts membrane potential in growing Staphylococcus aureus. *Antimicrob Agents Chemother*. 35:2282-2287.

Allen, N.E., W.E. Alborn, Jr., and J.N. Hobbs, Jr. 1991. Inhibition of membrane potential-dependent amino acid transport by daptomycin. *Antimicrob Agents Chemother*. 35:2639-2642.

Allen, N.E., J.N. Hobbs, and W.E. Alborn, Jr. 1987. Inhibition of peptidoglycan biosynthesis in gram-positive bacteria by LY146032. *Antimicrob Agents Chemother*. 31:1093-1099.

Antachopoulos, C., E. Iosifidis, K. Sarafidis, F. Bazoti, E. Gikas, A. Katragkou, V. Drossou-Agakidou, and E. Roilides. 2012. Serum levels of daptomycin in pediatric patients. *Infection*. 40:367-371.

Armstrong, J.K., R.B. Wenby, H.J. Meiselman, and T.C. Fisher. 2004. The hydrodynamic radii of macromolecules and their effect on red blood cell aggregation. *Biophys J*. 87:4259-4270.

Baltz, R.H. 2009. Daptomycin: mechanisms of action and resistance, and biosynthetic engineering. *Curr Opin Chem Biol*. 13:144-151.

Bankevich, A., S. Nurk, D. Antipov, A.A. Gurevich, M. Dvorkin, A.S. Kulikov, V.M. Lesin, S.I. Nikolenko, S. Pham, A.D. Prjibelski, A.V. Pyshkin, A.V. Sirotkin, N. Vyahhi, G. Tesler, M.A. Alekseyev, and P.A. Pevzner. 2012. SPAdes: a new genome assembly algorithm and its applications to single-cell sequencing. *J Comput Biol*. 19:455-477.

Batrakov, S.G., and L.D. Bergelson. 1978. Lipids of the Streptomycettes. Structural investigation and biological interrelation a review. *Chem Phys Lipids*. 21:1-29.

Bayer, A.S., N.N. Mishra, L. Chen, B.N. Kreiswirth, A. Rubio, and S.J. Yang. 2015. Frequency and Distribution of Single-Nucleotide Polymorphisms within mprF in Methicillin-Resistant Staphylococcus aureus Clinical Isolates and Their Role in Cross-Resistance to Daptomycin and Host Defense Antimicrobial Peptides. *Antimicrob Agents Chemother*. 59:4930-4937.

Bayer, A.S., N.N. Mishra, A.L. Cheung, A. Rubio, and S.J. Yang. 2016. Dysregulation of mprF and dltABCD expression among daptomycin-non-susceptible MRSA clinical isolates. *J Antimicrob Chemother*. 71:2100-2104.

Bayer, A.S., N.N. Mishra, G. Sakoulas, P. Nonejuie, C.C. Nast, J. Pogliano, K.T. Chen, S.N. Ellison, M.R. Yeaman, and S.J. Yang. 2014. Heterogeneity of mprF sequences in methicillin-resistant Staphylococcus aureus clinical isolates: role in cross-resistance between daptomycin and host defense antimicrobial peptides. *Antimicrob Agents Chemother*. 58:7462-7467.

Bayer, A.S., T. Schneider, and H.G. Sahl. 2013. Mechanisms of daptomycin resistance in Staphylococcus aureus: role of the cell membrane and cell wall. *Ann N Y Acad Sci*. 1277:139-158.

Baym, M., S. Kryazhimskiy, T.D. Lieberman, H. Chung, M.M. Desai, and R. Kishony. 2015. Inexpensive multiplexed library preparation for megabase-sized genomes. *PLoS One*. 10:e0128036.

Baym, M., L.K. Stone, and R. Kishony. 2016. Multidrug evolutionary strategies to reverse antibiotic resistance. *Science*. 351:aad3292.

Bligh, E.G., and W.J. Dyer. 1959. A rapid method of total lipid extraction and purification. *Can J Biochem Physiol*. 37:911-917.

Boudjemaa, R., R. Briandet, M. Revest, C. Jacqueline, J. Caillon, M.P. Fontaine-Aupart, and K. Steenkeste. 2016. New Insight into Daptomycin Bioavailability and Localization in Staphylococcus aureus Biofilms by Dynamic Fluorescence Imaging. *Antimicrob Agents Chemother*. 60:4983-4990.

Cesar A. Arias, M.D., Ph.D., Diana Panesso, Ph.D.,, P.D. Danielle M. McGrath, Xiang Qin, Ph.D., Maria F. Mojica, M.Sc., Corwin Miller, B.A., Lorena Diaz, B.Sc., Truc T. Tran, Pharm.D.,, M.S. Sandra Rincon, E. Magda Barbu, Ph.D., Jinnethe Reyes, M.Sc.,, and P.D. Jung H. Roh, Elizabeth Lobos, Ph.D., Erica Sodergren, Ph.D., Renata Pasqualini, Ph.D., Wadih Arap, M.D., Ph.D., John P. Quinn, M.D., Yousif Shamoo, Ph.D., Barbara E. Murray, M.D., and George M. Weinstock, Ph.D. 2001. Genetic Basis for In Vivo Daptomycin Resistance in Enterococci. *The New England Journal of Medicine*. 365:892-900.

Chatzopoulou, M., T. Koufakis, I. Voulgaridi, I. Gabranis, and M. Tsiakalou. 2016. A case of fatal sepsis due to multidrug-resistant Corynebacterium striatum. *Hippokratia*. 20:67-69.

Chen, Y.F., T.L. Sun, Y. Sun, and H.W. Huang. 2014. Interaction of daptomycin with lipid bilayers: a lipid extracting effect. *Biochemistry*. 53:5384-5392.

Cingolani, P., V.M. Patel, M. Coon, T. Nguyen, S.J. Land, D.M. Ruden, and X. Lu. 2012a. Using Drosophila melanogaster as a Model for Genotoxic Chemical Mutational Studies with a New Program, SnpSift. *Front Genet*. 3:35.

Cingolani, P., A. Platts, L. Wang le, M. Coon, T. Nguyen, L. Wang, S.J. Land, X. Lu, and D.M. Ruden. 2012b. A program for annotating and predicting the effects of single nucleotide

polymorphisms, SnpEff: SNPs in the genome of Drosophila melanogaster strain w1118; iso-2; iso-3. *Fly (Austin)*. 6:80-92.

Conesa, A., S. Gotz, J.M. Garcia-Gomez, J. Terol, M. Talon, and M. Robles. 2005. Blast2GO: a universal tool for annotation, visualization and analysis in functional genomics research. *Bioinformatics*. 21:3674-3676.

Cotroneo, N., R. Harris, N. Perlmutter, T. Beveridge, and J.A. Silverman. 2008. Daptomycin exerts bactericidal activity without lysis of Staphylococcus aureus. *Antimicrob Agents Chemother*. 52:2223-2225.

D'Costa, V.M., T.A. Mukhtar, T. Patel, K. Koteva, N. Waglechner, D.W. Hughes, G.D. Wright, and G. De Pascale. 2012. Inactivation of the lipopeptide antibiotic daptomycin by hydrolytic mechanisms. *Antimicrob Agents Chemother*. 56:757-764.

Dynamics, C.f.D. 2015. State of the World's Antibiotics, 2015. *Economics & Policy*. CDDEP: Washington, D.C.

Epand, R.M., S. Rotem, A. Mor, B. Berno, and R.F. Epand. 2008. Bacterial membranes as predictors of antimicrobial potency. *J Am Chem Soc*. 130:14346-14352.

Ernst, C.M., P. Staubitz, N.N. Mishra, S.J. Yang, G. Hornig, H. Kalbacher, A.S. Bayer, D. Kraus, and A. Peschel. 2009. The bacterial defensin resistance protein MprF consists of separable domains for lipid lysinylation and antimicrobial peptide repulsion. *PLoS Pathog*. 5:e1000660.

Garcia-de-la-Maria, C., J.M. Pericas, A. Del Rio, X. Castaneda, X. Vila-Farres, Y. Armero, P.A. Espinal, C. Cervera, D. Soy, C. Falces, S. Ninot, M. Almela, C.A. Mestres, J.M. Gatell, J. Vila, A. Moreno, F. Marco, J.M. Miro, and G. Hospital Clinic Experimental Endocarditis Study. 2013. Early in vitro and in vivo development of high-level daptomycin resistance is common in mitis group Streptococci after exposure to daptomycin. *Antimicrob Agents Chemother*. 57:2319-2325.

Gaupp, R., S. Lei, J.M. Reed, H. Peisker, S. Boyle-Vavra, A.S. Bayer, M. Bischoff, M. Herrmann, R.S. Daum, R. Powers, and G.A. Somerville. 2015. Staphylococcus aureus metabolic adaptations during the transition from a daptomycin susceptibility phenotype to a daptomycin nonsusceptibility phenotype. *Antimicrob Agents Chemother*. 59:4226-4238.

Gelband, h., m. Miller-petrie, s. Pant, s. Gandra, j. Levinson, d. Barter, a. White, and r. Laxminarayan. 2015. The state of the world's antibiotics 2015 center for disease dynamics, economics & policy, washington dc.

Gomila, M., F. Renom, C. Gallegos Mdel, M. Garau, D. Guerrero, J.B. Soriano, and J. Lalucat. 2012. Identification and diversity of multiresistant Corynebacterium striatum clinical isolates by MALDI-TOF mass spectrometry and by a multigene sequencing approach. *BMC Microbiol*. 12:52.

Gonzales, P.R., M.W. Pesesky, R. Bouley, A. Ballard, B.A. Biddy, M.A. Suckow, W.R. Wolter, V.A. Schroeder, C.A. Burnham, S. Mobashery, M. Chang, and G. Dantas. 2015. Synergistic, collaterally sensitive beta-lactam combinations suppress resistance in MRSA. *Nat Chem Biol*. 11:855-861.

Hachmann, A.B., E.R. Angert, and J.D. Helmann. 2009. Genetic analysis of factors affecting susceptibility of Bacillus subtilis to daptomycin. *Antimicrob Agents Chemother*. 53:1598-1609.

Hachmann, A.B., E. Sevim, A. Gaballa, D.L. Popham, H. Antelmann, and J.D. Helmann. 2011. Reduction in membrane phosphatidylglycerol content leads to daptomycin resistance in Bacillus subtilis. *Antimicrob Agents Chemother*. 55:4326-4337.

Hahn, W.O., B.J. Werth, S.M. Butler-Wu, and R.M. Rakita. 2016. Multidrug-Resistant Corynebacterium striatum Associated with Increased Use of Parenteral Antimicrobial Drugs. *Emerg Infect Dis*. 22.

Hayami, M. 1979. [Lipid composition of autoplast and stable L-form from Staphylococcus aureus (author's transl)]. *Nihon Saikingaku Zasshi*. 34:685-692.

Hayami, M., A. Okabe, R. Kariyama, M. Abe, and Y. Kanemasa. 1979. Lipid composition of Staphylococcus aureus and its derived L-forms. *Microbiol Immunol*. 23:435-442.

Hines, K.M., A. Waalkes, K. Penewit, E.A. Holmes, S.J. Salipante, B.J. Werth, and L. Xu. 2017. Characterization of the Mechanisms of Daptomycin Resistance among Gram-Positive Bacterial Pathogens by Multidimensional Lipidomics. *mSphere*. 2.

Ho, S.W., D. Jung, J.R. Calhoun, J.D. Lear, M. Okon, W.R. Scott, R.E. Hancock, and S.K. Straus. 2008. Effect of divalent cations on the structure of the antibiotic daptomycin. *Eur Biophys J*. 37:421-433.

Hobbs, J.K., K. Miller, A.J. O'Neill, and I. Chopra. 2008. Consequences of daptomycin-mediated membrane damage in Staphylococcus aureus. *J Antimicrob Chemother*. 62:1003-1008.

Humphries, R.M., T. Kelesidis, R. Tewhey, W.E. Rose, N. Schork, V. Nizet, and G. Sakoulas. 2012. Genotypic and phenotypic evaluation of the evolution of high-level daptomycin nonsusceptibility in vancomycin-resistant Enterococcus faecium. *Antimicrob Agents Chemother*. 56:6051-6053.

Jimah, J.R., N.D. Salinas, M. Sala-Rabanal, N.G. Jones, L.D. Sibley, C.G. Nichols, P.H. Schlesinger, and N.H. Tolia. 2016. Malaria parasite CelTOS targets the inner leaflet of cell membranes for pore-dependent disruption. *Elife*. 5.

Jimah, J.R., P.H. Schlesinger, and N.H. Tolia. 2017. Liposome Disruption Assay to Examine Lytic Properties of Biomolecules. *Bio Protoc*. 7.

Jorgensen, J.H., S.A. Crawford, C.C. Kelly, and J.E. Patterson. 2003. In vitro activity of daptomycin against vancomycin-resistant enterococci of various Van types and comparison of susceptibility testing methods. *Antimicrob Agents Chemother*. 47:3760-3763.

Jorgensen, J.H., L.A. Maher, and J.S. Redding. 1987. In vitro activity of LY146032 (daptomycin) against selected aerobic bacteria. *Eur J Clin Microbiol*. 6:91-96.

Jung, D., J.P. Powers, S.K. Straus, and R.E. Hancock. 2008. Lipid-specific binding of the calcium-dependent antibiotic daptomycin leads to changes in lipid polymorphism of model membranes. *Chem Phys Lipids*. 154:120-128.

Jung, D., A. Rozek, M. Okon, and R.E. Hancock. 2004. Structural transitions as determinants of the action of the calcium-dependent antibiotic daptomycin. *Chem Biol*. 11:949-957.

Kaisersberger Vincek, M., A. Mor, S. Gorgieva, and V. Kokol. 2017. Antibacterial activity and cytotoxycity of gelatine-conjugated lysine-based peptides. *J Biomed Mater Res A*. 105:3110-3126.

Kanehisa, M., and S. Goto. 2000. KEGG: kyoto encyclopedia of genes and genomes. *Nucleic acids research*. 28:27-30.

Kaur, R., V. Gautam, P. Ray, G. Singh, L. Singhal, and R. Tiwari. 2012. Daptomycin susceptibility of methicillin resistant Staphylococcus aureus (MRSA). *Indian J Med Res*. 136:676-677.

Kelley, L.A., S. Mezulis, C.M. Yates, M.N. Wass, and M.J. Sternberg. 2015. The Phyre2 web portal for protein modeling, prediction and analysis. *Nat Protoc*. 10:845-858.

Kelley, L.A., and M.J. Sternberg. 2009. Protein structure prediction on the Web: a case study using the Phyre server. *Nat Protoc*. 4:363-371.

Khatib, T.O., H. Stevenson, M.R. Yeaman, A.S. Bayer, and A. Pokorny. 2016. Binding of Daptomycin to Anionic Lipid Vesicles Is Reduced in the Presence of Lysyl-Phosphatidylglycerol. *Antimicrob Agents Chemother*. 60:5051-5053.

Kinouchi, H., M. Onishi, and H. Kamimori. 2013. Lipid membrane-binding properties of daptomycin using surface plasmon resonance. *Anal Sci*. 29:297-301.

Krawczyk, B., A. Samet, M. Bronk, A. Hellmann, and J. Kur. 2004. Emerging linezolid-resistant, vancomycin resistant Enterococcus faecium from a patient of a haematological unit in Poland. *Pol J Microbiol*. 53:193-196.

Kreutzberger, M.A., A. Pokorny, and P.F. Almeida. 2017. Daptomycin-Phosphatidylglycerol Domains in Lipid Membranes. *Langmuir*. 33:13669-13679.

Laganas, V., J. Alder, and J.A. Silverman. 2003. In vitro bactericidal activities of daptomycin against Staphylococcus aureus and Enterococcus faecalis are not mediated by inhibition of lipoteichoic acid biosynthesis. *Antimicrob Agents Chemother*. 47:2682-2684.

Lakey, J.H., and E.J. Lea. 1986. The role of acyl chain character and other determinants on the bilayer activity of A21978C an acidic lipopeptide antibiotic. *Biochim Biophys Acta*. 859:219-226.

Lakey, J.H., and M. Ptak. 1988. Fluorescence indicates a calcium-dependent interaction between the lipopeptide antibiotic LY146032 and phospholipid membranes. *Biochemistry*. 27:4639-4645.

Langmead, B., and S.L. Salzberg. 2012. Fast gapped-read alignment with Bowtie 2. *Nat Methods*. 9:357-359.

Lee, M.T., W.C. Hung, M.H. Hsieh, H. Chen, Y.Y. Chang, and H.W. Huang. 2017. Molecular State of the Membrane-Active Antibiotic Daptomycin. *Biophys J*. 113:82-90.

Li, S., Y. Yin, H. Chen, Q. Wang, X. Wang, and H. Wang. 2017. Fitness Cost of Daptomycin-Resistant Staphylococcus aureus Obtained from in Vitro Daptomycin Selection Pressure. *Front Microbiol*. 8:2199.

Liquet, B., K.A. Le Cao, H. Hocini, and R. Thiebaut. 2012. A novel approach for biomarker selection and the integration of repeated measures experiments from two assays. *BMC Bioinformatics*. 13:325.

Liu, H., W. Tian, B. Li, G. Wu, M. Ibrahim, Z. Tao, Y. Wang, G. Xie, H. Li, and G. Sun. 2012. Antifungal effect and mechanism of chitosan against the rice sheath blight pathogen, Rhizoctonia solani. *Biotechnol Lett*. 34:2291-2298.

LLP, K. 2014. The global economic impact of anti-microbial resistance. *www.KPMG.co.uk*.

Love, M.I., W. Huber, and S. Anders. 2014. Moderated estimation of fold change and dispersion for RNA-seq data with DESeq2. *Genome Biol.* 15:550.

Maragakis, L.L., E.N. Perencevich, and S.E. Cosgrove. 2008. Clinical and economic burden of antimicrobial resistance. *Expert Rev Anti Infect Ther*. 6:751-763.

Mascio, C.T., J.D. Alder, and J.A. Silverman. 2007. Bactericidal action of daptomycin against stationary-phase and nondividing Staphylococcus aureus cells. *Antimicrob Agents Chemother*. 51:4255-4260.

Mattos-Guaraldi, A.L., L.C. Guimaraes, C.S. Santos, A.A. Veras, A.R. Carneiro, S.C. Soares, J.N. Ramos, C. Souza, V.V. Vieira, R. Hirata, Jr., V. Azevedo, L.G. Pacheco, A. Silva, and R.T. Ramos. 2015. Draft Genome Sequence of Corynebacterium striatum 1961 BR-

RJ/09, a Multidrug-Susceptible Strain Isolated from the Urine of a Hospitalized 37-Year-Old Female Patient. *Genome Announc*. 3.

McElvania TeKippe, E., B.S. Thomas, G.A. Ewald, S.J. Lawrence, and C.A. Burnham. 2014. Rapid emergence of daptomycin resistance in clinical isolates of Corynebacterium striatum... a cautionary tale. *Eur J Clin Microbiol Infect Dis*. 33:2199-2205.

McMullen, A.R., N. Anderson, M.A. Wallace, A. Shupe, and C.A. Burnham. 2017a. When Good Bugs Go Bad: Epidemiology and Antimicrobial Resistance Profiles of Corynebacterium striatum, an Emerging Multidrug Resistant, Opportunistic Pathogen. *Antimicrob Agents Chemother*.

McMullen, A.R., N. Anderson, M.A. Wallace, A. Shupe, and C.A. Burnham. 2017b. When Good Bugs Go Bad: Epidemiology and Antimicrobial Resistance Profiles of Corynebacterium striatum, an Emerging Multidrug-Resistant, Opportunistic Pathogen. *Antimicrob Agents Chemother*. 61.

Michael, G.B., C. Freitag, S. Wendlandt, C. Eidam, A.T. Fessler, G.V. Lopes, K. Kadlec, and S. Schwarz. 2015. Emerging issues in antimicrobial resistance of bacteria from food-producing animals. *Future Microbiol*. 10:427-443.

Mishra, B., T. Lushnikova, and G. Wang. 2015. Small lipopeptides possess anti-biofilm capability comparable to daptomycin and vancomycin. *RSC Adv*. 5:59758-59769.

Mishra, N.N., and A.S. Bayer. 2013. Correlation of cell membrane lipid profiles with daptomycin resistance in methicillin-resistant Staphylococcus aureus. *Antimicrob Agents Chemother*. 57:1082-1085.

Mishra, N.N., A.S. Bayer, C. Weidenmaier, T. Grau, S. Wanner, S. Stefani, V. Cafiso, T. Bertuccio, M.R. Yeaman, C.C. Nast, and S.J. Yang. 2014. Phenotypic and genotypic characterization of daptomycin-resistant methicillin-resistant Staphylococcus aureus strains: relative roles of mprF and dlt operons. *PLoS One*. 9:e107426.

Mishra, N.N., S.J. Yang, A. Sawa, A. Rubio, C.C. Nast, M.R. Yeaman, and A.S. Bayer. 2009. Analysis of cell membrane characteristics of in vitro-selected daptomycin-resistant strains of methicillin-resistant Staphylococcus aureus. *Antimicrob Agents Chemother*. 53:2312-2318.

Muller, A., M. Wenzel, H. Strahl, F. Grein, T.N. Saaki, B. Kohl, T. Siersma, J.E. Bandow, H.G. Sahl, T. Schneider, and L.W. Hamoen. 2016. Daptomycin inhibits cell envelope synthesis by interfering with fluid membrane microdomains. *Proc Natl Acad Sci U S A*.

Muraih, J.K., J. Harris, S.D. Taylor, and M. Palmer. 2012. Characterization of daptomycin oligomerization with perylene excimer fluorescence: stoichiometric binding of phosphatidylglycerol triggers oligomer formation. *Biochim Biophys Acta*. 1818:673-678.

Muraih, J.K., and M. Palmer. 2012. Estimation of the subunit stoichiometry of the membrane-associated daptomycin oligomer by FRET. *Biochim Biophys Acta*. 1818:1642-1647.

Muraih, J.K., A. Pearson, J. Silverman, and M. Palmer. 2011. Oligomerization of daptomycin on membranes. *Biochim Biophys Acta*. 1808:1154-1160.

Murillo, O., C. Garrigos, M.E. Pachon, G. Euba, R. Verdaguer, C. Cabellos, J. Cabo, F. Gudiol, and J. Ariza. 2009. Efficacy of high doses of daptomycin versus alternative therapies against experimental foreign-body infection by methicillin-resistant Staphylococcus aureus. *Antimicrob Agents Chemother*. 53:4252-4257.

O'Neill, J. 2014. Antimicrobial Resistance: Tackling a crisis for the health and wealth of nations. *The Review on Antimicrobial Resistance*.

O'Neill, J. 2015. Antimicrobials in Agriculture and Environment: Reducing Unnecessary use and Waste. *Review on Antimicrobial Resistance*.

Oh, J., A.L. Byrd, C. Deming, S. Conlan, N.C.S. Program, H.H. Kong, and J.A. Segre. 2014. Biogeography and individuality shape function in the human skin metagenome. *Nature*. 514:59-64.

OptumRx. 2016. Cubicin (daptomycin) - First-Time Generic. Vol. 2017. OptumRx Clinical Services Department, https://professionals.optumrx.com/content/dam/optum3/professional-optumrx/news/rxnews/new-generics/newgenerics_cubicin_2016-0915.pdf.

Palmer, A.C., and R. Kishony. 2013. Understanding, predicting and manipulating the genotypic evolution of antibiotic resistance. *Nat Rev Genet*. 14:243-248.

Peschel, A., and L.V. Collins. 2001. Staphylococcal resistance to antimicrobial peptides of mammalian and bacterial origin. *Peptides*. 22:1651-1659.

Pogliano, J., N. Pogliano, and J.A. Silverman. 2012. Daptomycin-mediated reorganization of membrane architecture causes mislocalization of essential cell division proteins. *J Bacteriol*. 194:4494-4504.

Prevention, U.S.D.o.H.a.H.S.C.f.D.C.a. 2013. Antibiotic Resistance Threats in the United States, 2013. *CDC*.

Quinn, B., S. Hussain, M. Malik, K. Drlica, and X. Zhao. 2007. Daptomycin inoculum effects and mutant prevention concentration with Staphylococcus aureus. *J Antimicrob Chemother*. 60:1380-1383.

Raad, I., H. Hanna, Y. Jiang, T. Dvorak, R. Reitzel, G. Chaiban, R. Sherertz, and R. Hachem. 2007. Comparative activities of daptomycin, linezolid, and tigecycline against catheter-

related methicillin-resistant Staphylococcus bacteremic isolates embedded in biofilm. *Antimicrob Agents Chemother*. 51:1656-1660.

Randall, C.P., K.R. Mariner, I. Chopra, and A.J. O'Neill. 2013. The target of daptomycin is absent from Escherichia coli and other gram-negative pathogens. *Antimicrob Agents Chemother*. 57:637-639.

Reyes, J., D. Panesso, T.T. Tran, N.N. Mishra, M.R. Cruz, J.M. Munita, K.V. Singh, M.R. Yeaman, B.E. Murray, Y. Shamoo, D. Garsin, A.S. Bayer, and C.A. Arias. 2015. A liaR deletion restores susceptibility to daptomycin and antimicrobial peptides in multidrug-resistant Enterococcus faecalis. *J Infect Dis*. 211:1317-1325.

Rizvi, M., J. Ahmad, F. Khan, I. Shukla, A. Malik, and H. Sami. 2015. Synergy of drug combinations in treating multidrug-resistant Pseudomonas aeruginosa. *Australas Med J*. 8:1-6.

Rubio, A., J. Moore, M. Varoglu, M. Conrad, M. Chu, W. Shaw, and J.A. Silverman. 2012. LC-MS/MS characterization of phospholipid content in daptomycin-susceptible and -resistant isolates of Staphylococcus aureus with mutations in mprF. *Mol Membr Biol*. 29:1-8.

Rybak, M.J., E. Hershberger, T. Moldovan, and R.G. Grucz. 2000. In vitro activities of daptomycin, vancomycin, linezolid, and quinupristin-dalfopristin against Staphylococci and Enterococci, including vancomycin- intermediate and -resistant strains. *Antimicrob Agents Chemother*. 44:1062-1066.

Saito, M., S.J. Korsmeyer, and P.H. Schlesinger. 2000a. BAX-dependent transport of cytochrome c reconstituted in pure liposomes. *Nat Cell Biol*. 2:553-555.

Saito, M., S.J. Korsmeyer, and P.H. Schlesinger. 2000b. BAX-dependent transport of cytochrome c reconstituted in pure liposomes. *Nat Cell Biol*. 2:553-555.

Sauermann, R., M. Rothenburger, W. Graninger, and C. Joukhadar. 2008. Daptomycin: a review 4 years after first approval. *Pharmacology*. 81:79-91.

Scott, W.R., S.B. Baek, D. Jung, R.E. Hancock, and S.K. Straus. 2007. NMR structural studies of the antibiotic lipopeptide daptomycin in DHPC micelles. *Biochim Biophys Acta*. 1768:3116-3126.

Seemann, T. 2014. Prokka: rapid prokaryotic genome annotation. *Bioinformatics*. 30:2068-2069.

Silverman, J.A., N.G. Perlmutter, and H.M. Shapiro. 2003. Correlation of daptomycin bactericidal activity and membrane depolarization in Staphylococcus aureus. *Antimicrob Agents Chemother*. 47:2538-2544.

Souza, C., Y.V. Faria, O. Sant'Anna Lde, V.G. Viana, S.H. Seabra, M.C. Souza, V.V. Vieira, R. Hirata Junior, O. Moreira Lde, and A.L. Mattos-Guaraldi. 2015. Biofilm production by

multiresistant Corynebacterium striatum associated with nosocomial outbreak. *Mem Inst Oswaldo Cruz*. 110:242-248.

Srinivasan, A. 2017. Antibiotic stewardship: Why we must, how we can. *Cleve Clin J Med*. 84:673-679.

Srinivasan, A., and L.E. Davidson. 2017. Improving Patient Safety Through Antibiotic Stewardship: The Veterans Health Administration Leads the Way, Again. *Infect Control Hosp Epidemiol*. 38:521-523.

Staubitz, P., H. Neumann, T. Schneider, I. Wiedemann, and A. Peschel. 2004. MprF-mediated biosynthesis of lysylphosphatidylglycerol, an important determinant in staphylococcal defensin resistance. *FEMS Microbiol Lett*. 231:67-71.

Straus, S.K., and R.E. Hancock. 2006. Mode of action of the new antibiotic for Gram-positive pathogens daptomycin: comparison with cationic antimicrobial peptides and lipopeptides. *Biochim Biophys Acta*. 1758:1215-1223.

Szoka, F., Jr., and D. Papahadjopoulos. 1978. Procedure for preparation of liposomes with large internal aqueous space and high capture by reverse-phase evaporation. *Proc Natl Acad Sci U S A*. 75:4194-4198.

Taylor, R., D. Beriashvili, S. Taylor, and M. Palmer. 2017a. Daptomycin Pore Formation Is Restricted by Lipid Acyl Chain Composition. *ACS Infect Dis*.

Taylor, R., D. Beriashvili, S. Taylor, and M. Palmer. 2017b. Daptomycin Pore Formation Is Restricted by Lipid Acyl Chain Composition. *ACS Infect Dis*. 3:797-801.

Taylor, R., K. Butt, B. Scott, T. Zhang, J.K. Muraih, E. Mintzer, S. Taylor, and M. Palmer. 2016. Two successive calcium-dependent transitions mediate membrane binding and oligomerization of daptomycin and the related antibiotic A54145. *Biochim Biophys Acta*. 1858:1999-2005.

Taylor, S.D., and M. Palmer. 2016. The action mechanism of daptomycin. *Bioorg Med Chem*. 24:6253-6268.

Teatero, S., A. McGeer, A. Li, J. Gomes, C. Seah, W. Demczuk, I. Martin, J. Wasserscheid, K. Dewar, R.G. Melano, and N. Fittipaldi. 2015. Population Structure and Antimicrobial Resistance of Invasive Serotype IV Group B Streptococcus, Toronto, Ontario, Canada. *Emerg Infect Dis*. 21:585-591.

Teo, J., T.P. Lim, L.Y. Hsu, T.Y. Tan, S. Sasikala, P.Y. Hon, A.L. Kwa, and A. Apisarnthanarak. 2015. Extensively drug-resistant Acinetobacter baumannii in a Thai hospital: a molecular epidemiologic analysis and identification of bactericidal Polymyxin B-based combinations. *Antimicrob Resist Infect Control*. 4:2.

Tran, T.T., S. Jaijakul, C.T. Lewis, L. Diaz, D. Panesso, H.B. Kaplan, B.E. Murray, A. Wanger, and C.A. Arias. 2012. Native valve endocarditis caused by Corynebacterium striatum with heterogeneous high-level daptomycin resistance: collateral damage from daptomycin therapy? *Antimicrob Agents Chemother*. 56:3461-3464.

Tran, T.T., D. Panesso, N.N. Mishra, E. Mileykovskaya, Z. Guan, J.M. Munita, J. Reyes, L. Diaz, G.M. Weinstock, B.E. Murray, Y. Shamoo, W. Dowhan, A.S. Bayer, and C.A. Arias. 2013. Daptomycin-resistant Enterococcus faecalis diverts the antibiotic molecule from the division septum and remodels cell membrane phospholipids. *MBio*. 4.

Trapnell, C., D.G. Hendrickson, M. Sauvageau, L. Goff, J.L. Rinn, and L. Pachter. 2013. Differential analysis of gene regulation at transcript resolution with RNA-seq. *Nat Biotechnol*. 31:46-53.

Trapnell, C., B.A. Williams, G. Pertea, A. Mortazavi, G. Kwan, M.J. van Baren, S.L. Salzberg, B.J. Wold, and L. Pachter. 2010. Transcript assembly and quantification by RNA-Seq reveals unannotated transcripts and isoform switching during cell differentiation. *Nat Biotechnol*. 28:511-515.

Vanessa M. D'Costa, K.M.M., Donald W. Hughes, Gerard D. Wright. 2006. Sampling the Antibiotic Resistome. *Science*. 311:374-377.

Walker, B.J., T. Abeel, T. Shea, M. Priest, A. Abouelliel, S. Sakthikumar, C.A. Cuomo, Q. Zeng, J. Wortman, S.K. Young, and A.M. Earl. 2014. Pilon: an integrated tool for comprehensive microbial variant detection and genome assembly improvement. *PLoS One*. 9:e112963.

Wang, J., Y. Wang, X. Du, J. Cui, K. Wang, L. Zhang, and Y. Han. 2016. Rapid transmission of multidrug-resistant Corynebacterium striatum among susceptible patients in a tertiary hospital in China. *J Infect Dev Ctries*. 10:1299-1305.

Wang, W., Z. Wei, T.W. Lam, and J. Wang. 2011. Next generation sequencing has lower sequence coverage and poorer SNP-detection capability in the regulatory regions. *Sci Rep*. 1:55.

Weis, F., A. Beiras-Fernandez, and G. Schelling. 2008. Daptomycin, a lipopeptide antibiotic in clinical practice. *Curr Opin Investig Drugs*. 9:879-884.

Werth, B.J., W.O. Hahn, S.M. Butler-Wu, and R.M. Rakita. 2016. Emergence of High-Level Daptomycin Resistance in Corynebacterium striatum in Two Patients with Left Ventricular Assist Device Infections. *Microb Drug Resist*. 22:233-237.

Wong, K.Y., Y.C. Chan, and C.Y. Wong. 2010. Corynebacterium striatum as an emerging pathogen. *J Hosp Infect*. 76:371-372.

Y Tang, K.I., L Hong T Ishizone, H Yokoyama. 2016 Tunable thermoresponsive mesoporous block copolymer. *Macromolecules*. 49:7886-7896.

Yang, S.J., N.N. Mishra, A. Rubio, and A.S. Bayer. 2013. Causal role of single nucleotide polymorphisms within the mprF gene of Staphylococcus aureus in daptomycin resistance. *Antimicrob Agents Chemother*. 57:5658-5664.

Yang, S.J., C.C. Nast, N.N. Mishra, M.R. Yeaman, P.D. Fey, and A.S. Bayer. 2010. Cell wall thickening is not a universal accompaniment of the daptomycin nonsusceptibility phenotype in Staphylococcus aureus: evidence for multiple resistance mechanisms. *Antimicrob Agents Chemother*. 54:3079-3085.

Yao, F., J. Coquery, and K.A. Le Cao. 2012. Independent Principal Component Analysis for biologically meaningful dimension reduction of large biological data sets. *BMC Bioinformatics*. 13:24.

Yoneda, A., W.R. Henson, N.K. Goldner, K.J. Park, K.J. Forsberg, S.J. Kim, M.W. Pesesky, M. Foston, G. Dantas, and T.S. Moon. 2016. Comparative transcriptomics elucidates adaptive phenol tolerance and utilization in lipid-accumulating Rhodococcus opacus PD630. *Nucleic Acids Res*. 44:2240-2254.

Zhang, T., J.K. Muraih, B. MacCormick, J. Silverman, and M. Palmer. 2014a. Daptomycin forms cation- and size-selective pores in model membranes. *Biochim Biophys Acta*. 1838:2425-2430.

Zhang, T., J.K. Muraih, E. Mintzer, N. Tishbi, C. Desert, J. Silverman, S. Taylor, and M. Palmer. 2013. Mutual inhibition through hybrid oligomer formation of daptomycin and the semisynthetic lipopeptide antibiotic CB-182,462. *Biochim Biophys Acta*. 1828:302-308.

Zhang, T., J.K. Muraih, N. Tishbi, J. Herskowitz, R.L. Victor, J. Silverman, S. Uwumarenogie, S.D. Taylor, M. Palmer, and E. Mintzer. 2014b. Cardiolipin prevents membrane translocation and permeabilization by daptomycin. *J Biol Chem*. 289:11584-11591.

Chapter 4: Conclusion

This dissertation set out to answer four crucial questions about the biology of daptomycin. 1) How do bacteria become hyper-resistant to daptomycin? 2) What is the *in vivo* membrane target of daptomycin? 3) How does daptomycin interact with the membrane? 4) What is daptomycin's mechanism of killing? In our first paper (Chapter 2), we conclude that *C. striatum*, an emerging commensal opportunistic pathogen, develops high-level daptomycin resistance through the rapid adaptive evolution of loss-of-function *pgsA2* (PG synthase) mutations. This mutation, in any variation that results in loss of function, results in the significant loss or removal of membrane PG, which is necessary and sufficient for high-level daptomycin resistance (HLDR) in *C. striatum*. HLDR leads to catastrophic daptomycin treatment failure in patients. No additional genomic or transcriptomic compensation mechanisms are evident for the evolved HLDR phenotype. The HLDR mutants also have no changes in cell wall thickness, cell surface charge, conversion of PG to cardiolipin, or membrane shape, which are all previously implicated mechanisms in lower-level daptomycin resistance. (Bayer et al., 2015; Bayer et al., 2016; Bayer et al., 2014; Bayer et al., 2013; D'Costa et al., 2012; Gaupp et al., 2015; Mishra et al., 2015; Mishra et al., 2009; Quinn et al., 2007; Raad et al., 2007; Reyes et al., 2015; Vanessa M. D'Costa, 2006; Zhang et al., 2014) Rebalancing of membrane composition to include more PI in the absence of PG as observed by lipidomic profiling likely results in membrane stability. *C. striatum*'s ability to completely remove PG from its membrane, with simple loss-of-function point mutations in PG synthase, further demonstrates that PG is the *in vivo* and *in vitro* target of daptomycin. These data give a clear identification of daptomycin's *in vivo* membrane target, as well as the mechanism of high-level daptomycin resistance development in bacteria.

We were able to answer both these questions effectively; however, several mechanisms remained unclear. All of the evidence (genomic, transcriptomic and lipidomic) suggest that there is only one mutation, the loss-of-function mutation in *pgsA2*, that is essential; however, all attempts to knock the gene out have been unsuccessful, due in large part to *C. striatum* not being a model organism with robust genetic tools that would allow us to effectively manipulate its genome. Given the importance of *C. striatum* as a potential model organism for screening future lipopeptide antibiotics, new genetic tools should be developed to more intensely interrogate gene function. Additionally, while we were able to demonstrate that *C. striatum* can survive incredible shifts in membrane composition, it remains unclear how. Future experiments should focus on characterizing the metabolic activity of the proteins involved in the various lipid synthesis pathways of *C. striatum*. Specifically, it will be necessary to identify how Glua-Dag, CDP-DAG and PI metabolism shifts during the transition between WT to HLDR, as well as after HLDR is established. Finally, it is critical to understand whether the mutations that lead to HLDR are endemic in the population of *C. striatum*, or if HLDR is as a result of an unknown or uncharacterized stress response that randomly inserts these mutations into the genome.

In our second paper (Chapter 3) we identify how daptomycin interacts with the membrane, and daptomycin's mechanism of killing bacteria. Based on our data, we concluded that when daptomycin binds to the cell membrane, it stably integrates into the membrane in a calcium- and phosphatidylglycerol (PG)-dependent manner, at a defined ~1:1 ratio of PG to daptomycin. It then recruits or colocalizes with other daptomycin molecules to form stable pores with an approximate Stokes radius of 8 nm. The resulting pore allows cytoplasmic metabolites, ions and other intracellular components to leave the cell. When a high enough concentration of PG is present in

bacterial membranes, enough daptomycin pores can be formed to release biologically essential metabolites, ultimately killing the cell.

Further work will be needed to characterize the structure and formation of the pore *in vivo*, establish an upper limit on the size of expelled metabolites, and determine how daptomycin co-localizes for pore formation once it has integrated into the membrane. To characterize the structure of the pore, Cryo-EM, membrane NMR, or small angle x-ray diffraction could be employed. All three methods could be effectively carried out using *in vitro* model systems such as liposomes. Cryo-EM could determine the structure of pores using a more biologically relevant model, daptomycin-susceptible *C. striatum*. Establishing the structure of the pore would allow us to establish the size of the channel and unequivocally point to large pore formation as the mechanism of killing. Alternatively, matrix-assisted laser desorption/ionization time-of-flight (MALDI-TOF) could be employed to establish the upper limit of the size of metabolites or proteins leaking out of the pore, giving a biologically relevant determination of the size of biological material leaving the inside of the bacterial cell. One drawback of our original experiment looking at differential metabolite leakage was that it was optimized for small molecular weight metabolites, which prevent us from establishing the upper limit of the pore size. MALDI-TOF could address this issue. Finally, it is essential to understand how daptomycin forms pores once daptomycin molecules have bound and integrated into the membrane. The rapid nature of daptomycin activity *in vitro* makes this difficult to visualize or measure. One solution is to develop computational models that generate the membrane and daptomycin dynamics over a larger timescale. A drawback to this technique is the cost of computing power and the time necessary to render membrane dynamics, even on the nanosecond scale. Attempts to use fluorescent probes *in vitro* and *in vivo* to determine how daptomycin co-localizes and forms a pore have yielded unsatisfying results. The addition of

these probes often interferes with the activity of daptomycin, rendering the data uninformative or speculative at best. New techniques to study peptide-lipid interaction in membranes will be required to understand how daptomycin transitions from integration to pore formation without the use of fluorescence.

Appendix 1: Comparative transcriptomics elucidates adaptive phenol tolerance and utilization in lipid-accumulating *Rhodococcus opacus* PD630

Aki Yoneda[1,2,†], William R. Henson[3,†], Nicholas K. Goldner[2], Kun Joo Park[3], Kevin J. Forsberg[2] , Soo Ji Kim[3], Mitchell W. Pesesky[2], Marcus Foston[3], Gautam Dantas[1, 2, 4, 5,*] and Tae Seok Moon[3,*]

[1] Department of Pathology and Immunology, Washington University in St. Louis School of Medicine, St. Louis, MO, 63108, USA

[2] Center for Genome Sciences and Systems Biology, Washington University in St. Louis School of Medicine, St. Louis, MO, 63108, USA

[3] Department of Energy, Environmental & Chemical Engineering, Washington University in St. Louis, St. Louis, MO, 63130, USA

[4] Department of Biomedical Engineering, Washington University, St Louis, MO, 63130, USA

[5] Department of Molecular Microbiology, Washington University School of Medicine, St. Louis, MO, 63108, USA

† The authors wish it to be known that, in their opinion, the first two authors should be regarded as joint First Authors.

A1.1 Abstract

Lignin-derived (e.g. phenolic) compounds can compromise the bioconversion of lignocellulosic biomass to fuels and chemicals due to their toxicity and recalcitrance. The lipid-accumulating bacterium *Rhodococcus opacus* PD630 has recently emerged as a promising microbial host for lignocellulose conversion to value-added products due to its natural ability to tolerate and utilize phenolics. To gain a better understanding of its phenolic tolerance and utilization mechanisms, we adaptively evolved *R. opacus* over 40 passages using phenol as its sole carbon source (up to 373% growth improvement over wild-type), and extensively characterized two strains from passages 33

and 40. The two adapted strains showed higher phenol consumption rates (~20 mg/l/h) and ~2-fold higher lipid production from phenol than the wild-type strain. Whole-genome sequencing and comparative transcriptomics identified highly-upregulated degradation pathways and putative transporters for phenol in both adapted strains, highlighting the important linkage between mechanisms of regulated phenol uptake, utilization, and evolved tolerance. Our study shows that the R. opacus mutants are likely to use their transporters to import phenol rather than export them, suggesting a new aromatic tolerance mechanism. The identified tolerance genes and pathways are promising candidates for future metabolic engineering in R. opacus for improved lignin conversion to lipid-based products.

A1.2 Introduction

Lignocellulosic biomass, comprised of cellulose, hemicellulose and lignin (1,2), remains an underutilized substrate in sustainable microbial production of fuels and chemicals (3–6). One main challenge is that current biorefinery pretreatment approaches release diverse toxic degradation compounds from lignin during conversion of lignocellulosic biomass to fermentable sugars (7). These lignin degradation compounds include a wide array of phenolics that can severely inhibit microbial production of fuels or chemicals, leading to lower yields (8). Currently, unconverted lignin is typically burned to provide thermal energy onsite, but the amount of waste lignin is predicted to escalate as lignocellulose-based biorefinery output increases (4,9,10).

Lignin, the second most abundant terrestrial polymer, constitutes ~15–30% of lignocellulose (11) and is more energy dense than cellulose and hemicellulose due to its higher carbon-to-oxygen ratio. Unfortunately, lignin is much more difficult to depolymerize due to its complex molecular

structure. Structural heterogeneity also leads to a broad spectrum of breakdown products, substantially compromising the efficiency of chemical catalysis approaches for product synthesis and purification. Some bacteria and fungi can consume lignin breakdown products and utilize them as carbon sources (12), potentiating fuel and chemical production via lignin consolidated bioprocessing (13–15). One such bacterium, Rhodococcus opacus, is a promising microbial host for converting lignocellulose to useful products due to its naturally robust lipid production and ability to both tolerate and metabolize diverse phenolic compounds (14,16–18).

Rhodococcus strains are found in diverse environments (19,20) and can tolerate environmental stresses such as desiccation and high salinity (21,22) as well as chemical stresses such as high concentrations of butanol (23,24). Often isolated from polluted or contaminated environmental samples (25,26), R. opacus strains have a strong innate tolerance to benzene, toluene and lignocellulosic hydrolysates from different sources (27,28) and can metabolize aromatic compounds (14,16). Rhodococcus species can convert aromatics to acetyl-CoA and succinyl-CoA (12,29), which are important precursors for converting phenolics to bioproducts (30). Originally isolated from soil at a gas works plant, R. opacus PD630 (hereafter R. opacus unless specified) is known to accumulate large amounts of the biodiesel precursors triacylglycerols (TAGs, up to 76% of cell dry weight) when using sugars as a carbon source. Thus, R. opacus has been a target strain for commercial-scale lipid production using sugars derived from lignocellulose (18,31–34).

Growth inhibition by toxic compounds (either end-product or feedstock) is a major limiting factor for commercialization of biochemical processes (35,36). Developing production hosts with natural

tolerance to toxic inhibitors may significantly reduce time and efforts for host optimization. The tolerance capabilities of R. opacus are hypothesized to come from its highly hydrophobic cell wall (22) and/or its ability to consume a diverse array of compounds (20), but few studies have directly investigated phenolic tolerance mechanisms in this organism. While we have recently explored the central metabolism in wild-type (WT) R. opacus and found simultaneous utilization of glucose and phenol (i.e. no catabolite repression) using 13C-metabolite fingerprinting (37), more work is necessary to thoroughly characterize the catabolic pathways of aromatic compounds and global metabolism to elucidate tolerance mechanisms in R. opacus.

In this study, we adaptively evolved increased phenol tolerance of R. opacus by sequentially sub-culturing in phenol as a sole carbon source and screening fast-growing mutants over 40 passages. We selected phenol as a model lignin degradation product to avoid the confounding effects of many compounds present in heterogeneous lignin degradation product streams. Phenol has a shared substructure to many of the compounds that can be derived from lignin (38), and it also has a similar level of toxicity to that of other compounds derived from lignin (39,40).

Even though previous studies have demonstrated bioconversion of lignocellulose-derived compounds into lipids by R. opacus (14,27,40–44), the connection between the tolerance phenotype and specific cellular mechanisms remains elusive. Here, we present a combined adaptive evolution/omics approach leveraging multiple phenol-adapted strains to identify possible mechanisms for phenolic tolerance and utilization in R. opacus (Supplemental Figure A1.1). This approach builds on previous studies by examining multiple paths to phenolic tolerance from the

same strain background and resolving these tolerance strategies by comparing the transcriptomic response in different growth conditions. We performed adaptive evolution of R. opacus on increasing concentrations of phenol to select for increasingly tolerant strains and identified two high-performing strains through in-depth phenotyping. Next, we performed whole-genome sequencing of the selected strains to identify genomic alterations during adaptive evolution and employed comparative transcriptomics to identify transcriptional changes between strains in different growth conditions (i.e. in glucose and different concentrations of phenol). This approach proved to be effective in gaining insights into tolerance mechanisms and identifying promising gene candidates that can facilitate future metabolic engineering efforts in Rhodococcus to produce fuels and chemicals directly from lignin breakdown products or from lignocellulosic hydrolysates rich in toxic lignin degradation compounds.

A1.3 Materials and Methods

A1.3.1 Adaptive evolution

To increase the strain's tolerance to phenol, R. opacus PD630 was adapted to grow in increasing concentrations of phenol for 40 successive subcultures. To start the experiment, the WT strain was grown in 2 ml of 0.3 g/l phenol for 2 days, and then subcultured at 0.3 g/l phenol with an initial OD600 of 0.03 during the first 10 subcultures. Once the culture reached an OD600 of 0.3 within 24–36 h, the phenol concentration was increased in increments of 0.25 g/l up to a final concentration of 1.5 g/l phenol. Frozen stocks of each subculture were saved for later testing. To pick phenol-tolerant strains, frozen stocks from intermediate subcultures were streaked onto minimal media plates supplemented with 1.5% agar containing 0.3 g/l phenol. From three of the intermediate subcultures (17, 26 and 33) and the final subculture (40), six colonies were picked

for growth screening and lipid assays in 96 well plates. The two fastest growing strains with best lipid productivities (named evol33 and evol40) were chosen from this screening for further analysis.

A1.3.2 Lipid assay

The two best performing strains were chosen for lipid assays using Nile red. Growth experiments were started with single colonies from LB plates, and cells were cultured in 2 ml of 0.3 g/l phenol in a 50 ml glass tube for 36–48 h. Next, 2 ml of cells was subcultured in 10 ml of 0.3 g/l phenol for 24 h in a 50 ml glass tube. Next, 10 ml of cells was added to 140 ml of 0.3 g/l phenol in a 250 ml flask and grown for 24 h. Cells were centrifuged at 3000 x g for 10 min, resuspended in carbon- and nitrogen-free media, and then each condition (1 g/l glucose, 0.75 g/l phenol or 1.5 g/l phenol) was tested for each strain with an initial OD600 = 0.3 in low nitrogen conditions (0.05 g/l (NH4)2SO4) at a 10 ml volume in a 50 ml glass culture tube. Cells were stained by Nile red according to the reported method (45) with some modifications. Briefly, 200 µl of cell culture was stored in 20% DMSO at −20°C until staining. For staining, cells were centrifuged at 1000 x g and room temperature for 3 min and resuspended in 200 µl of 1x PBS. 5 µl of 1 mM Nile red in DMSO was added to each sample in a 96-well plate, which was subsequently incubated in the dark at room temperature for 30 min. The plate was wrapped in foil, centrifuged at 1000 x g for 3 min and washed twice with 0.9% NaCl solution. Flow cytometry analysis was performed using a Millipore Guava EasyCyte High Throughput flow cytometer with a 488 nm excitation laser and a 575 nm emission filter. For all data, at least 5000 events were collected and gated by forward and side scatter. Samples were stained and analyzed on the same day to decrease variability. FlowJo (TreeStar Inc.) was used to obtain the arithmetic mean of the Nile red fluorescence distributions of stained cells, and the autofluorescence of unstained cells was subtracted from each measurement

value. Because of differences in lag phases between strains, the lipid productivity was calculated as the average change in Nile red fluorescence (per cell per time) between at least four time points taken from the exponential to the stationary phase.

A1.3.3 Illumina library preparation

A protocol adapted from Bowman et al. and Fisher et al. (46,47) was used to generate Illumina sequencing libraries. Double-stranded cDNA (for RNA-Seq) or genomic DNA (for whole genome sequencing) in 50 µl elution buffer (Qiagen) was fragmented to 200–400 bp using Covaris E-220 and microTUBEs at a recommended setting by Covaris. ~50 µl of fragmented DNA in Buffer EB (Qiagen) was recovered from Covaris tubes and transferred to a semi-skirted 96-well polymerase chain reaction (PCR) plate. 20 µl of end repair mix (7 µl 10x T4 ligase buffer, 2.8 µl 10 mM dNTPs, 3.5 µl T4 polymerase, 3.5 µl T4 polynucleotide kinase, 0.7 µl Escherichia coli DNA polymerase I and 2.5 µl nuclease-free water; all enzymes were purchased from NEB) was added to the fragmented DNA to blunt and phosphorylate the ends at room temperature for 30 min. 130 µl of AMPure XP beads (Agencourt) were added to each well to remove reagents from the previous step. The 96-well plate was placed on a magnetic plate after pipetting thoroughly to mix, and supernatant was discarded when it became clear. The beads with DNA on the walls of 96 wells were washed with 150 µl 80% ethanol once, before eluting the DNA with 32 µl of water. 18 µl of dA-tailing mix (5 µl 10x NEBuffer 2, 1 mM dATP and 3 µl Klenow fragment (3′-5′ exo-)) was added to the beads with eluted DNA to add a dA-tail at 37ºC for 30 min. After dA-tailing, 110 µl of 20% polyethylene glycol (PEG) 8000 in 2.5 M NaCl was used to precipitate DNA onto the magnetic beads. The plate was placed on a magnet again to collect DNA and washed with 80% ethanol. Barcoded adapters were added to the eluted DNA (20.5 µl water added to DNA with beads) to a 10:1 molar ratio, and 6.5 µl of ligation mix was added to ligate adapters at room

temperature for 20 min. 21 µl of 20% PEG in 2.5 M NaCl was added to precipitate DNA onto the beads, and two barcoded samples were pooled after washing for elution. Adapter-ligated DNA was then PCR-amplified using KAPA HiFi Hot start Readymix (KAPA Biosystems) and gel purified using a Zymoclean Gel DNA Recovery Kit (Zymo Research). The resulting purified DNA samples were quantified using a Qubit DNA HS kit, combined and diluted with Buffer EB to yield a 10 nM pool. 20 µl of the pool was submitted to HiSeq-2500 sequencing at the Center for Genome Sciences & Systems Biology, Washington University in St. Louis School of Medicine. For other details regarding DNA and RNA preparations, see Supplemental Materials and Methods.**A1.3.4**

A1.3.4 Genome sequencing and SNP analysis

Raw Illumina reads were demultiplexed by barcodes and trimmed using an in-house Python script, and mapped to an indexed genome of R. opacus (both annotated supercontigs maintained by Broad Institute (Genbank#ABRH01000000 (20)) and the finished genome by Chinese Academy of Science (ASM59954v1 (48)) using Bowtie2 (49). The mapped SAM files were converted to sorted BAM files with BAM index files using SAMtools (50,51). SNPs and possible indels were analyzed using Pilon (52). SNPs that were also found in the WT strain were filtered out using an in-house Python script (see Supplemental Computational Methods). Additionally, MIRA (53) was used to confirm SNPs and indels predicted by Pilon. In addition to utilizing MIRA's SNP detection function, we performed de novo-assembly of a genome for each strain using MIRA. Assembled genomes were then used to further confirm presence or absence of SNPs in each strain. This deep sequencing confirmation eliminated SNPs that were inconsistently found due to Illumina sequencing errors or biases during Illumina preparations. Table Table1A1A shows all SNPs found in evolved strains and not in WT.

A1.3.5 RNA-Seq data analysis

After demultiplexing and trimming, raw Illumina reads were mapped to an indexed genome of R. opacus (both annotated supercontigs (20) and the finished genome (48)) using Bowtie2 (49). The mapped SAM files were converted to sorted BAM files with BAM index files using SAMtools (50,51). FeatureCounts (54) was used to count the number of reads per coding sequence, and the raw result was used for differential expression analysis using DESeq2 (55) as implemented in the R software package.

A1.4 Results

A1.4.1 Adaptive evolution of *R. opacus* PD630 using phenol as a sole carbon source

In the adaptive evolution approach, we increased phenol concentrations in a minimal salts medium (MSM) over time to select for the fastest growing strains using phenol as a sole carbon source (Supplemental Figure S1). Growth of the WT strain on phenol was characterized by a lag phase that increases with higher concentrations of phenol (Figure A1). To prevent long lag phases in adapted strains, cells were grown in non-inhibitory concentrations of phenol for the initial rounds of selection before increasing to inhibitory phenol concentrations. Serial transfers were performed when exponential phase was reached (optical density at 600 nm (OD600) of ~0.3). For the total adaptive evolution experiment (40 serial passages), the estimated cumulative cell divisions (56) were ~6 × 109, assuming four doublings per subculture and an initial cell concentration of ~1 × 107 CFU/ml (colony forming unit per ml; initial OD600 of ~0.03 was experimentally determined to be ~1 × 107 CFU/ml). Over the course of the 40 serial transfers (~200 generations), six colonies each from passages 17, 26, 33 and 40 (total of 24 colonies) were randomly selected for high-throughput phenotypic screening, along with WT (Supplemental Figure A1.1). We chose the two best-performing phenol-adapted strains based on improved growth rate, biomass yields and lipid

yields: one derived from passage 33 (named evol33) and the other from passage 40 (evol40). These two adapted strains were subjected to further phenotypic characterization (i.e. growth profiles and lipid accumulation assay), deep whole-genome sequencing and comparative transcriptomic profiling by RNA-Seq.

A1.4.2 Phenotypic characterization of phenol-adapted strains

To characterize improvements in tolerance from adaptive evolution, both adapted and WT strains were cultivated in a range of concentrations of phenol (Figure A1.1). We characterized phenol tolerance by comparing growth rates, final biomass accumulation (OD600), lag phases and estimated IC50 (half maximal inhibitory concentration; Supplemental Figure A1.2). The adapted strains evol33 and evol40 had 20% and 24% higher IC50 values than WT, respectively, after 45 h of culture ($P < 0.001$ for both evol33 and evol40, one mean, two-tailed Student's t-test). Both adapted strains also reached 22–373% higher cell densities ($P < 0.05$) than WT in all concentrations of phenol tested where growth was observed (0.75–2 g/l), with evol33 and evol40 having a 92% and 102% increase in OD600 at 1.5 g/l ($P = 0.0005$ and $P = 0.0002$, respectively; Supplemental Table A1.1). The lag phase of the adapted strains was 17–54% shorter compared to that of the WT strain, with evol33 showing a 46% shorter lag phase at 1.5 g/l ($P = 0.029$) and evol40 showing a 34% shorter lag phase compared to WT ($P = 0.054$; Supplemental Table A1.2). The adapted strains also demonstrated significant growth rate increases at intermediate concentrations of phenol, with 30% and 38% increases in growth rates at 1.5 g/l for evol33 ($P = 0.03$) and evol40 ($P = 0.04$), respectively (Supplemental Table A1.3). When cells were grown in 1.5 g/l phenol, we also observed significantly higher phenol consumption rates in the adapted strains compared to the WT strain ($P = 0.002$ and $P = 0.003$ for evol33 and evol40, respectively), suggesting that phenol uptake, consumption and growth are related (Supplemental Figure A1.3).

To determine whether adaptive evolution affected lipid accumulation, we measured lipid amounts under nitrogen-limited conditions using either glucose or phenol as a sole carbon source (Figure A1.2 and Supplemental Table A1.4). WT R. opacus accumulates intracellular lipids in the form of TAGs under nitrogen limitation in the stationary phase (18). Strains were grown in 1 g/l glucose ('glucose'), 0.75 g/l phenol ('low phenol') or 1.5 g/l phenol ('high phenol') as sole carbon sources. Relative lipid amounts at different time points were estimated by staining cells with Nile red and measuring single cell fluorescence, which has been used to characterize total lipid contents in many oleaginous organisms (15,45) and correlates well with total lipid content (Supplemental Figure A1.4). Peak lipid accumulation occurs in the mid-stationary phase, followed by a decrease in lipid contents due to lipid consumption caused by extended carbon starvation. Because cells would be harvested at peak lipid accumulation for an industrial-scale process, we used the maximum Nile red fluorescence in the stationary phase to compare the lipid titer (Supplemental Table A1.4) between strains. The adapted strains showed similar maximum Nile red fluorescence to that of the WT strain when grown in glucose ($P = 0.1$ and $P = 0.09$ for evol33 and evol40, respectively). In contrast, when grown in low phenol, evol33 and evol40 showed a 2.5-fold ($P = 5 \times 10{-}5$) and 1.9-fold ($P = 0.001$) increase in maximum Nile red fluorescence compared to WT, respectively (Supplemental Table A1.4). The adapted strains also showed high lipid accumulation in high phenol (Supplemental Table A1.4 and Supplemental Figure A1.5). In addition to titer, productivity is also an important factor for industrial scale processes, and we compared lipid productivity between strains by examining the average increase in Nile red fluorescence over time in exponential to stationary phase (Figure A1.2, Supplemental Table A1.5, and Supplemental Figure A1.5). Here, we define lipid productivity as the lipid amount per cell per unit time. In glucose, all

three strains showed similar lipid productivities ranging from 7.8 to 8.4 arbitrary unit (a.u.) h−1. While the WT strain demonstrated a lower lipid productivity in low phenol (5.8 a.u. h−1), the adapted strains showed similar or higher lipid productivities in low phenol compared to glucose conditions (13.6 and 8.9 a.u. h−1 for evol33 and evol40, respectively). Compared to the WT strain, evol33 and evol40 has a 2.3- and 1.5-fold increase in lipid productivity in low phenol. The adapted strains also had higher lipid productivity in high phenol compared to glucose conditions (16.5 a.u. h−1, $P = 0.001$ for evol33; and 19.4 a.u. h−1, $P = 0.0001$ for evol40). These results prompted us to further characterize these strains using whole-genome sequencing and RNA-Seq.

A1.4.3 Deep whole-genome sequencing of phenol-adapted strains

We sequenced the genomes of phenol-adapted R. opacus strains evol33 and evol40 along with the original wild-type strain to > 90X-coverage. For a reference genome, we used both annotated supercontigs maintained by the Broad Institute (Genbank # ABRH01000000 (20); OPAG_#s) and the finished genome by the Chinese Academy of Science (ASM59954v1 (48); LPD#s). Contrary to our initial expectations, there were no single nucleotide polymorphisms (SNPs) or insertion/deletions (indels) in promoter regions, transcriptional regulators, or sensors. In fact, the numbers of mutations were low, and when excluding mutations that were found in WT as well, there were only three consistent mutations (which were not due to sequencing errors) in evol40 and four mutations in evol33. While we explored the possibility of large duplications as genomes of Rhodococcus species are known to contain duplications (57–59), we could not obtain consistent large duplication prediction based on short read sequencing only. The three common point mutations shared in the genomes of both evol33 and evol40 (Table A1.1A) are the following: LPD03112, annotated as ‘cytochrome c oxidase/cytochrome aa3 quinol oxidase’, contained a Phe to Ser mutation at amino acid position 335. LPD03747, annotated as ‘dicarboxylate carrier

protein/citrate transporter/MFS transporter', contained an Ile296 to Phe mutation. The third shared mutation occurred in OPAG_05248, which is annotated as 'acyl-CoA thioesterase II', and had a silent mutation of G to A (Phe120) when mapped to the supercontigs (20). When mapped to the complete genome (48), however, this mutation occurred in an intergenic region between LPD04711 and LPD04712 (Table A1.1A). Regardless of the annotations, overall reads mapped to this region were very low (reads per kilobase of transcript per million reads (rpkm) 0–10) and not phenol-responsive (Table A1.1B,C),suggesting caution when considering the biological implication of this mutation. evol33 additionally had a gene LPD00118 with a SNP; this gene is annotated as '4-hydroxyphenylacetate permease/MFS transporter' (Gly162 to Val). Given two transporter/permease genes containing consistently found SNPs, these results suggest that adapted strains have altered transport of phenol or related compounds.

A1.4.4 Transcriptomic analysis of phenol-adapted strains

A1.4.4.1 Stress adaptation in evol33 and evol40 compared to WT

To investigate tolerance mechanisms further, we employed a comparative transcriptomic approach by sequencing ribosomal RNA-depleted total RNA from WT, evol33 and evol40 in the three medium conditions described in Materials and Methods. High phenol (1.5 g/l) was used for adapted strains only, since the wild-type strain did not reach adequate cell densities at this culture condition. High phenol condition data were used to assess whether the up- or downregulation of genes was phenol concentration-dependent. Three biological replicates of each strain and condition showed consistent gene expression results (Figure A1.3 and Supplemental Figure A1.7; in Figure A1.3, each square on a heat map represents a biological replicate). In addition to coping with the low nutrient-culture conditions (cells were grown in minimal media with low nitrogen to

promote lipid accumulation), cells came in contact with phenol, which is generally toxic to cell membranes and cellular macromolecules (60,61). As expected, multiple putative stress genes were upregulated due to nitrogen-limited growth conditions and the toxicity of phenol. Some of the annotated stress genes that were upregulated in all strains in phenol growth conditions were 'DNA protection during starvation protein' LPD04106, 'heat shock protein 20 homolog' LPD07748 and 'molecular chaperone DnaK' LPD02079 (Table A1.2 and Supplemental Table A1.6, Sheet 13). LPD04106 was highly expressed in glucose, but even more upregulated in low phenol in WT and evol40 (Table A1.2 and Supplemental Table A1.6). evol33 showed modest upregulation of LPD04106 (2.64-fold) in low phenol. In adapted strains in high phenol, expression levels of LPD04106 were similar to that of glucose (no change in evol33 and 1.3-fold downregulation in evol40). LPD07748 was highly upregulated in low phenol in all strains, but to a less extent in adapted strains in high phenol compared to low phenol (Table A1.2 and Supplemental Table A1.6). LPD02079 was 16-fold upregulated in WT in phenol, while it was 3.1- to 6.3- fold upregulated in adapted strains in phenol (Table A1.2 and Supplemental Table A1.6). These results suggest that adapted strains show less stress response to phenol-containing media than WT.

A1.4.4.2 Phenol degradation and utilization genes were highly upregulated in adapted strains

Genes that were more than 1024-fold upregulated in phenol compared to glucose across all strains were LPD06575 and LPD06576, which are annotated as 'flavin-dependent monooxygenase, reductase subunit/phenol monooxygenase reductase' and '4-hydroxyphenylacetate 3-monooxygenase', respectively. In addition to these two genes, LPD06740, LPD06741 and LPD06742 were also more than ~1000-fold upregulated in phenol in evol33 and evol40 (Figure A1.3, Table A1.2, and Supplemental Figure A1.8). LPD06740 and LPD06741 have high identity to LPD06575 and LPD06576, and are in the same orientation in tandem (Figure A1.4B).

LPD06742 is annotated as catechol 1,2-dioxygenase (Figures A1.3 and A1.4). WT did upregulate the LPD06740 operon in phenol, but the expression levels were 3- to 18-fold lower than that of the adapted strains (Figure A1.3, Table A1.2, and Supplemental Figure A1.8). LPD06575/LPD06740 and LPD6576/LPD06741 are likely to be small and large components of two-component phenol hydroxylase, where LPD06575/LPD06740 are flavin reductases and LPD6576/LPD06741 are NADH-dependent phenol hydroxylases, as there are reports of biochemically proven two-component phenol hydroxylases in other Rhodococcus species (62,63). Gene duplication of this region is also documented, and R. opacus strain 1CP is thought to have a third copy of the genes (59). Based on our transcriptional data, R. opacus appears to utilize both copies of the two-component phenol hydroxylase genes, but the adapted strains have the ability to upregulate the second copy (phenol degradation cluster #2; Figures A1.3 and A1.4B) more than the WT strain. Notably, the second copy of the phenol hydroxylase genes is directly upstream of a catechol 1,2-dioxygenase gene (Figure A1.4B), which is the first gene in the catechol branch of the β-ketoadipate pathway (Figure A1.4A; 12). Both copies were tightly regulated by the presence of phenol, and AraC-family transcriptional regulators are found in the same operons (Figures A1.3 and A1.4B). Moreover, other downstream genes in the β-ketoadipate pathway, such as muconolactone delta isomerase and muconate cycloisomerase, are upregulated more in the adapted strains, especially in high phenol (~2000-fold; Figures A1.3 and A1.4A), and they are located in the same operon as IclR-family regulators (LPD05454, LPD06569 and LPD06698; Figures A1.3 and A1.4A). We searched for genomic mutations near differentially regulated operons such as the phenol degradation cluster #2, but the closest SNP observed was over 2 Mbp upstream of differentially regulated genes in adapted strains, suggesting that the differential gene expression

could be affected by an indirect cause, such as intracellular concentrations of regulatory molecules or metabolites.

RNA-Seq also revealed that R. opacus upregulates the gentisate pathway of aromatic degradation and utilization when phenol concentration was elevated to 1.5 g/l, while predicted meta-cleavage aromatic degradation pathway genes and anaerobic aromatic degradation genes did not seem utilized (Supplemental Figures A1.9 and A1.10). These results strongly suggest that adapted strains efficiently detoxify phenol mainly via the ortho-cleavage pathway and utilize it as a carbon source through the β-ketoadipate pathway (12).

There are over 380 genes annotated as transcriptional regulators or regulatory proteins in R. opacus. Of those, ten genes are annotated as 'probable thc operon regulatory protein' (AraC-family transcriptional regulator). Of the ten genes, LPD06577, LPD06739 and potentially LPD06574 are putative regulators of the highly phenol-responsive phenol degradation genes based on the proximity of the genes to phenol degradation genes and expression profiles (Figure A1.3). A gene annotated as 'xylose repressor' (LPD06565) may be involved in regulating the β-ketoadipate pathway cluster #2 because it is co-regulated with the genes in the cluster. β-ketoadipate pathway operons seem to be associated with genes annotated as Pca regulon regulatory protein (IclR family transcriptional regulator; LPD05454, LPD06569 and LPD06698). Although the gentisate pathway operon was adjacent to an AraC-family transcriptional regulator (LPD03777), their expression patterns were not similar (Supplemental Figure A1.9). However, their expression patterns were similar to an annotated serine/threonine-protein kinase gene (LPD03770) downstream of the gentisate pathway genes (Supplemental Figure A1.9).

Genes most downregulated by phenol in WT were LPD02697 (NDMA-dependent methanol dehydrogenase/lactaldehyde reductase; >6500-fold downregulated) and two hypothetical protein genes downstream of LPD02697 (Table A1.2 and Supplemental Table A1.6, Sheet 14). Adapted strains did not show dramatic downregulation of this gene in low phenol, but did show strong downregulation in high phenol (Table A1.2 and Supplemental Table A1.6, Sheets 15-18). A homolog of LPD02697 is implicated in oligotrophic growth of Rhodococcus erythropolis N9T-4 (64). In all strains, methane monooxygenase component genes were among the most downregulated in phenol conditions.

When comparing the low phenol and glucose conditions in terms of global regulatory changes, evol33 had higher average levels of upregulation from fewer genes than WT and evol40, and both adapted strains had fewer downregulated genes than WT, which were also generally downregulated to a lesser extent than WT (Supplemental Tables A1.6 and A1.7 and Supplemental Figure A1.11).

A1.4.4.3 Upregulation of transporter genes in phenol

While genomic data suggested that phenol transport could be altered in the adapted strains, it did not give a complete picture about how the adapted strains could tolerate and utilize higher concentrations of phenol compared to WT. Significant expression differences were not observed between WT and adapted strains in transporter genes identified to have SNPs by whole-genome sequencing. However, a few other putative transporter genes were observed to have altered expression levels (Table A1.2 and Supplemental Table A1.6). We identified a highly upregulated gene in both adapted strains (401-fold and 102-fold upregulated in evol33 and evol40, respectively,

compared to 5-fold in WT in low phenol, and upregulated to higher degrees in high phenol in adapted strains), which is annotated as a shikimate transporter gene (LPD06699). Shikimate is a cyclohexene compound that is a precursor for aromatic amino acids, and it contains functional groups similar to many phenolic compounds derived from lignin (65). LPD07505, also annotated as a shikimate transporter, was 3.2-fold downregulated in WT in low phenol, but was upregulated in both low and high phenol in adapted strains, especially in evol33 (8.5-fold compared to glucose in high phenol; Table A1.2 and Supplemental Table A1.6). No other genes annotated as shikimate transporters showed similar upregulation patterns, and shikimate utilization genes were not upregulated in phenol (Supplemental Table A1.6, Sheet 12). Moreover, phenol was more quickly consumed by the adapted strains than WT (Supplemental Figure A1.3), suggesting that increased phenol uptake may play a role in phenol tolerance and utilization in R. opacus.

A1.4.4.4 Lipid biosynthesis and metabolism genes were differentially regulated in adapted strains.

R. opacus TadA is a heparin-binding hemagglutinin-like protein required for normal lipid droplet morphology, which is thought to colocalize with lipid droplets (48,66). Interestingly, the gene encoding TadA (LPD06283 (48,66)) was upregulated in phenol in all strains (Supplemental Table A1.6, Sheet 13; >24-fold in WT and >27-fold in evol33). This finding prompted us to speculate that lipid droplet morphology may be different in R. opacus strains depending on the carbon source. However, there was no marked change in size or number of lipid droplets when comparing cells in glucose to cells in phenol (Supplemental Figure A1.12). LPD05549, annotated as a fatty acid synthesis gene (FASI), was upregulated 33- to 64-fold in all strains in phenol compared to glucose. 8 out of the 11 genes annotated as stearoyl-CoA 9-desaturase or stearoyl-CoA 9-desaturase electron transfer partner genes were at least 4-fold upregulated in WT in phenol,

whereas 24 of the 45 genes annotated as fatty acid –CoA ligase were greater than 2-fold downregulated in phenol in WT (19/45 genes in evol33 and 22/45 genes in evol40 were >2-fold upregulated), although the degree of fold change differed significantly between WT and adapted strains (representative genes shown in Table A1.2 and Supplemental Table A1.6, Sheet 13).

A1.4.4.5 Effects of nitrogen limitation on R. opacus transcriptome

In glucose, strain-to-strain variation in global expression was low (Supplemental Figures A1.7 and A1.13), and the most highly expressed genes assessed by DESeq2 were LPD00472 (porin protein), LPD04147 (linear gramicidin synthase subunit C/non-ribosomal peptide synthase), LPD03031 (nitrite extrusion protein) and LPD03032 (nitrite reductase; Supplemental Table S6). LPD00472 was a highly abundant transcript and was slightly downregulated (up to 4-fold) in phenol growth conditions, probably reflecting the hydrophobic nature of phenol compared to hydrophilic glucose. Normalized counts using plotCounts function of DESeq2 comparing these genes, phenol degradation genes and constitutively highly expressed housekeeping genes (such as DNA-dependent RNA polymerase subunits (LPD06131/6132), ClpX (LPD05487), and elongation factor Tu (LPD06091)) are shown in Table A1.2. Because we used a minimal salts medium with a reduced nitrogen concentration, we expected that genes involved in nitrogen limitation would be highly expressed. This speculation was confirmed by the extremely high expression of LPD03031 and LPD03032 (Table A1.2). In fact, some of the most highly expressed genes across all strains in all medium conditions included proteasome genes LPD04933 (Mpa homolog/ATPase) and LPD04928 (proteasome endopeptidase complex beta subunit). As shown in R. erythropolis (67), R. opacus is likely equipped with a complete set of components to constitute active proteasomes, where proteins are presumably recycled and utilized in nitrogen-limited conditions. Changes in

carbon source (glucose or phenol) did not seem to affect proteasome gene expression (Table A1.2; less than 2-fold up- or downregulated).

A1.5 Discussion

In this work, we analyzed genomic and transcriptomic changes between adaptively evolved R. opacus mutants and the WT strain grown in phenol. Laboratory adaptive evolution has been used for many different bacteria to improve growth on diverse compounds (68). We used phenol as a sole carbon source in our adaptive evolution process and identified strains with higher tolerance to the toxic chemical by measuring their total biomass accumulation, lag phase and growth rate (Figure A1.1 and Supplemental Tables A1.1–A1.3). After ∼200 generations, adapted strains contained 3–4 SNPs in the genomes, which was more rapid accumulation of SNPs than reported by Lenski et al. in their long-term evolution experiment and other labs ($8.9 \times 10{-}11$ per base-pair per generation; 69). Strong selective pressure by the toxic compound being the sole carbon source probably contributed to the faster rate of SNP accumulation compared to the E. coli experiment, although the 'normal' rate of SNP accumulation during adaptive evolution in R. opacus has not been determined. Unfortunately, we did not identify 'obvious' SNPs that contributed to the striking transcriptomic profile difference between WT and evolved strains. The two adapted strains had improved growth profiles with increased biomass accumulation and shorter lag phases that could be due to altered transport of phenol in the mutants, leading to changes in intracellular concentrations of phenol and thus expression of phenol-responsive genes for phenol detoxification and degradation.

Differences were also observed between WT and adapted strains in terms of lipid accumulation. From RNA-Seq expression data, phenol appears to be mainly degraded into acetyl-CoA and

succinyl-CoA via the β-ketoadipate pathway (12). Acetyl-CoA can be integrated directly into fatty acid biosynthesis pathways, and succinyl-CoA can enter the TCA cycle to generate reducing equivalents and ATP for cell growth and lipid synthesis (70). Compared to WT, the adapted strains maintained the ability to synthesize and accumulate lipids when grown in glucose, but they both accumulated significantly more lipids than WT when grown in phenol (Figure A1.2, Supplemental Tables A1.4 and A1.5).

The adapted strains in this study demonstrated high phenol consumption capabilities that match or surpass other phenol-degrading bacterial strains and mixed cultures. Pseudomonas putida MTCC1194, which was adapted for growth in phenol as a sole carbon source, had maximum phenol degradation rates of ~12 mg phenol/l/h during growth at its maximum phenol concentration of 1 g/l (71). Another approach used mixed cultures to increase phenol degradation capacity, with tolerances up to 0.8 g/l phenol and degradation rates of 15.4 mg/l/h (72). Another approach is to isolate strains directly from environments such as contaminated wastewater. Bacillus brevis, isolated from an industrial wastewater, showed the highest phenol tolerance and utilization at concentrations up to 1.75 g/l phenol with degradation rates of ~20 mg/l/h (73). Our adapted strains showed higher tolerance than B. brevis with growth in 2 g/l phenol, and experiments at 1.5 g/l showed phenol degradation rates of 22 and 21 mg/l/h for evol33 and evol40, respectively (Supplemental Figure A1.3). In summary, evol33 and evol40 demonstrated comparative phenol degradation rates and tolerances to the best-performing environmental isolates.

Our transcriptomic data suggested that phenol-adapted strains express lower levels of stress-response genes in the conditions tested (low nitrogen, minimal media and phenol as a sole carbon source). Phenol is known to cause oxidative stress response in bacteria (74). In our study, R. opacus upregulated 'DNA protection during starvation protein' LPD04106, or Dps, which is thought to

be involved in oxidative stress resistance (75,76). It seems likely that low nutrient condition can induce the gene, but the adapted strain, especially evol33, showed significantly lower upregulation of this gene compared to WT in phenol, suggesting that evolved strains sensed less oxidative stress in our experiment. A similar trend was observed with the major housekeeping chaperone genes. DnaK is a major bacterial Hsp70 (70 kDa heat shock protein) and functions with co-chaperones GrpE and DnaJ to prevent aggregation of denatured proteins (77,78). R. opacus expressed 2 copies of the dnaK operons (LPD2079–02081 and LPD03845–03847) in the conditions we tested, and the major operon appeared to be LPD02079 and the following 3 genes. All DnaK and co-chaperone genes were upregulated more in WT than in the phenol-adapted strains in low phenol, indicating that the low-nutrient, phenol medium condition encountered by WT may cause proteins to misfold, and that the phenol-adapted strains encounter lower level of cellular stress than WT at the same concentration of phenol in the media.

We observed clear patterns of altered gene regulation in phenol-adapted strains compared to WT R. opacus in response to phenol. In WT, one of the two copies of phenol hydroxylase genes was dominantly upregulated, but in adapted strains the second copy (LPD06740 and LPD06741) was also upregulated to the same or even higher level (Figure A1.3, Table A1.2 and Supplemental Figure A1.8). Both SNP analysis and RNA-Seq results suggest that transport of phenol or compounds related to its metabolism is altered in the adapted strains. In fact, phenol was consumed at faster rates by the adapted strains than the WT strain (Supplemental Figure A1.3). evol33, which additionally had a putative transporter gene with a single point mutation compared to evol40 (Table A1.1), upregulated phenol degradation genes more strongly than evol40 (Figure A1.3). It is well documented that many identified transcriptional regulators for aromatic degradation and

catabolism are AraC/XylS family (79–81). AraC/XylS-family transcriptional regulators bind to ligands (e.g. arabinose), and upregulation of effector genes is tunable by adjusting the concentration of ligands (82–84). Therefore, it is possible that adapted strains allow more phenol molecules to be transported into the cell, which in turn activate the second phenol degradation operons to the degree observed (6307-fold upregulation in evol33, 2624-fold upregulation in evo40 and 657-fold upregulation in WT; Figure A1.3 and Supplemental Table A1.6). Higher upregulation of β-ketoadipate pathway genes in adapted strains could also be influenced by higher intracellular concentrations of phenol or its downstream metabolite, catechol, which has been observed with aromatic degradation pathways in other organisms (79,80).

There are 46 genes annotated as shikimate transporters in the complete genome of R. opacus. Of the 46, LPD06699 was uniquely co-upregulated with phenol degradation genes, at 353- and 103-fold in evol33 and evol40 comparing low phenol to glucose, and 937- and 572-fold in evol33 and evol40 comparing high phenol to glucose, respectively. In WT, LPD06699 was upregulated 5-fold in low phenol compared to glucose. Except for LPD07505, which was upregulated in phenol only in adapted strains, none of the other genes annotated as a shikimate transporter were regulated in the same manner (Supplemental Table A1.6). Furthermore, predicted shikimate utilization genes LPD05461, LPD06023, LPD17011 and LPD05485 were not highly transcribed or upregulated in phenol (Supplemental Table A1.6), suggesting that LPD06699 and potentially LPD07505 may be involved in phenol transport.

Another interesting finding was the upregulation of a putative YRNA and Rsr (85) in adapted strains in phenol. YRNAs were recently found to exist in a wide variety of bacterial species, including R. opacus (86). R. opacus Rsr homolog, LPD06269, caught our attention because of its phenol-responsive upregulation in evolved strains, even though it was annotated as a hypothetical protein. LPD06269 was constitutively expressed at a medium-low level in all strains in glucose but upregulated 52-fold in low phenol compared to glucose and 115-fold in high phenol compared to glucose in evol33 (8.3-fold and 17-fold in evol40), and upregulation of the predicted YRNA region showed the same pattern (Supplemental Figure A1.14). In WT, transcript levels of LPD06269 slightly decreased in low phenol (0.87-fold), and no upregulation of YRNA region was observed, suggesting that this response was phenol-dependent and specific to the adapted strains. We are in a process of focusing on small noncoding RNAs in R. opacus, since we removed the majority of small RNAs from the total RNA samples in order to obtain maximal amount of mRNA in this study. Nonetheless, our results indicate that small RNA-mediated global response may also be involved in adaptive evolution of R. opacus against phenol as a sole carbon source, and it may explain the ability of R. opacus to rapidly adapt to diverse environments without accumulating substantial genomic changes.

This work suggests that characterizing funneling pathways (which convert lignin-derived compounds into pathway metabolites such as catechol; 87) and transporters for phenolics is important for conversion of phenolics into fuels and chemicals. Genes converting phenol to catechol were some of the most highly upregulated genes when strains were grown in phenol compared to glucose, suggesting that phenol-to-catechol conversion may be a limiting step for growth on phenol. Under the condition that we tested (low nitrogen, minimal medium and aerobic

condition), phenol seems to be degraded mainly by ortho-cleavage via the catechol branch of the β-ketoadipate pathway into succinyl-CoA and acetyl-CoA, consistent with our previous result obtained from WT cultures grown in 0.5 g/l phenol supplemented with 13C glucose (37). Other phenolic compounds would require other funneling enzymes to convert them into precursors such as catechol and protocatechuic acid for degradation (87). This study also identified putative transporters for phenol, and transport of many different phenolic compounds would require either promiscuity for transporters or different transporters for each compound. Note that while previous studies on transporters of toxic chemicals focused on efflux pumps to minimize the intracellular concentrations of these compounds (88–90), R. opacus is likely to use its transporters to import toxic phenolics, suggesting a new mechanism of bacterial aromatic tolerance. Increased phenolic compound flux into the cell requires balancing between transport and degradation to prevent accumulation of toxic compounds within the cell.

A recent study demonstrated that adaptive evolution can increase R. opacus tolerance to lignocellulose-derived inhibitors (40). While they used media supplemented with glucose, our evolution process is different in that phenol was used as a sole carbon source to obtain highly tolerant mutants to phenol. Consequently, we were able to decouple the effects of other potentially available carbon sources in lignocellulose-derived feedstock on changes in the genome and transcriptome. We also demonstrated that phenol as a sole carbon source can support R. opacus for both growth and accumulation of lipids (biodiesel precursors) and that adaptive evolution can increase lipid productivity, an important factor for current lignin conversion processes (15). Combining adaptive evolution and omics analyses, our approach provides insights into the

tolerance mechanism of the promising production host, facilitating future lignocellulose, specifically lignin, valorization efforts.

A1.6 Tables and Figures

A. SNP summary

CAS gene ID	MIT gene ID	Annotation	WT	SNP	Amino acid change
Both Evol33 and Evol40					
Between LPD04711 and LPD04712	OPAG_05248	Intergenic (CAS)/ acyl-CoA thioesterase II	ttc	ttt	F120 to F (silent)
LPD03112	OPAG_03447	cytochrome aa3 quinol oxidase, subunit I	ttc	tcc	F335 to S
LPD03747	OPAG_04053	dicarboxylate carrier protein/citrate transporter/MFS transporter	atc	ttc	I296 to F
Evol33 only					
LPD00118	OPAG_07911	4-hydroxyphenylacetate permease	gga	gta	G162 to V

B. Expression levels using DESeq2 calculation (average of triplicates)

Gene ID	WT Glc	WT LowP	evol33 Glc	evol33 LowP	evol33 HighP	evol40 Glc	evol40 LowP	evol40 HighP
LPD04711	3	6	2	10	13	3	12	4
LPD04712	11	14	13	9	5	11	8	2
LPD03112	2580	18633	2908	9718	12462	2373	13083	13086
LPD03747	152	29	116	136	165	119	59	75
LPD00118	376	64	289	312	343	312	163	165

C. Expression levels using rpkm calculation (average of triplicates)

Gene ID	WT Glc	WT LowP	evol33 Glc	evol33 LowP	evol33 HighP	evol40 Glc	evol40 LowP	evol40 HighP
LPD04711	2	3	1	5	6	2	7	2
LPD04712	6	7	8	5	2	7	4	1
LPD03112	152	900	189	498	591	153	753	697
LPD03747	11	2	9	8	9	9	4	5
LPD00118	27	4	23	20	20	25	12	11

Table A1: Single nucleotide polymorphisms (SNPs) found in the adapted strains.

(A) All SNPs found in the adapted strains but not in the WT strain are summarized. The mutations were called by both Pilon and MIRA. (B) Expression levels of the genes listed in A, shown in DESeq2-normalized counts, using plotCounts function. (C) Expression levels of the same genes listed in A, in Reads per Kilobase of transcript per Million mapped reads (rpkm). Rpkm values are calculated as explained in the Materials and Method section, and the average of triplicate samples is shown. Glc, 1 g/l glucose; LowP, 0.75 g/l phenol; HighP, 1.5 g/l phenol.

Gene ID	Annotation / Strain:conditions	WT LowP	evol33 LowP	evol33 HighP	evol40 LowP	evol40 HighP
Genes with SNPs (* evol33 only)						
LPD03112	Probable cytochrome c oxidase subunit 1-alpha	2.83	1.75	2.09	2.46	2.45
LPD03747	Uncharacterized protein YfdE/MFS transporter	0.32	−0.40	0.62	0.62	1.59
Between LPD04711 and 04712 (OPAG_05248)	Acyl-CoA thioesterase II	0.56	−0.12	−0.55	0.55	−1.03
LPD00118*	Putative tartrate transporter/4-hydroxyphenylacetate permease	−2.54	0.13	0.25	−1.25	−0.92
Differentially expressed phenol degradation and utilization genes						
LPD05449	Probable succinyl-CoA:3-ketoacid-coenzyme A transferase subunit A	4.12	4.45	6.00	4.09	6.41
LPD05450	Protocatechuate 3,4-dioxygenase beta chain	4.78	6.39	8.07	5.73	8.24
LPD05451	Protocatechuate 3,4-dioxygenase alpha chain	4.84	6.08	7.72	5.92	8.15
LPD05452	3-carboxy-cis,cis-muconate cycloisomerase	6.14	5.75	7.55	5.26	7.81
LPD05453	3-oxoadipate enol-lactonase 2	5.99	5.41	7.19	5.07	7.30
LPD05454	Pca regulon regulatory protein	4.63	4.12	5.60	4.09	5.99
LPD05455	Probable acetyl-CoA acyltransferase	4.10	3.69	5.08	3.73	5.23
LPD06565	Xylose repressor	4.14	4.62	5.09	3.68	5.19
LPD06566	Muconolactone Delta-isomerase	7.44	9.88	10.34	8.85	11.01
LPD06567	Muconate cycloisomerase 1	7.19	9.73	10.12	8.67	10.46
LPD06568	Catechol 1,2-dioxygenase	6.33	9.27	9.81	8.03	9.99
LPD06570	Catechol 1,2-dioxygenase	2.77	6.66	7.13	5.08	6.42
LPD06575	Two-component phenol hydroxylase, reductase component	12.57	12.51	12.11	12.88	12.21
LPD06576	Two-component phenol hydroxylase, oxygenase component	12.18	11.48	11.24	10.98	10.99
LPD06740	Two-component phenol hydroxylase, reductase component	9.36	12.53	12.52	11.34	11.37
LPD06741	Two-component phenol hydroxylase, oxygenase component	9.17	12.25	11.87	10.43	10.45
LPD06742	Catechol 1,2-dioxygenase	8.36	11.97	11.53	9.95	9.94
LPD06743	Putative 3-oxoadipate enol-lactonase	5.24	9.74	9.48	7.45	7.49
LPD06744	Putative beta-ketoadipyl CoA thiolase	0.13	4.68	4.82	2.01	2.32
Putative phenol transporters (> 2 fold up in HighP compared to Glc)						
LPD06699	Shikimate transporter	2.34	8.46	9.87	6.68	9.16
LPD07505	Shikimate transporter	−1.68	2.82	3.09	0.61	1.53
Stress response genes						
LPD04106	DNA protection during starvation protein	3.69	1.40	0.04	2.03	−0.44
LPD07748	18 kDa antigen 2/heat shock protein 20	5.33	3.69	3.32	4.31	3.40
LPD02079	Chaperone protein DnaK	4.00	1.63	2.48	2.66	2.24
Highly expressed genes (count data below)						
LPD00472	Hypothetical protein/ porin protein	−1.59	−0.72	−1.94	−0.84	−1.98
LPD04147	Linear gramicidin synthase subunit C	−1.15	−0.79	−1.81	−1.55	−2.51
LPD03031	Nitrite extrusion protein 1	−0.32	−0.37	1.19	−0.15	1.49
LPD03032	Nitrite reductase NAD(P)H large subunit	−0.57	−1.37	0.94	−1.05	1.24
LPD06131	DNA-directed RNA polymerase subunit beta'	0.41	−0.64	0.22	−0.40	−0.04
LPD06132	DNA-directed RNA polymerase subunit beta	0.16	−0.25	0.17	−0.09	−0.03
LPD05487	ATP-dependent Clp protease ATP-binding subunit ClpX	−0.18	−0.28	−0.05	−0.07	0.45
LPD06091	Elongation factor Tu	−0.29	−0.91	0.36	−0.74	0.15
LPD04933	Proteasome-associated ATPase	0.01	−0.42	−0.86	0.03	−0.67
LPD04928	Proteasome subunit beta	0.12	−0.26	−0.53	−0.13	−0.64

Expression levels of differentially expressed phenol degradation/utilization genes and highly expressed genes using plotCounts function (average counts from triplicate samples)

	WT Glc	WT LowP	evol33 Glc	evol33 LowP	evol33 HighP	evol40 Glc	evol40 LowP	evol40 HighP
LPD05449	34	592	47	995	3036	46	784	4008
LPD05450	25	702	30	2446	8167	35	1862	10944
LPD05451	23	609	21	1472	4716	20	1236	5917
LPD05452	27	2085	31	1626	5905	32	1233	7366
LPD05453	32	2108	42	1803	6392	46	1511	7274
LPD05454	44	1140	61	1065	3031	51	862	3286
LPD05455	87	1525	101	1270	3411	100	1315	3793
LPD06565	110	1962	145	3527	5008	128	1632	4750
LPD06566	6	991	8	8152	11264	5	2407	10971
LPD06567	48	7001	59	48979	67851	43	17726	62444
LPD06568	91	7284	101	61673	94392	80	21091	83313
LPD06569	12	193	11	654	696	10	430	759
LPD06570	4	32	6	640	862	7	237	605
LPD06574	642	425	549	1601	1548	611	850	1618
LPD06575	20	138793	30	190664	144683	25	186689	120411
LPD06576	226	1115301	534	1546914	1339798	495	1147992	1052801
LPD06577	372	3206	288	6635	7135	312	5360	4835
LPD06698	144	229	134	7329	18985	141	2107	8299
LPD06699	77	419	74	26215	70678	77	8062	45006
LPD06739	356	485	269	5067	4041	278	1392	2480
LPD06740	27	18588	29	224065	186503	26	67421	70570
LPD06741	119	69820	200	1005004	779070	166	229458	238395
LPD06742	50	16975	74	312714	232725	65	63793	65619
LPD06743	50	1944	48	41968	35435	44	7767	8113
LPD06744	255	282	265	6691	7520	297	1187	1496
LPD05449	34	592	47	995	3036	46	784	4008
LPD05450	25	702	30	2446	8167	35	1862	10944
LPD05451	23	609	21	1472	4716	20	1236	5917
LPD00472	391881	130913	280688	168207	72748	307073	171411	78144
LPD04147	276825	125049	254571	145768	71941	321709	109833	56532
LPD03031	176283	141517	213166	163206	485834	161971	145702	460250
LPD03032	199408	134490	234314	89615	450441	165498	79799	394788
LPD06131	34784	46649	37322	23675	43500	35730	27179	35080
LPD06132	44905	50714	40698	33754	45703	43683	40984	43259
LPD05487	15674	13971	13293	10789	12796	13163	12571	18072
LPD06091	20925	17195	26436	13873	29313	24111	14338	31098
LPD04933	104368	105771	108367	79769	59627	95300	97451	60274
LPD04928	47296	52024	41704	34480	28722	43987	40396	28430
Most downregulated in phenol								
Gene ID	**Annotation / Strain:conditions**	**WT LowP**	**evol33 LowP**	**evol33 HighP**	**evol40 LowP**	**evol40 HighP**		
LPD02697	NDMA-dependent methanol dehydrogenase	−12.68	−7.24	−6.78	−7.01	−10.83		
LPD02728	Inner membrane metabolite transport protein yhjE	−10.00	−6.56	−5.51	−8.71	−8.58		
LPD04550	Methane monooxygenase component A alpha chain	−9.02	−8.26	−6.55	−7.57	−9.00		
LPD04551	Methane monooxygenase component C	−8.40	−8.35	−6.50	−8.64	−8.44		
LPD04552	Methane monooxygenase component A beta chain	−7.38	−7.07	−6.56	−7.57	−6.93		
LPD04555	Uncharacterized protein MJ1129	−7.41	−7.35	−7.09	−7.31	−7.59		
LPD04556	NAD-dependent alcohol dehydrogenase	−7.91	−7.24	−6.78	−7.01	−6.98		
LPD04557	60 kDa chaperonin 3	−7.64	−7.03	−6.67	−6.43	−6.56		
Lipid biosynthesis/metabolism								
LPD06283	Heparin-binding hemagglutinin (TadA)	4.67	4.76	3.77	4.58	3.14		
LPD05549	Putative sterigmatocystin biosynthesis fatty acid synthase subunit alpha	6.01	5.04	5.84	5.04	5.82		
LPD00131	Stearoyl-CoA 9-desaturase	11.80	5.10	6.66	6.52	6.24		
LPD00130	Long-chain specific acyl-CoA dehydrogenase, mitochondrial	8.06	2.65	5.14	3.79	3.79		
LPD03000	Stearoyl-CoA 9-desaturase	7.24	5.15	5.67	5.48	5.85		
LPD05528	Stearoyl-CoA 9-desaturase	6.18	4.52	7.55	5.03	6.31		
LPD05529	Stearoyl-CoA 9-desaturase electron transfer partner	5.80	4.23	6.93	4.79	5.85		
LPD01195	Long-chain-fatty-acid--CoA ligase FadD19	−5.92	−2.13	−2.98	−4.41	−5.03		
LPD06540	Long-chain specific acyl-CoA dehydrogenase, mitochondrial	−3.82	−2.20	−1.27	−2.50	−2.72		
LPD04435	Long-chain-fatty-acid--CoA ligase	−2.34	−2.71	−3.93	−2.66	−3.51		
LPD03408	Long-chain specific acyl-CoA dehydrogenase, mitochondrial	−3.76	−2.88	−2.76	−3.12	−3.06		
LPD07841	Long-chain-fatty-acid--CoA ligase	−4.16	−3.66	−3.73	−3.96	−2.94		
LPD03067	Short/branched chain specific acyl-CoA dehydrogenase, mitochondrial	−3.08	−3.71	−2.96	−3.10	−2.72		
LPD03066	Short-chain specific acyl-CoA dehydrogenase, mitochondrial	−3.36	−3.78	−3.19	−3.35	−3.26		
Transcriptional regulators								
LPD06577	Probable thc operon regulatory protein	3.09	4.52	4.61	4.09	3.93		
LPD06739	Probable thc operon regulatory protein	0.44	4.23	3.89	2.31	3.14		
LPD06574	Probable thc operon regulatory protein	−0.59	1.55	1.49	0.47	1.39		
LPD03777	Probable thc operon regulatory protein	−1.78	−0.78	1.09	−2.19	0.81		
LPD03770	Probable serine/threonine-protein kinase pknK	0.38	0.08	1.62	−0.30	1.62		

Table A1.2: Summarized fold changes of selected genes.

WT LowP, WT in low phenol versus glucose; evol33 LowP, evol33 in low phenol versus glucose; evol33 HighP, evol33 in high phenol versus glucose; evol40 LowP, evol40 in low phenol versus glucose; evol40 HighP, evol40 in high phenol versus glucose. For DESeq2-normalized count data, counts are shown in each condition specified, rather than comparing to glucose (Glc, 1 g/l glucose; LowP, 0.75 g/l phenol; HighP, 1.5 g/l phenol). Count numbers were obtained using plotCounts

function of DESeq2 and averaging triplicate samples. More information of this chart can be found in Supplemental Table S6.

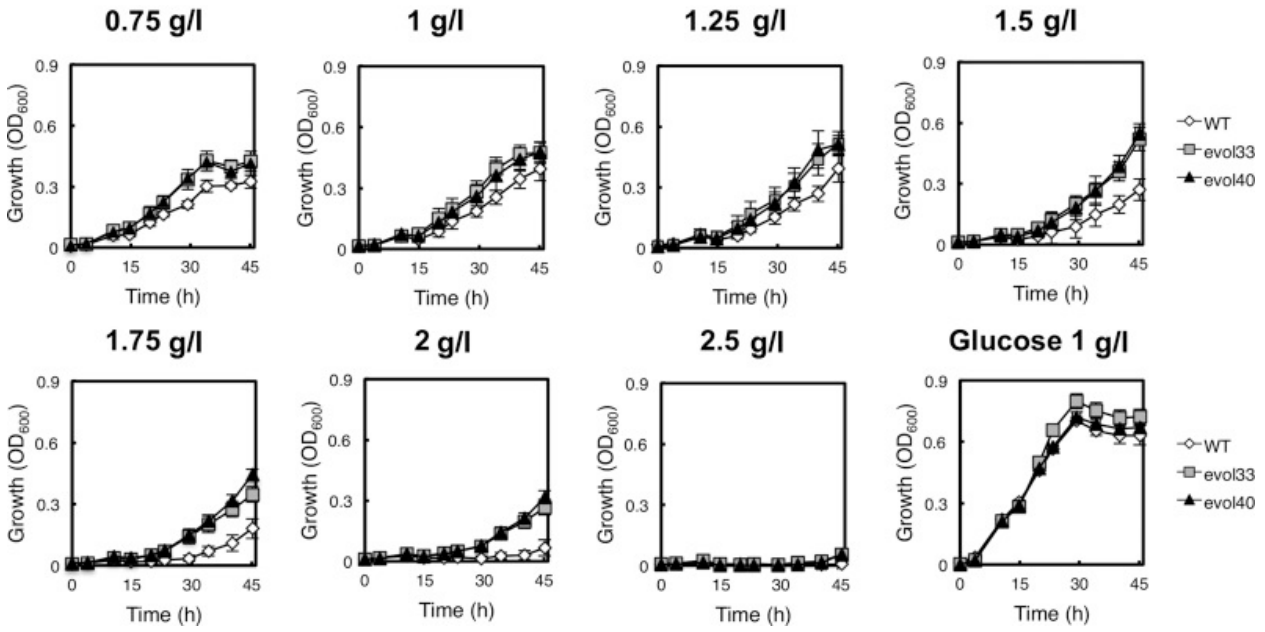

Figure A1.1: Growth comparison between the two phenol-adapted strains and the WT strain in diverse growth conditions.

The adapted strains and the WT strain were grown in multiple concentrations of phenol as their sole carbon source to characterize improvements in tolerance after adaptive evolution (phenol concentrations as indicated; 1 g/l ammonium sulfate). The adapted strains grew to higher optical densities than the WT strain in all concentrations of phenol (Supplemental Table S1), had shorter lag phases in higher concentrations of phenol (Supplemental Table S2) and demonstrated growth even in 2 g/l phenol. White diamonds, gray squares and black triangles represent WT, evol33 and evol40, respectively. Data show the average of six biological replicates grown in 96 well plates (with 200 µl culture each). The error bars represent one standard deviation.

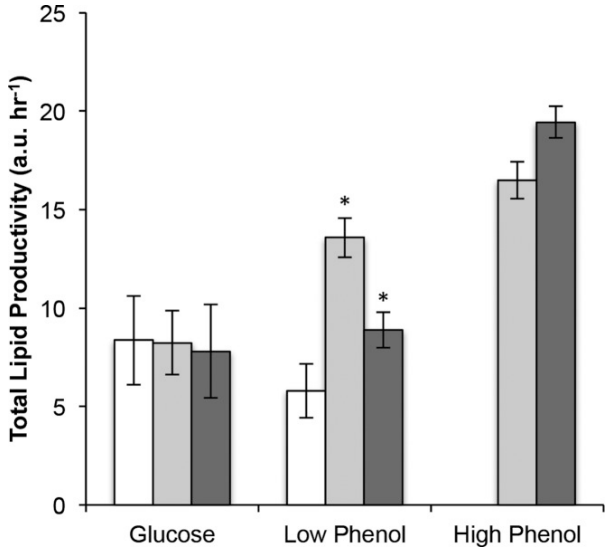

Figure A1.2: Characterization of lipid accumulation.

Comparison of total lipid (Nile red fluorescence) productivity between WT and the adapted strains. For all experiments, the nitrogen source was 0.05 g/l ammonium sulfate and an initial OD600 was 0.3 with a culture volume of 10 ml. White bar = WT, gray bar = evol33 and black bar = evol40. Glucose = 1 g/l, Low Phenol = 0.75 g/l and High Phenol = 1.5 g/l. The data are the average of the arithmetic means of the Nile red fluorescence distribution obtained from three biological replicates. To take into account differences in the lag phase for each condition, time points were taken from the exponential to the stationary phase to determine the average increase in Nile red fluorescence over time for each condition. The asterisk indicates significant increases in lipid productivity compared to that of WT in the same condition ($P < 0.05$; one mean, two-tailed Student's t-test). No growth was observed for the WT strain in 1.5 g/l phenol (<1 cell doubling in 10 ml cultures). Error bars represent one standard deviation with all staining and flow cytometry measurements performed on the same day.

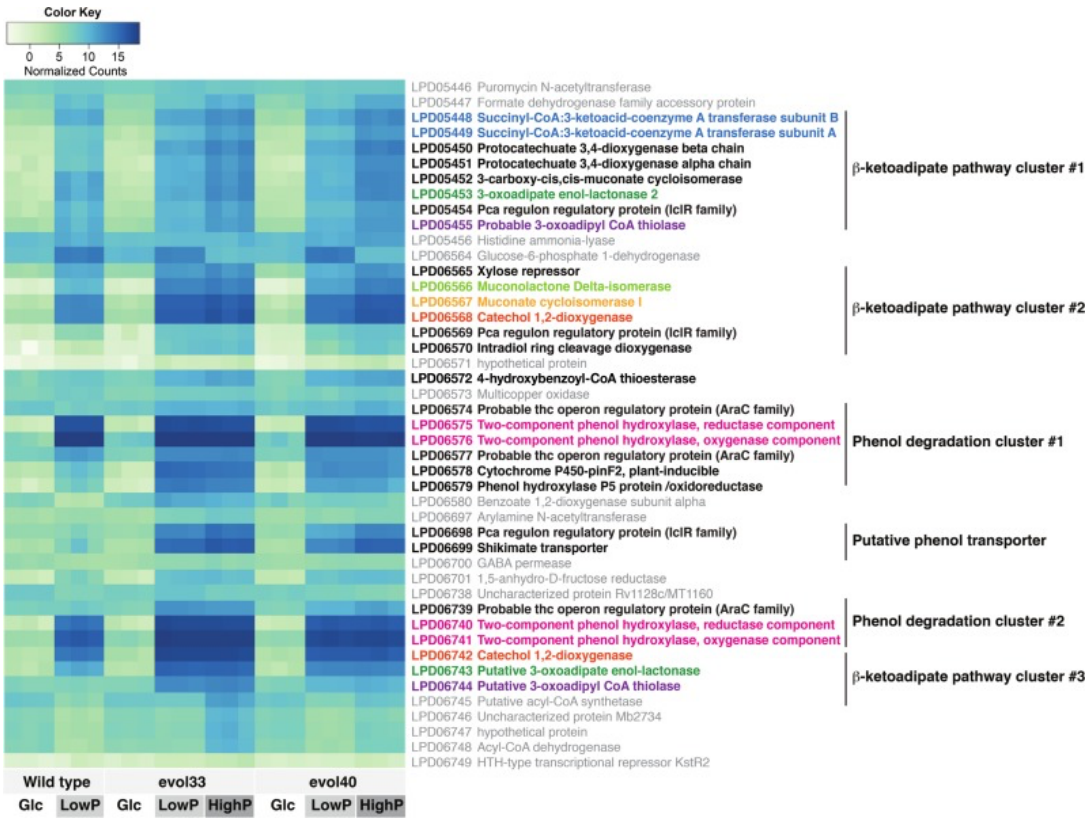

Figure A1.3: Transcriptomic and genomic information of genes involved in phenol degradation and utilization.

(**A**) Transcriptomic and genomic information of genes involved in phenol degradation and utilization. Differential expression is shown for the phenol-responsive degradation operons, β-ketoadipate pathway gene clusters, a putative phenol transporter gene and transcriptional regulator genes. Raw counts were normalized using variance stabilizing transformation in DESeq2 to fit in the range of 20 across all genes. Darker colors indicate higher normalized counts (as shown in Color Key). Glc, 1 g/l glucose; LowP, 0.75 g/l phenol; and HighP, 1.5 g/l phenol. The color scheme is the same throughout Figures Figures33 and 4 for each step of the pathway. Each square on the heat map represents a biological replicate.

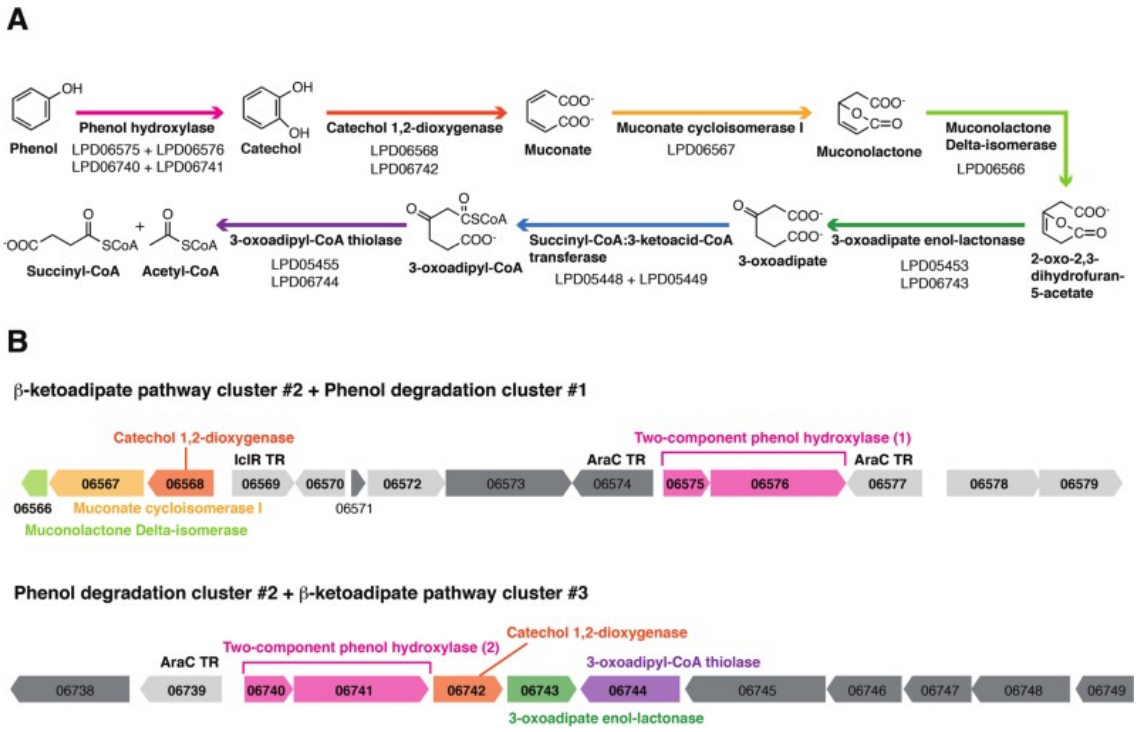

Figure A1.4 Pathway and genome maps showing genes involved in phenol degradation and utilization.

(A) Ortho-cleavage branch of the β-ketoadipate pathway in R. opacus. An expanded pathway map including other phenol degradation pathways can be found in Supplemental Figure S10. The color scheme is the same throughout Figures 3 and 4 for each step of the pathway. (B) Genomic organization of the two phenol degradation operons. Light gray genes are highly upregulated in phenol. Darker gray genes are flanking genes that were not upregulated in phenol.

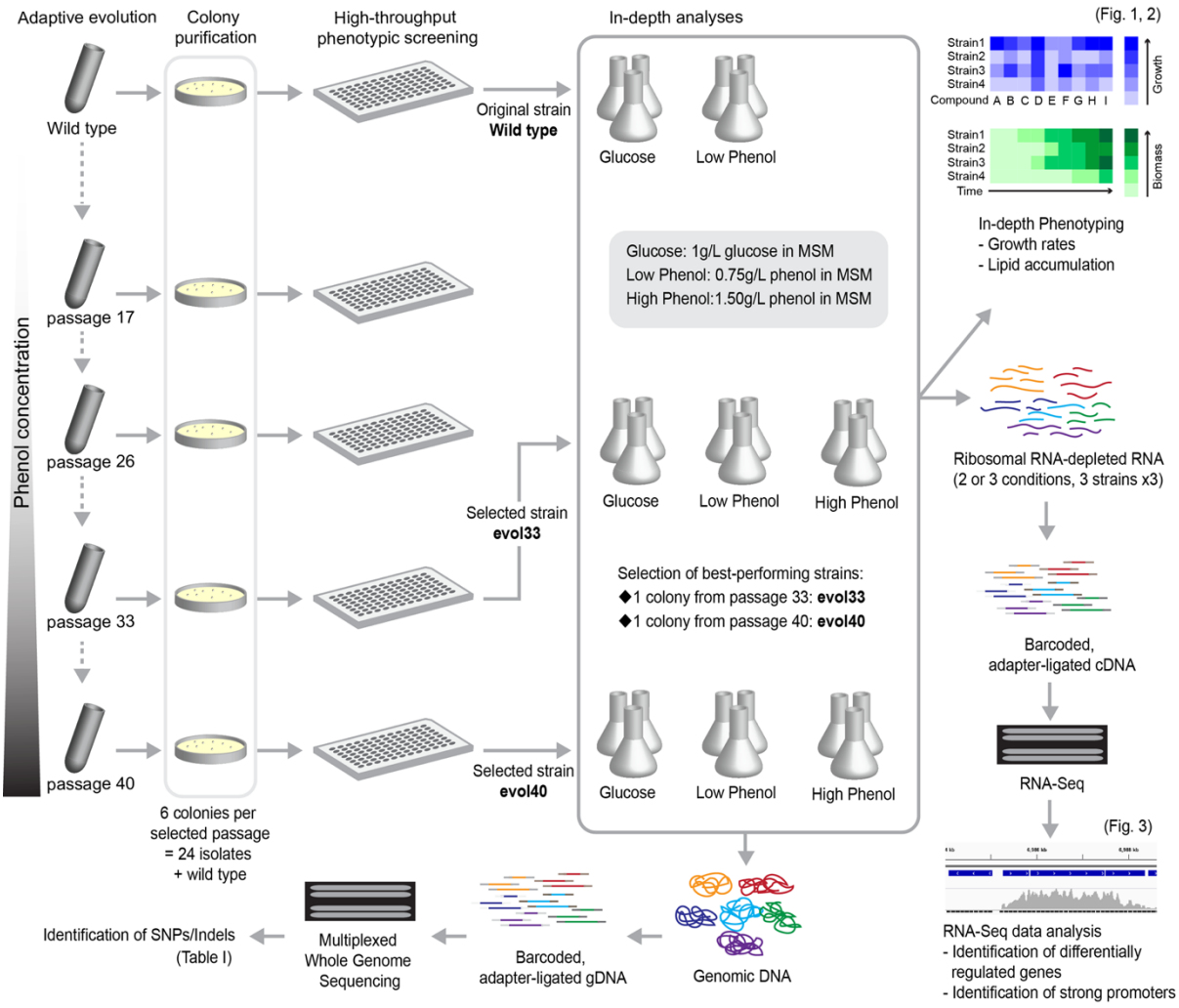

Supplemental Figure A1.1: Experimental approach.

R. opacus PD630 wild-type (WT) strain was passaged in a minimal salts medium (MSM) with increasing concentrations of phenol as a sole carbon source, and an aliquot of the liquid culture was taken and stored at -80ºC at each passage. Of the 40 passages, 6 colonies per passage were purified from passages 17, 26, 33, and 40. Growth and lipid accumulation profiles of the isolated strains were analyzed, and two top performing colonies, evol33 and evol40, were chosen. WT, evol33, and evol40 were further analyzed by whole genome sequencing (Table 1), RNA-Seq

(Table 2 and Figure 3), and in-depth phenotyping including determination of growth profiles on different concentrations of phenol (Figure 1) and total lipid productivity (Figure 2).

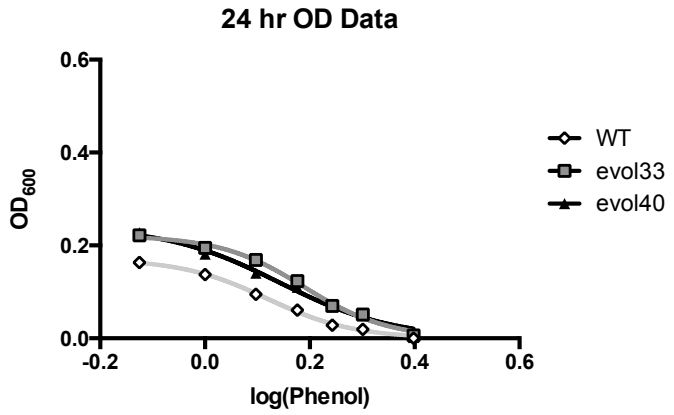

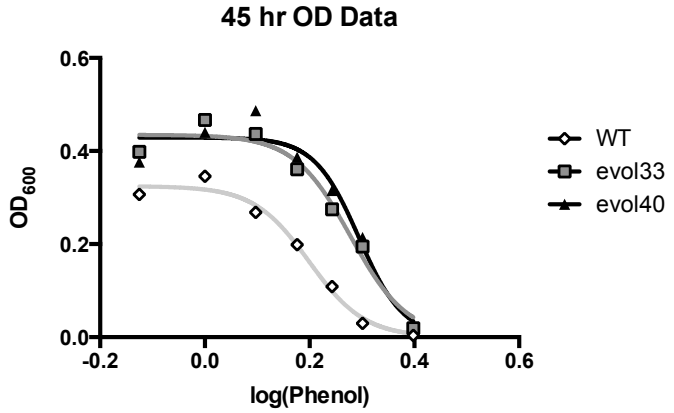

	WT	evol33	evol40	evol33 improvement (%)	evol40 improvement (%)
24 hr IC_{50} (g/L)	1.29 ± 0.10	1.49 ± 0.19	1.44 ± 0.11	15.5	11.6
45 hr IC_{50} (g/L)	1.58 ± 0.08	1.90 ± 0.05	1.96 ± 0.06	20.3	24.1

Supplemental Figure A1.2: Characterization of IC_{50} values for WT and adapted strains.

Optical densities (OD_{600}) measured from cultures grown in various concentrations of phenol and high nitrogen (1 g/L ammonium sulfate) at 24 and 45 hours were fitted in Prism using a four-parameter inhibitor response curve to calculate the IC_{50} values. R^2 values were greater than 0.88

for all fittings. The fitted values for each biological replicate were averaged to calculate p values for significance (one mean, two-tailed Student's *t*-test). IC_{50} values at 24 hours are not significantly different from WT for both adapted strains ($p = 0.07$ and $p = 0.06$ for evol33 and evol40, respectively), but IC_{50} values for both evol33 and evol40 at 45 hours are significantly higher than that of WT ($p = 0.0004$ and $p = 0.0002$ for evol33 and evol40, respectively). Error represents one standard deviation of fitted values from six biological replicates grown in 96 well plates. Improvement was calculated as $(evolX_{IC50}-WT_{IC50}) / WT_{IC50} \times 100\%$, where X = 33 or 40.

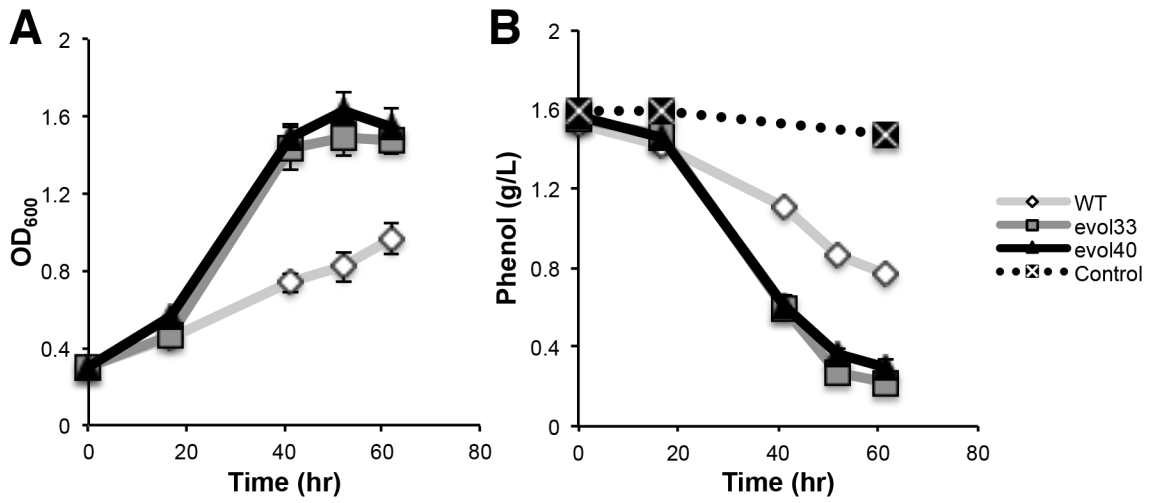

Supplemental Figure A1.3: Growth and phenol consumption profiles of WT and adapted strains.

Cells were grown in 100 mL of high nitrogen (1 g/L) minimal salts medium containing 1.5 g/L phenol as the sole carbon source. White diamonds = WT, gray squares = evol33, black triangles = evol40, and black square with white cross = no cell control (1.5 g/L phenol). **A**, Growth profile of WT and adapted strains. **B**, Phenol consumption profiles of WT and adapted strains. Phenol (g/L) was estimated by measuring absorbance of culture supernatants at 280 nm (see the Supplemental Materials and Methods). For both plots, each point is the average of three biological replicates and the error bars represent one standard deviation of three biological replicates.

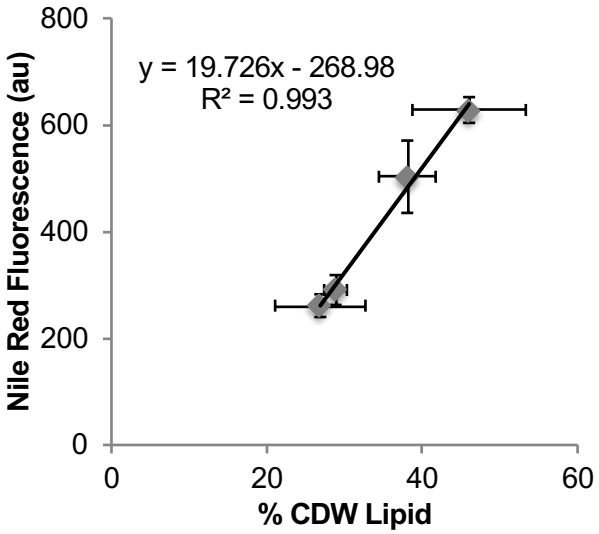

Supplemental Figure A1.4: Correlation between Nile red fluorescence and total lipid content (% CDW lipid).

The WT strain was grown in four different ammonium sulfate concentrations (1, 0.2, 0.1, and 0.025 g/L) as a sole nitrogen source and 1 g/L glucose as a sole carbon source for 24 hours. Three 200 μL aliquots of each biological replicate were used for Nile red fluorescence measurement. Cells from each biological replicate were lyophilized, and the cell dry weight lipid content (% CDW lipid) of each biomass sample was calculated from the total lipids extracted using the Folch procedure (See Materials and Methods). The Nile red fluorescence values represent the average of three technical replicates from two biological replicates for a total of six replicates. The % CDW lipid values are the average of two biological replicates. The error bars represent the standard error.

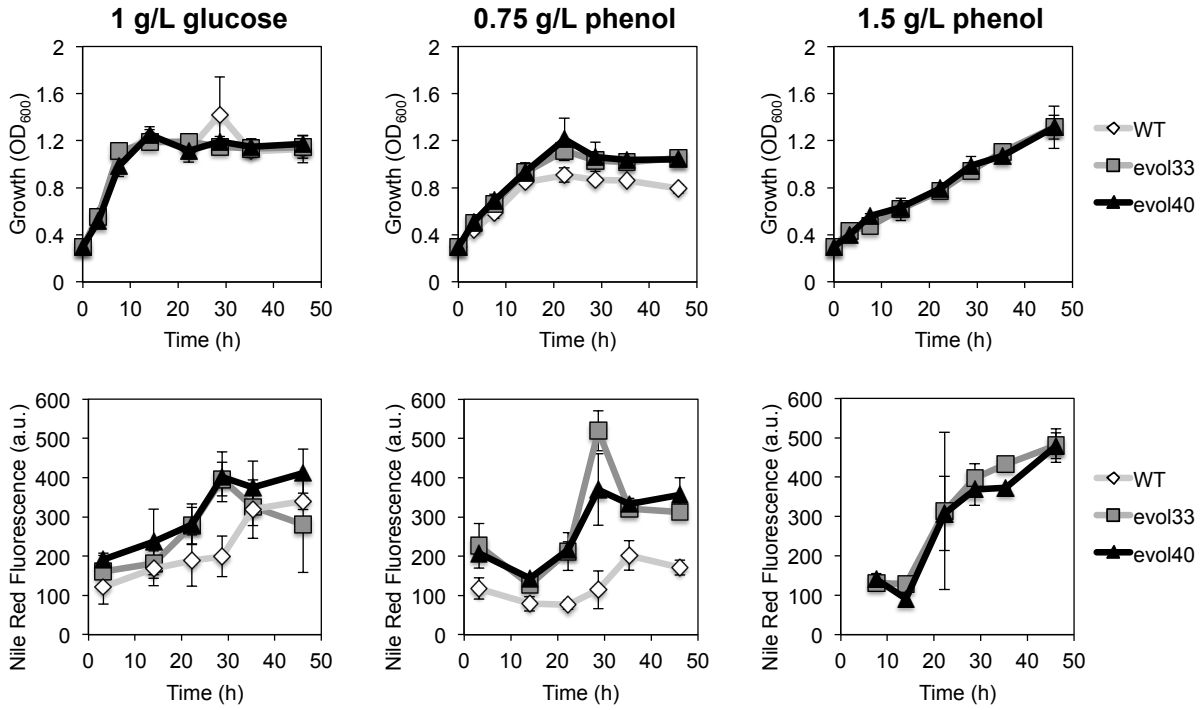

Supplemental Figure A1.5: Nile red fluorescence and growth kinetics of WT and adapted strains.

The top row shows the growth profile of each strain in low nitrogen conditions (0.05 g/L ammonium sulfate), and the bottom row shows the average Nile red fluorescence of each strain over time. No growth was observed for the WT strain in 1.5 g/L phenol with low nitrogen (<1 cell doubling in 10 mL cultures). Each data point represents the average of three biological replicates. Each Nile red fluorescence value is the arithmetic mean of the Nile red fluorescence distribution obtained using flow cytometry (see Materials and Methods for more information). Error bars represent one standard deviation.

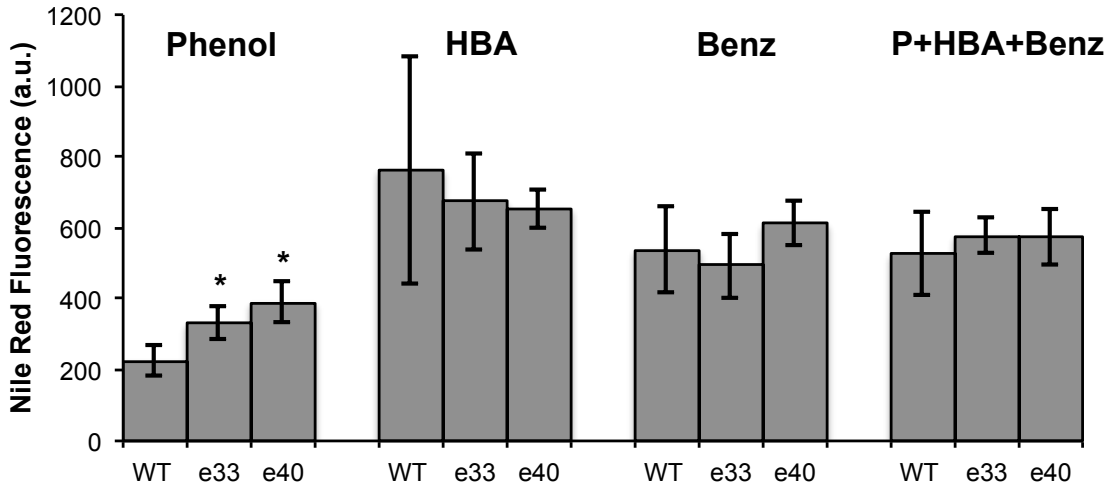

Supplemental Figure A1.6: Lipid accumulation using lignin model compounds.

Cultures were grown in 96 well plates at 200 μL volumes in low nitrogen (0.05 g/L) minimal medium using 1 g/L of total phenolics as a carbon source. Cells were harvested after 48 hours and analyzed for lipid content by Nile red analysis (see Materials and Methods). HBA = 4-hydroxybenzoic acid, Benz = sodium benzoate, P+HBA+Benz = 1 g/L total phenolics; 0.33 g/L phenol, 0.33 g/L HBA, and 0.33 g/L Benz. e33 = evol33 and e40 = evol40. Stars represent significantly higher lipid accumulation compared to WT ($p < 0.05$, one tailed Student's t-test). evol33 and evol40 show significantly higher lipid accumulation in phenol compared to WT ($p = 0.009$ for evol33, $p = 0.005$ for evol40). However, the adapted strains do not show increased lipid production, compared to that of WT, on other lignin model compounds, although all strains have higher lipid accumulation using hydroxybenzoic acid and sodium benzoate as carbon sources than using phenol ($p < 0.04$ for all cases). Bars represent the average of five biological replicates, and error bars represent one standard deviation.

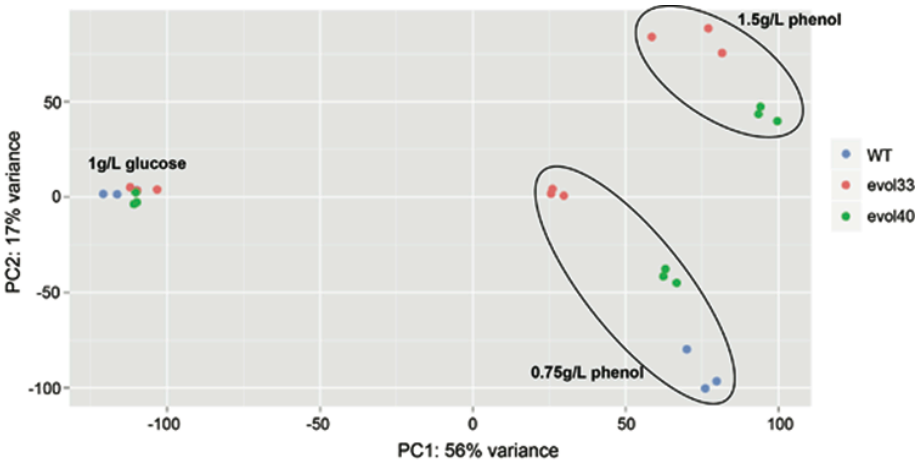

Supplemental Figure A1.7:

Principal component analysis plot of all 8945 genes from RNA-Seq triplicate samples, generated by using the plotPCA function of DESeq2. Blue, WT; pink, evol33; green, evol40. Medium conditions are indicated in the plot.

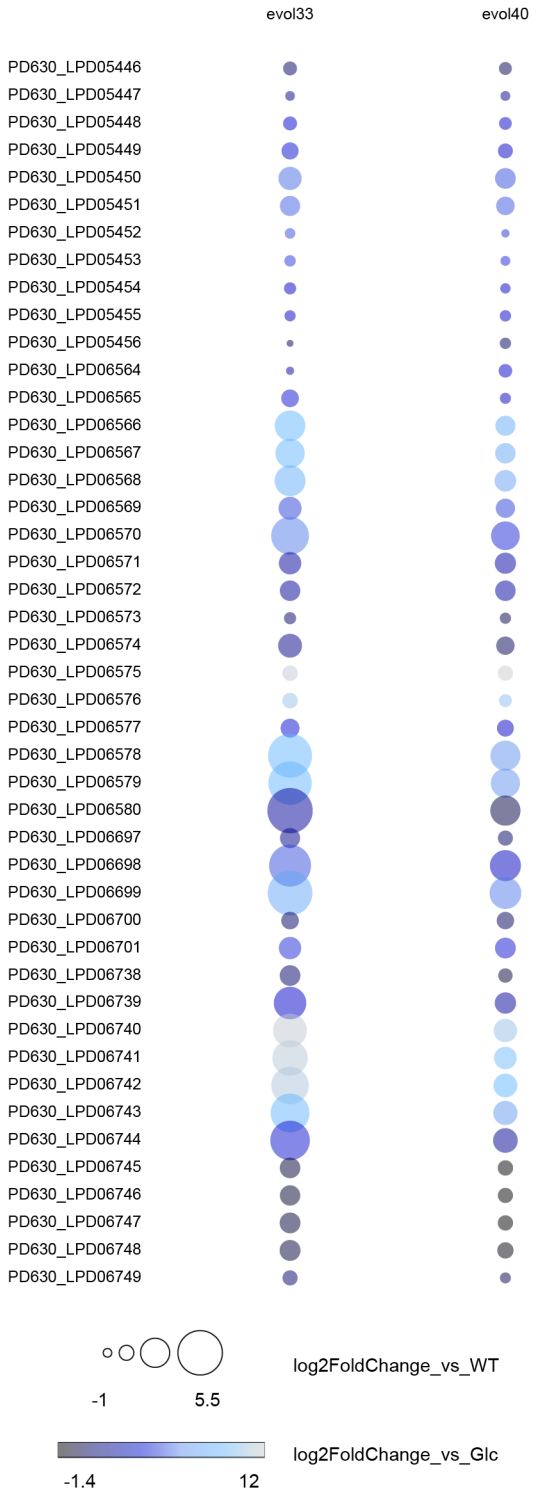

Supplemental Figure A1.8:

Bubble plot representation of fold changes in phenol degradation and utilization genes in low phenol (0.75 g/L). Sizes of the bubbles indicate $\log_2$ fold change compared to the same medium condition in WT, and colors indicate $\log_2$ fold change compared to the indicated adapted strain in glucose (1 g/L).

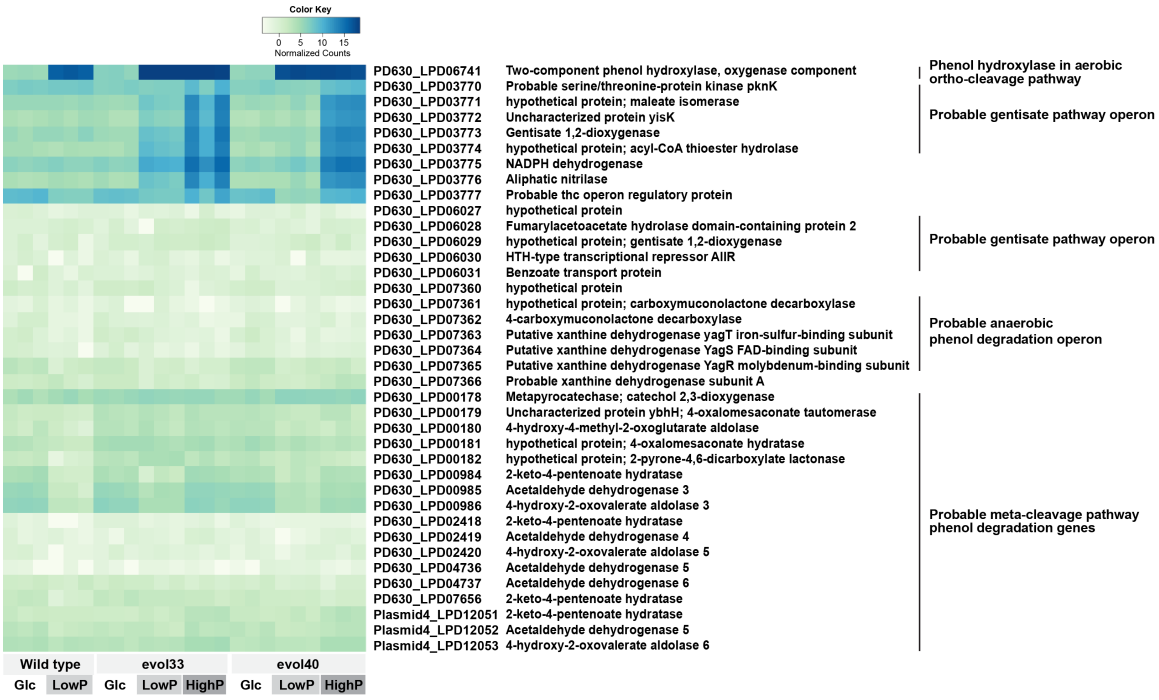

Supplemental Figure A1.9: Expression profiles of other annotated phenolic degradation genes.

Heat map of genes annotated as alternative phenol degradation pathways by RhodoCyc (http://rhodocyc.broadinstitute.org/) is shown. LPD gene IDs were converted from OPAG gene IDs using NCBI BLAST. Glc, 1 g/L glucose; LowP, 0.75 g/L phenol; and HighP, 1.5 g/L phenol.

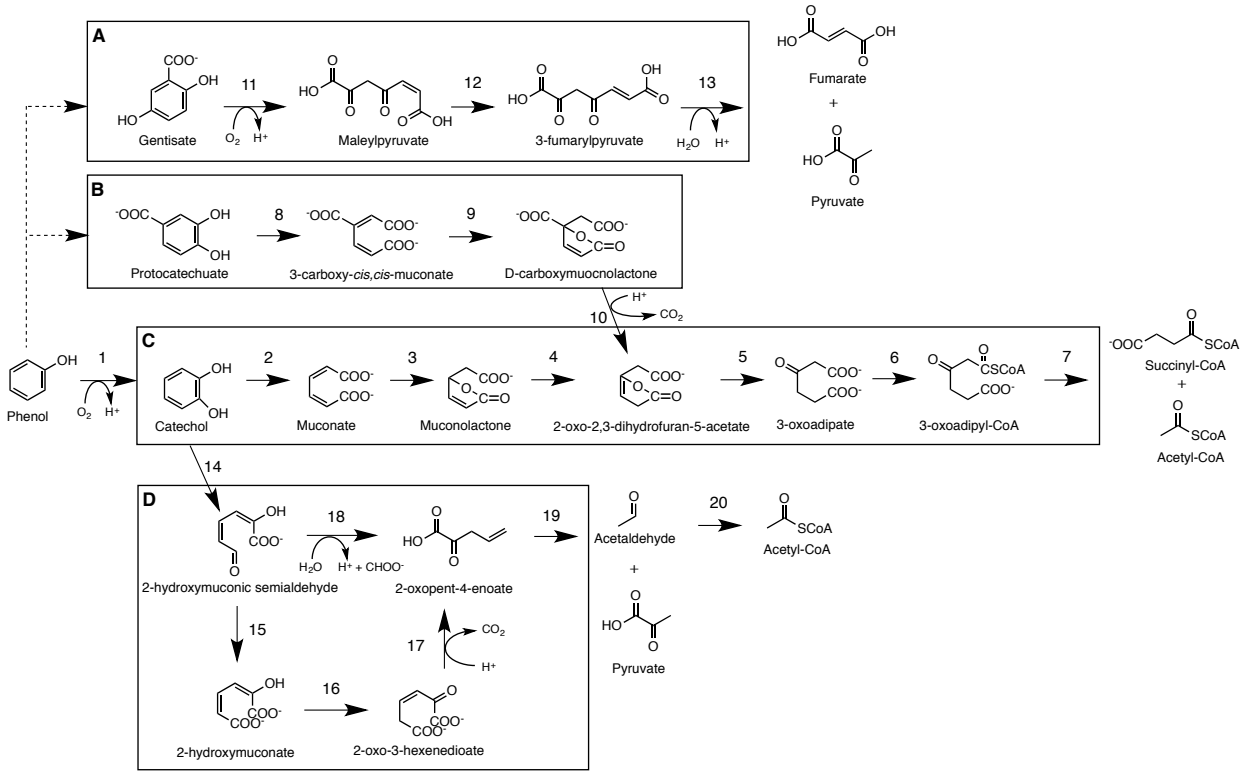

Supplemental Figure A1.10: Phenolic degradation pathways present in *R. opacus* PD630.

Each enzymatic reaction is listed as a number that can be found in Supplemental Table S8 with enzyme name, E.C. number, and Gene ID number(s). Dotted lines represent alternate aromatic degradation pathways that could be involved in phenol degradation. **A**, Gentisate degradation pathway. **B**, Protocatechuate *ortho*-cleavage branch of β-ketoadipate pathway. **C**, Catechol *ortho*-cleavage branch of β-ketoadipate pathway. **D**, Catechol *meta*-cleavage branch of β-ketoadipate pathway. Pathway information shown was matched to the KEGG database (Kanehisa and Goto, 2000).

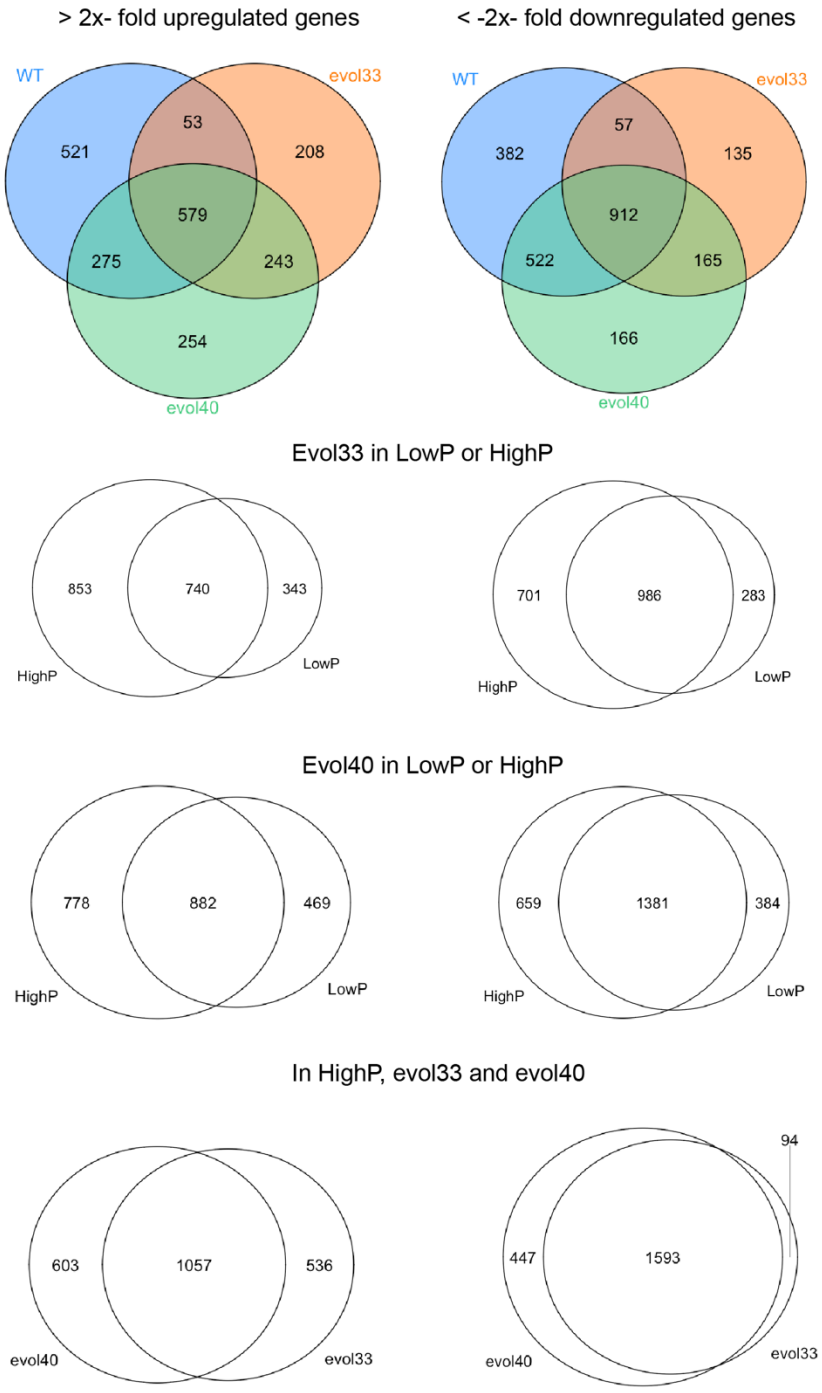

Supplemental Figure A1.11:

Venn diagrams of genes >2-fold upregulated and < -2-fold downregulated in phenol in WT, evol33, and evol40 ($p_{adj} < 0.01$). Glucose vs. low phenol conditions were compared for all 3 strains;

genes with > |2|-fold changes in low phenol (0.75 g/L, LowP) and high phenol (1.5 g/L, HighP) compared to glucose are shown in the same strains. > |2|-fold upregulated and downregulated genes in HighP in evol33 and evol40 are also shown. All genes have adjusted p values of < 0.01.

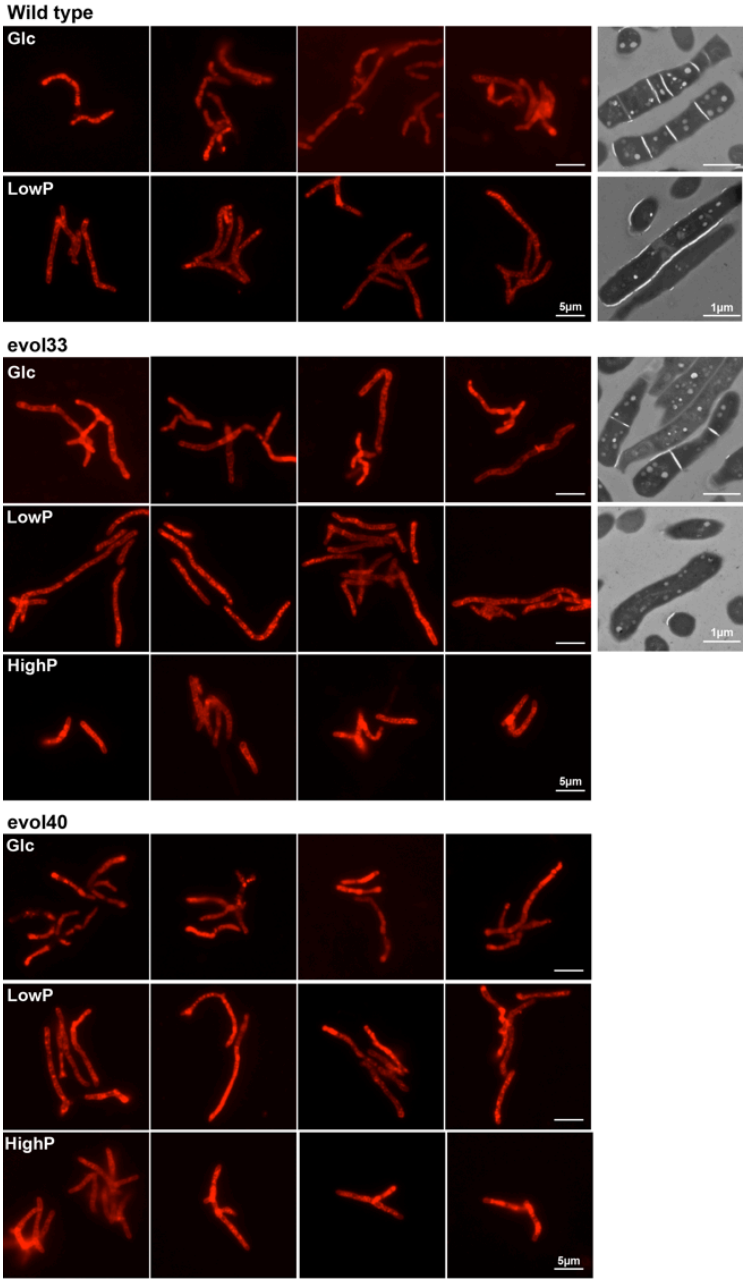

Supplemental Figure A1.12: Microscopy images of *R. opacus* PD630 under nitrogen-limited conditions.

The left four columns are epifluorescence micrographs of Nile red-stained, stationary phase *R. opacus* PD630 cells grown in nitrogen-limited conditions. The far-right column shows transmission electron micrographs of *R. opacus* cells grown in the same conditions.

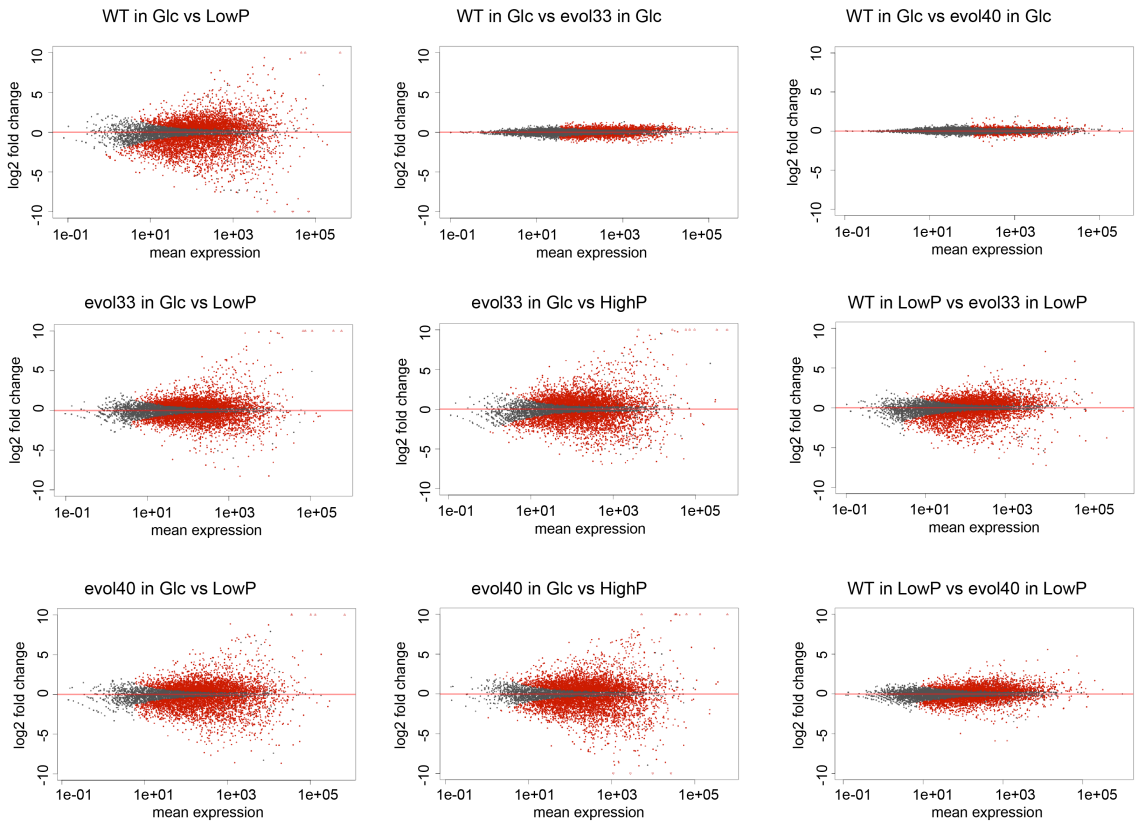

Supplemental Figure A1.13: MA Plot Summary.

Each panel shows the up- or down-regulation of all genes in an indicated strain and medium composition compared to a different strain and medium composition. Expression difference of each gene is plotted as log2 fold change (y axis) and mean expression (x axis) of the gene. The gray dots represent insignificant fold changes in expression, and the red dots represent significant fold changes in expression where significance threshold is defined as the adjusted p value < 0.1 (false discovery rate (Benjamini-Hochberg procedure) calculated using DESeq2 (Love et al., 2014). Glc, 1 g/L glucose; LowP, 0.75 g/L phenol; and HighP, 1.5 g/L phenol.

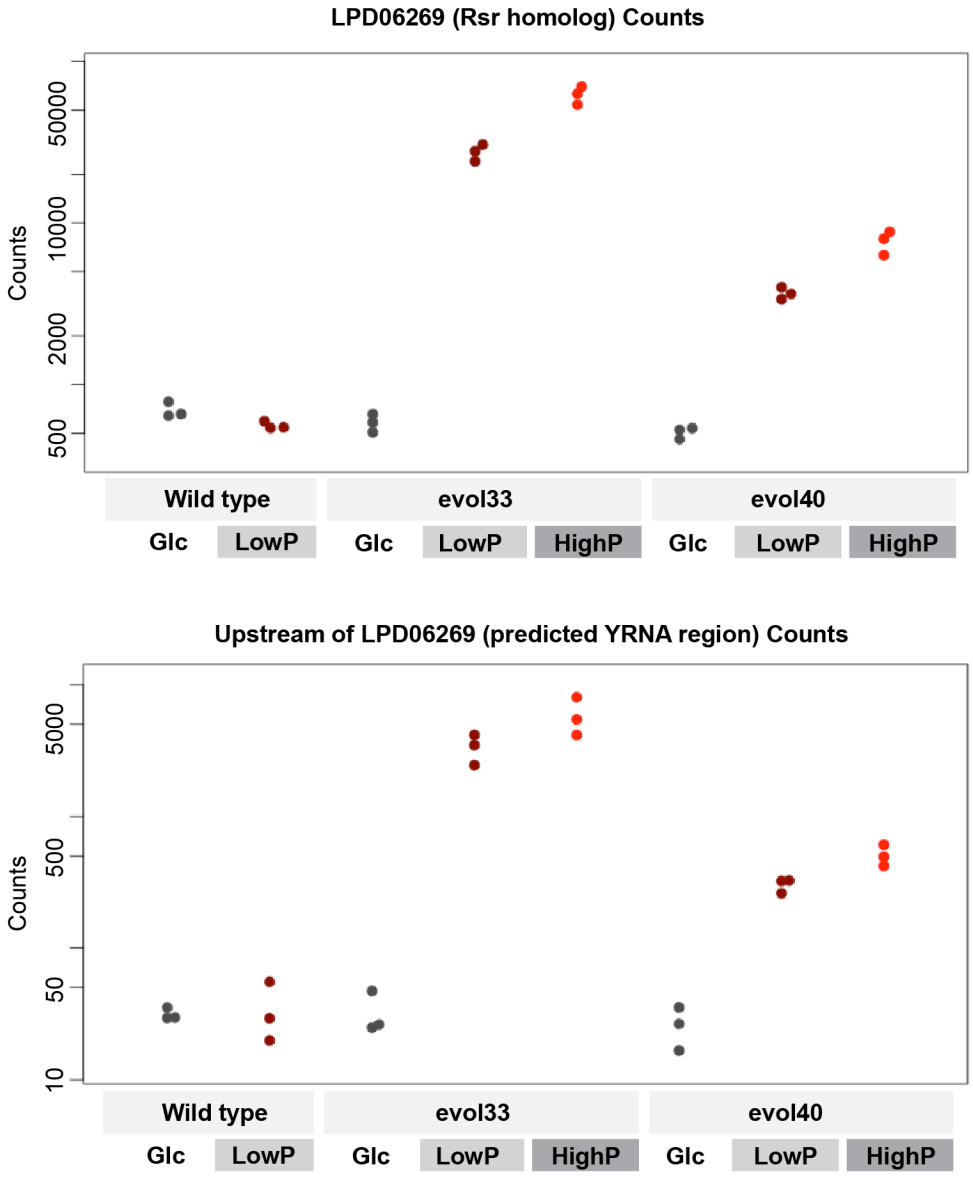

Supplemental Figure A1.14: Expression profile of Rsr and YRNA homologs in different growth conditions.

Top, Rsr homolog expression profile. Raw counts were normalized using the plotCounts function in DESeq2 (Love et al., 2014) and plotted using Beeswarm package (https://cran.r-project.org/web/packages/beeswarm/index.html). **Bottom**, RNA reads mapped to the noncoding

region upstream of LPD06269 (predicted YRNA). Glc, 1 g/L glucose; LowP, 0.75 g/L phenol; and HighP, 1.5 g/L phenol.

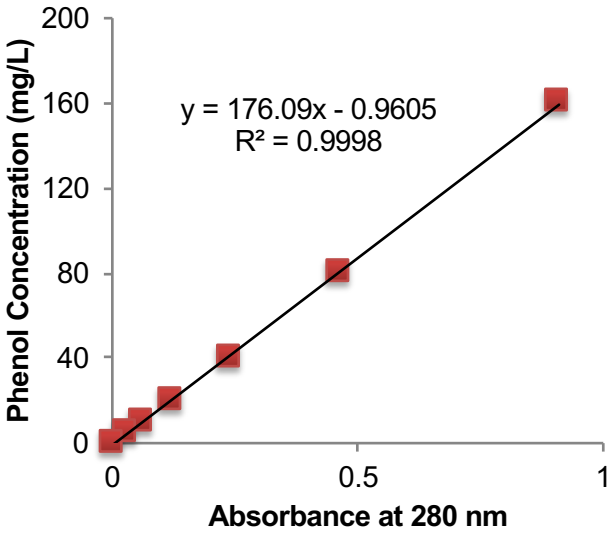

Supplemental Figure A1.15: Calibration curve obtained by using known concentrations of phenol in minimal medium and measuring absorbance at 280 nm.

Supplemental Table A1.1: Comparison of WT, evol33, and evol40 maximum biomass accumulation.

Initial OD_{600} was 0.01, and cells were grown in high nitrogen conditions (1 g/L ammonium sulfate). Biomass accumulation values reported are the highest attained OD_{600} value after 45 hours of growth. Significance was determined by a one mean, two-tailed Student's t-test ($p < 0.05$). Error represents one standard deviation of six biological replicates grown in 96 well plates. Improvement was calculated as (evolX-WT) / WT x 100%, where X = 33 or 40. See Materials and Methods for more details.

Phenol (g/L)	WT (OD_{600})	evol33 (OD_{600})	evol40 (OD_{600})	Significantly higher than WT?	evol33 improvement (%)	evol40 improvement (%)
0.75	0.33 ± 0.03	0.45 ± 0.03	0.44 ± 0.04	Yes, both	36.1	32.5
1	0.40 ± 0.06	0.48 ± 0.05	0.48 ± 0.04	Yes, both	21.5	22.0
1.25	0.39 ± 0.07	0.52 ± 0.05	0.53 ± 0.05	Yes, both	32.2	33.4
1.5	0.27 ± 0.04	0.52 ± 0.06	0.55 ± 0.06	Yes, both	92.3	102.4
1.75	0.18 ± 0.05	0.35 ± 0.04	0.44 ± 0.03	Yes, both	92.3	145.9
2	0.07 ± 0.04	0.27 ± 0.04	0.32 ± 0.03	Yes, both	297.6	372.5

Supplemental Table A1.2: Comparison of WT, evol33, and evol40 lag phase.

Initial OD_{600} was 0.01, and cells were grown in high nitrogen conditions (1 g/L ammonium sulfate). Lag phase was calculated as the time for more than two doublings to occur ($OD_{600} > 0.04$). Significance was determined by a one mean, two-tailed Student's t-test ($p < 0.05$). Error represents one standard deviation of six biological replicates grown in 96 well plates. Improvement was calculated as (WT-evolX) / WT x 100%, where X = 33 or 40. See Materials and Methods for more details.

Phenol (g/L)	WT (h)	evol33 (h)	evol40 (h)	Significantly lower than WT?	evol33 improvement (%)	evol40 improvement (%)
0.75	4.7 ± 2.4	3.3 ± 1.3	3.8 ± 0.1	No	28.4	18.2
1	7.9 ± 5.7	6.6 ± 5.1	3.8 ± 0.1	No	17.3	51.9
1.25	10.7 ± 5.7	7.2 ± 6.4	6.6 ± 5.1	No	32.6	38.6
1.5	17.3 ± 2.7	9.3 ± 5.9	11.5 ± 5.0	Evol33 only	46.4	33.6
1.75	25.4 ± 4.3	14.2 ± 5.2	12.0 ± 5.1	Yes, both	44.3	52.6
2	39.9 ± 5.7	18.4 ± 3.2	18.4 ± 3.2	Yes, both	53.9	53.9

Supplemental Table A1.3: Comparison of WT, evol33, and evol40 growth rates.

Initial OD_{600} was 0.01, and cells were grown in high nitrogen conditions (1 g/L ammonium sulfate). Specific growth rates were calculated from fitting optical density measurements in the exponential phase. Significance was determined by a one mean, two-tailed Student's t-test ($p < 0.05$). Error represents one standard deviation of six biological replicates grown in 96 well plates. The fitted values for each biological replicate were averaged to calculate p values for significance. N/A = not applicable. * = not enough growth to calculate accurate growth rate. Improvement was calculated as (evolX-WT) / WT x 100%, where X = 33 or 40. See Materials and Methods for more details.

Phenol (g/L)	WT (hr^{-1})	evol33 (hr^{-1})	evol40 (hr^{-1})	Significantly higher than WT?	evol33 improvement (%)	evol40 improvement (%)
0.75	0.06 ± 0.01	0.08 ± 0.03	0.07 ± 0.01	No	27.6	9.7
1	0.09 ± 0.02	0.12 ± 0.01	0.11 ± 0.02	evol33 only	27.7	12.8
1.25	0.08 ± 0.02	0.11 ± 0.02	0.12 ± 0.03	Yes, both	39.3	48.6
1.5	0.07 ± 0.01	0.09 ± 0.01	0.10 ± 0.02	Yes, both	29.6	37.7
1.75	0.08 ± 0.01	0.09 ± 0.01	0.09 ± 0.01	No	12.0	8.0
2	*	0.08 ± 0.01	0.09 ± 0.01	N/A	N/A	N/A

Supplemental Table A1.4: Maximum Nile red fluorescence in stationary phase.

Nile red fluorescence was measured using flow cytometry as described in Materials and Methods. Significance was determined by a one mean, two-tailed Student's t-test ($p < 0.05$). Error represents one standard deviation of three biological replicates. Improvement was calculated as (evolX-WT) / WT x 100%, where X = 33 or 40. N/A = not applicable. ** = no significant growth (< 1 cell doubling in 10 mL cultures). Glc = 1 g/L glucose, LowP = 0.75 g/L phenol, and HighP = 1.5 g/L phenol. Cells were grown in low nitrogen conditions (0.05 g/L ammonium sulfate).

Condition	WT (a.u.)	evol33 (a.u.)	evol40 (a.u.)	Significantly higher than WT?	evol33 improvement (%)	evol40 improvement (%)
Glc	355 ± 25	396 ± 43	413 ± 63	No	12	16
LowP	205 ± 33	519 ± 51	393 ± 62	Yes, both	153	92
HighP	**	542 ± 64	550 ± 24	N/A	N/A	N/A

Supplemental Table A1.5: Overall lipid productivity as measured by Nile red fluorescence.

Productivity was calculated as the change in Nile red fluorescence divided by time elapsed, including a minimum of four time points. Significance was determined by a one mean, two-tailed Student's t-test ($p < 0.05$). Error represents one standard deviation of three biological replicates. Improvement was calculated as (evolX-WT) / WT x 100%, where X = 33 or 40. N/A = not applicable. ** = no significant growth (< 1 cell doubling in 10 mL cultures). Glc = 1 g/L glucose, LowP = 0.75 g/L phenol, and HighP = 1.5 g/L phenol. Cells were grown in low nitrogen conditions (0.05 g/L ammonium sulfate).

Condition	WT (a.u. hr^{-1})	evol33 (a.u. hr^{-1})	evol40 (a.u. hr^{-1})	Significantly higher than WT?	evol33 improvement (%)	evol40 improvement (%)
Glc	8.4 ± 2.3	8.2 ± 1.6	7.8 ± 2.4	No	N/A	N/A
LowP	5.8 ± 1.4	13.6 ± 1.0	8.9 ± 0.9	Yes, both	134	53
HighP	**	16.5 ± 0.9	19.4 ± 0.8	N/A	N/A	N/A

Supplemental Table A1.7: Differentially regulated genes in WT and adapted strains.

A, The number of genes with indicated fold change in specified strains and conditions. Glc = 1 g/L glucose, LowP = 0.75 g/L phenol, and HighP = 1.5 g/L phenol. Lists of greater than 8-fold upregulated or downregulated genes with DESeq2 results are shown in Supplemental Table S6 (Sheet 1 through 10). **B**, Average fold change of the genes in specified conditions.

A

Fold change	> 4	> 8	>16	>256	< -4	< -8	< -16	< -256
WT LowP vs. Glc	395	164	85	7	592	318	180	9
evol33 LowP vs. Glc	302	112	70	13	287	90	38	2
evol40 LowP vs. Glc	327	141	74	8	564	253	101	1
evol33 HighP vs. Glc	411	200	118	16	507	220	101	0
evol40 HighP vs. Glc	440	197	116	10	721	348	166	10

B

	> 8-fold upregulated	< 8-fold downregulated
WT LowP vs. Glc	22.83	22.23
evol33 LowP vs. Glc	34.58	18.26
evol40 LowP vs. Glc	25.47	16.76
evol33 HighP vs. Glc	30.92	16.93
evol40 HighP vs. Glc	29.65	20.49

Supplemental Table A1.8: Annotation for phenolic degradation pathways present in *R. opacus* PD630 (Supplemental Figure S10). NA = none annotated.

# in Fig S10	Enzyme name	E.C.#	Gene IDs
1	phenol hydroxylase	1.14.13.7	PD630_LPD06575 + PD630_LPD06576, PD630_LPD6740 + PD630_LPD06741
2	catechol 1,2-dioxygenase	1.13.11.1	PD630_LPD06568, PD630_LPD06742
3	muconate cycloisomerase I	5.5.1.1	PD630_LPD06567
4	muconolactone D-isomerase	5.3.3.4	PD630_LPD06566
5	3-oxoadipate enol-lactonase	3.1.1.24	PD630_LPD05453
6	succinyl-CoA:3-ketoacid-CoA transferase	2.8.3.6	PD630_LPD05448 + PD630_LPD05449
7	3-oxoadipyl-CoA thiolase	2.3.1.174	PD630_LPD05455, PD630_LPD06744
8	protocatechuic 3,4-dioxygenase	1.13.11.3	PD630_LPD05450 + PD630_LPD05451
9	3-carboxymuconate cycloisomerase I	5.5.1.2	PD630_LPD05452, PD630_LPD07500
10	4-carboxymuconolactone decarboxylase	4.1.1.44	PD630_LPD07725, PD630_LPD07387, PD630_LPD07362, PD630_LPD06866, PD630_LPD06775, PD630_LPD06313
11	gentisate 1,2-dioxygenase	1.13.11.4	PD630_LPD03773, PD630_LPD06029
12	maleylpyruvate isomerase	5.2.1.4	PD630_LPD03771
13	fumarylpyruvate hydrolase	3.7.1.20	PD630_LPD03774, PD630_LPD06028
14	catechol 2,3-dioxygenase	1.13.11.2	PD630_LPD00178
15	2-hydroxymuconic semialdehyde dehydrogenase	1.2.1.85	NA
16	2-hydroxymuconate tautomerase	5.3.2.6	PD630_LPD00179

17	2-hydroxymuconic semialdehyde hydrolase	3.7.1.9	Plasmid5_LPD13074
18	2-oxo-3-hexenedioate decarboxylase	4.1.1.77	NA
19	2-oxopent-4-enoate hydratase	4.2.1.80	PD630_LPD02410, Plasmid4_LPD12051
20	acetaldehyde dehydrogenase (acylating)	1.2.1.10	PD630_LPD00985, PD630_02419, Plasmid4_LPD12052

Supplemental Table A1.9: Growth rate, lag phase, and maximum optical density of best-performing strains obtained from colony purification.

Cells were grown in 50 mL of minimal salts medium supplemented with 0.75 g/L phenol and 1 g/L nitrogen source (initial OD_{600} = 0.05). See the Materials and Methods for information on the calculation of growth rate and lag phase.

Strain	Specific Growth Rate (hr^{-1})	Lag Phase (h)	Max OD_{600}
WT	0.107	27	0.55
33-2 (evol33)	0.149	17	0.66
33-3	0.127	17	0.65
40-1 (evol40)	0.135	17	0.75
40-2	0.133	17	0.67
40-6	0.130	17	0.61

A1.7 References

1. Chundawat S.P., Beckham G.T., Himmel M.E., Dale B.E. Deconstruction of lignocellulosic biomass to fuels and chemicals. Annu. Rev. Chem. Biomol. Eng. 2011;2:121–145. [PubMed]

2. Sun Y., Cheng J. Hydrolysis of lignocellulosic materials for ethanol production: a review. Bioresour. Technol. 2002;83:1–11. [PubMed]

3. Peralta-Yahya P.P., Zhang F., del Cardayre S.B., Keasling J.D. Microbial engineering for the production of advanced biofuels. Nature. 2012;488:320–328. [PubMed]

4. Ragauskas A.J., Beckham G.T., Biddy M.J., Chandra R., Chen F., Davis M.F., Davison B.H., Dixon R.A., Gilna P., Keller M., et al. Lignin valorization: improving lignin processing in the biorefinery. Science. 2014;344:1246843. [PubMed]

5. Steen E.J., Kang Y., Bokinsky G., Hu Z., Schirmer A., McClure A., del Cardayre S.B., Keasling J.D. Microbial production of fatty-acid-derived fuels and chemicals from plant biomass. Nature. 2010;463:559–562. [PubMed]

6. Rubin E.M. Genomics of cellulosic biofuels. Nature. 2008;454:841–845. [PubMed]

7. Keating D.H., Zhang Y., Ong I.M., McIlwain S., Morales E.H., Grass J.A., Tremaine M., Bothfeld W., Higbee A., Ulbrich A., et al. Aromatic inhibitors derived from ammonia-pretreated lignocellulose hinder bacterial ethanologenesis by activating regulatory circuits controlling inhibitor efflux and detoxification. Front. Microbiol. 2014;5:402. [PMC free article] [PubMed]

8. Palmqvist E., Hahn-Hagerdal B. Fermentation of lignocellulosic hydrolysates. II: inhibitors and mechanisms of inhibition. Bioresour. Technol. 2000;74:25–33.

9. Strassberger Z., Tanase S., Rothenberg G. The pros and cons of lignin valorisation in an integrated biorefinery. RSC Adv. 2014;4:25310–25318.

10. Sannigrahi P., Ragauskas A.J. Characterization of Fermentation Residues from the Production of Bio-Ethanol from Lignocellulosic Feedstocks. J. Biobased Mater. Bioenergy. 2011;5:514–519.

11. Carrier M., Loppinet-Serani A., Denux D., Lasnier J.-M., Ham-Pichavant F., Cansell F., Aymonier C. Thermogravimetric analysis as a new method to determine the lignocellulosic composition of biomass. Biomass Bioenergy. 2011;35:298–307.

12. Harwood C.S., Parales R.E. The beta-ketoadipate pathway and the biology of self-identity. Annu. Rev. Microbiol. 1996;50:553–590. [PubMed]

13. Johnson C.W., Beckham G.T. Aromatic catabolic pathway selection for optimal production of pyruvate and lactate from lignin. Metab. Eng. 2015;28:240–247. [PubMed]

14. Kosa M., Ragauskas A.J. Bioconversion of lignin model compounds with oleaginous *Rhodococci*. Appl. Microbiol. Biotechnol. 2012;93:891–900. [PubMed]

15. Salvachua D., Karp E.M., Nimlos C.T., Vardon D.R., Beckham G.T. Towards lignin consolidated bioprocessing: simultaneous lignin depolymerization and product generation by bacteria. Green Chem. 2015;17:4951–4967.

16. Zaitsev G.M., Uotila J.S., Tsitko I.V., Lobanok A.G., Salkinoja-Salonen M.S. Utilization of Halogenated Benzenes, Phenols, and Benzoates by *Rhodococcus opacus* GM-14. Appl. Environ. Microbiol. 1995;61:4191–4201. [PMC free article] [PubMed]

17. Di Gennaro P., Terreni P., Masi G., Botti S., De Ferra F., Bestetti G. Identification and characterization of genes involved in naphthalene degradation in *Rhodococcus opacus* R7. Appl. Microbiol. Biotechnol. 2010;87:297–308. [PubMed]

18. Alvarez H.M., Mayer F., Fabritius D., Steinbuchel A. Formation of intracytoplasmic lipid inclusions by *Rhodococcus opacus* strain PD630. Arch. Microbiol. 1996;165:377–386. [PubMed]

19. Taylor C.R., Hardiman E.M., Ahmad M., Sainsbury P.D., Norris P.R., Bugg T.D. Isolation of bacterial strains able to metabolize lignin from screening of environmental samples. J. Appl. Microbiol. 2012;113:521–530. [PubMed]

20. Holder J.W., Ulrich J.C., DeBono A.C., Godfrey P.A., Desjardins C.A., Zucker J., Zeng Q., Leach A.L., Ghiviriga I., Dancel C., et al. Comparative and functional genomics of *Rhodococcus opacus* PD630 for biofuels development. PLoS Genet. 2011;7:e1002219. [PMC free article] [PubMed]

21. LeBlanc J.C., Goncalves E.R., Mohn W.W. Global response to desiccation stress in the soil actinomycete *Rhodococcus jostii* RHA1. Appl. Environ. Microbiol. 2008;74:2627–2636.[PMC free article] [PubMed]

22. de Carvalho C.C., Marques M.P., Hachicho N., Heipieper H.J. Rapid adaptation of *Rhodococcus erythropolis* cells to salt stress by synthesizing polyunsaturated fatty acids. Appl. Microbiol. Biotechnol. 2014;98:5599–5606. [PubMed]

23. Fischer C.R., Klein-Marcuschamer D., Stephanopoulos G. Selection and optimization of microbial hosts for biofuels production. Metab. Eng. 2008;10:295–304. [PubMed]

24. van der Geize R., Dijkhuizen L. Harnessing the catabolic diversity of rhodococci for environmental and biotechnological applications. Curr. Opin. Microbiol. 2004;7:255–261. [PubMed]

25. Uz I., Duan Y.P., Ogram A. Characterization of the naphthalene-degrading bacterium, *Rhodococcus opacus* M213. FEMS Microbiol. Lett. 2000;185:231–238. [PubMed]

26. Taki H., Syutsubo K., Mattison R.G., Harayama S. Identification and characterization of o-xylene-degrading *Rhodococcus* spp. which were dominant species in the remediation of o-xylene-contaminated soils. Biodegradation. 2007;18:17–26. [PubMed]

27. Wang B., Rezenom Y.H., Cho K.C., Tran J.L., Lee do G., Russell D.H., Gill J.J., Young R., Chu K.H. Cultivation of lipid-producing bacteria with lignocellulosic biomass: effects of inhibitory compounds of lignocellulosic hydrolysates. Bioresour. Technol. 2014;161:162–170. [PubMed]

28. Na K.S., Kuroda A., Takiguchi N., Ikeda T., Ohtake H., Kato J. Isolation and characterization of benzene-tolerant *Rhodococcus opacus* strains. J. Biosci. Bioeng. 2005;99:378–382. [PubMed]

29. Fuchs G., Boll M., Heider J. Microbial degradation of aromatic compounds - from one strategy to four. Nat. Rev. Microbiol. 2011;9:803–816. [PubMed]

30. Sainsbury P.D., Hardiman E.M., Ahmad M., Otani H., Seghezzi N., Eltis L.D., Bugg T.D. Breaking down lignin to high-value chemicals: the conversion of lignocellulose to vanillin in a gene deletion mutant of *Rhodococcus jostii* RHA1. ACS Chem. Biol. 2013;8:2151–2156. [PubMed]

31. Kurosawa K., Boccazzi P., de Almeida N.M., Sinskey A.J. High-cell-density batch fermentation of *Rhodococcus opacus* PD630 using a high glucose concentration for triacylglycerol production. J. Biotechnol. 2010;147:212–218. [PubMed]

32. Xiong X., Wang X., Chen S. Engineering of a xylose metabolic pathway in *Rhodococcus* strains. Appl. Environ. Microbiol. 2012;78:5483–5491. [PMC free article] [PubMed]

33. Kurosawa K., Wewetzer S.J., Sinskey A.J. Engineering xylose metabolism in triacylglycerol-producing *Rhodococcus opacus* for lignocellulosic fuel production. Biotechnol. Biofuels. 2013;6:134.[PMC free article] [PubMed]

34. Waltermann M., Luftmann H., Baumeister D., Kalscheuer R., Steinbuchel A. *Rhodococcus opacus*strain PD630 as a new source of high-value single-cell oil? Isolation and characterization of triacylglycerols and other storage lipids. Microbiology. 2000;146:1143–1149. [PubMed]

35. Nicolaou S.A., Gaida S.M., Papoutsakis E.T. A comparative view of metabolite and substrate stress and tolerance in microbial bioprocessing: From biofuels and chemicals, to biocatalysis and bioremediation. Metab. Eng. 2010;12:307–331. [PubMed]

36. Nielsen D.R., Moon T.S. From promise to practice. The role of synthetic biology in green chemistry. EMBO Rep. 2013;14:1034–1038. [PMC free article] [PubMed]

37. Hollinshead W.D., Henson W.R., Abernathy M., Moon T.S., Tang Y.J. Rapid metabolic analysis of *Rhodococcus opacus* PD630 via parallel ^{13}C-metabolite fingerprinting. Biotechnol. Bioeng. 2016;113:91–100. [PubMed]

38. van der Pol E.C., Bakker R.R., Baets P., Eggink G. By-products resulting from lignocellulose pretreatment and their inhibitory effect on fermentations for (bio)chemicals and fuels. Appl. Microbiol. Biotechnol. 2014;98:9579–9593. [PubMed]

39. Shumkova E.S., Solianikova I.P., Plotnikova E.G., Golovleva L.A. Phenol degradation by *Rhodococcus opacus* strain 1G. Prikl. Biokhim. Mikrobiol. 2009;45:51–57. [PubMed]

40. Kurosawa K., Laser J., Sinskey A.J. Tolerance and adaptive evolution of triacylglycerol-producing *Rhodococcus opacus* to lignocellulose-derived inhibitors. Biotechnol. Biofuels. 2015;8:76.[PMC free article] [PubMed]

41. Kosa M., Ragauskas A.J. Lignin to lipid bioconversion by oleaginous *Rhodococci*. Green Chem. 2013;15:2070–2074.

42. Wei Z., Zeng G., Huang F., Kosa M., Sun Q., Meng X., Huang D., Ragauskas A.J. Microbial lipid production by oleaginous *Rhodococci* cultured in lignocellulosic autohydrolysates. Appl. Microbiol. Biotechnol. 2015;99:7369–7377. [PubMed]

43. Wei Z., Zeng G., Kosa M., Huang D., Ragauskas A.J. Pyrolysis oil-based lipid production as biodiesel feedstock by *Rhodococcus opacus*. Appl. Biochem. Biotechnol. 2015;175:1234–1246. [PubMed]

44. Kurosawa K., Anthony Debono C., Sinskey A.J. Lignocellulose-derived inhibitors improve lipid extraction from wet *Rhodococcus opacus* cells. Bioresour. Technol. 2015;193:206–212. [PubMed]

45. Blazeck J., Hill A., Liu L., Knight R., Miller J., Pan A., Otoupal P., Alper H.S. Harnessing *Yarrowia lipolytica* lipogenesis to create a platform for lipid and biofuel production. Nat. Commun. 2014;5:3131.[PubMed]

46. Fisher S., Barry A., Abreu J., Minie B., Nolan J., Delorey T.M., Young G., Fennell T.J., Allen A., Ambrogio L., et al. A scalable, fully automated process for construction of sequence-ready human exome targeted capture libraries. Genome Biol. 2011;12:R1. [PMC free article] [PubMed]

47. Bowman S.K., Simon M.D., Deaton A.M., Tolstorukov M., Borowsky M.L., Kingston R.E. Multiplexed Illumina sequencing libraries from picogram quantities of DNA. BMC Genomics. 2013;14:466. [PMC free article] [PubMed]

48. Chen Y., Ding Y., Yang L., Yu J., Liu G., Wang X., Zhang S., Yu D., Song L., Zhang H., et al. Integrated omics study delineates the dynamics of lipid droplets in *Rhodococcus opacus* PD630. Nucleic Acids Res. 2014;42:1052–1064. [PMC free article] [PubMed]

49. Langmead B., Salzberg S.L. Fast gapped-read alignment with Bowtie 2. Nat. Methods. 2012;9:357–359. [PMC free article] [PubMed]

50. Li H., Handsaker B., Wysoker A., Fennell T., Ruan J., Homer N., Marth G., Abecasis G., Durbin R. The Sequence Alignment/Map format and SAMtools. Bioinformatics. 2009;25:2078–2079.[PMC free article] [PubMed]

51. Li H. A statistical framework for SNP calling, mutation discovery, association mapping and population genetical parameter estimation from sequencing data. Bioinformatics. 2011;27:2987–2993.[PMC free article] [PubMed]

52. Walker B.J., Abeel T., Shea T., Priest M., Abouelliel A., Sakthikumar S., Cuomo C.A., Zeng Q., Wortman J., Young S.K., et al. Pilon: an integrated tool for comprehensive microbial variant detection and genome assembly improvement. PLoS One. 2014;9:e112963. [PMC free article] [PubMed]

53. Chevreux B., Wetter T, Suhai S. Proceedings of the German Conference on Bioinformatics (GCB) Vol. 99. Hannover: 1999. Computer Science and Biology; pp. 45–56.

54. Liao Y., Smyth G.K., Shi W. featureCounts: an efficient general purpose program for assigning sequence reads to genomic features. Bioinformatics. 2014;30:923–930. [PubMed]

55. Love M.I., Huber W., Anders S. Moderated estimation of fold change and dispersion for RNA-seq data with DESeq2. Genome Biol. 2014;15:550. [PMC free article] [PubMed]

56. Lee D.H., Feist A.M., Barrett C.L., Palsson B.O. Cumulative number of cell divisions as a meaningful timescale for adaptive laboratory evolution of *Escherichia coli*. PLoS One. 2011;6:e26172.[PMC free article] [PubMed]

57. Leahy J.G., Batchelor P.J., Morcomb S.M. Evolution of the soluble diiron monooxygenases. FEMS Microbiol. Rev. 2003;27:449–479. [PubMed]

58. Choi K.Y., Kim D., Chae J.C., Zylstra G.J., Kim E. Requirement of duplicated operons for maximal metabolism of phthalate by *Rhodococcus* sp. strain DK17. Biochem. Biophys. Res. Commun. 2007;357:766–771. [PubMed]

59. Groning J.A., Eulberg D., Tischler D., Kaschabek S.R., Schlomann M. Gene redundancy of two-component (chloro)phenol hydroxylases in *Rhodococcus opacus* 1CP. FEMS Microbiol. Lett. 2014;361:68–75. [PubMed]

60. Sikkema J., de Bont J.A., Poolman B. Mechanisms of membrane toxicity of hydrocarbons. Microbiol. Rev. 1995;59:201–222. [PMC free article] [PubMed]

61. Putrins M., Ilves H., Lilje L., Kivisaar M., Horak R. The impact of ColRS two-component system and TtgABC efflux pump on phenol tolerance of *Pseudomonas putida* becomes evident only in growing bacteria. BMC Microbiol. 2010;10:110. [PMC free article] [PubMed]

62. Saa L., Jaureguibeitia A., Largo E., Llama M.J., Serra J.L. Cloning, purification and characterization of two components of phenol hydroxylase from *Rhodococcus erythropolis* UPV-1. Appl. Microbiol. Biotechnol. 2010;86:201–211. [PubMed]

63. Szokol J., Rucka L., Simcikova M., Halada P., Nesvera J., Patek M. Induction and carbon catabolite repression of phenol degradation genes in *Rhodococcus erythropolis* and *Rhodococcus jostii*. Appl. Microbiol. Biotechnol. 2014;98:8267–8279. [PubMed]

64. Ohhata N., Yoshida N., Egami H., Katsuragi T., Tani Y., Takagi H. An extremely oligotrophic bacterium, *Rhodococcus erythropolis* N9T-4, isolated from crude oil. J. Bacteriol. 2007;189:6824–6831.[PMC free article] [PubMed]

65. Maeda H., Dudareva N. The Shikimate Pathway and Aromatic Amino Acid Biosynthesis in Plants. Annu. Rev. Plant Biol. 2012;63:73–105. [PubMed]

66. MacEachran D.P., Prophete M.E., Sinskey A.J. The *Rhodococcus opacus* PD630 heparin-binding hemagglutinin homolog TadA mediates lipid body formation. Appl. Environ. Microbiol. 2010;76:7217–7225. [PMC free article] [PubMed]

67. Yun H.Y., Tamura N., Tamura T. *Rhodococcus* prokaryotic ubiquitin-like protein (Pup) is degraded by deaminase of pup (Dop) Biosci. Biotechnol. Biochem. 2012;76:1959–1966. [PubMed]

68. Dragosits M., Mattanovich D. Adaptive laboratory evolution—principles and applications for biotechnology. Microb. Cell Fact. 2013;12:64. [PMC free article] [PubMed]

69. Wielgoss S., Barrick J.E., Tenaillon O., Cruveiller S., Chane-Woon-Ming B., Medigue C., Lenski R.E., Schneider D. Mutation Rate Inferred From Synonymous Substitutions in a Long-Term Evolution Experiment With *Escherichia coli*. G3: Genes, Genomes, Genet. 2011;1:183–186. [PMC free article][PubMed]

70. Wells T., Jr, Ragauskas A.J. Biotechnological opportunities with the beta-ketoadipate pathway. Trends Biotechnol. 2012;30:627–637. [PubMed]

71. Kumar A., Kumar S., Kumar S. Biodegradation kinetics of phenol and catechol using *Pseudomonas putida* MTCC 1194. Biochem. Eng. J. 2005;22:151–159.

72. Saravanan P., Pakshirajan K., Saha P. Growth kinetics of an indigenous mixed microbial consortium during phenol degradation in a batch reactor. Bioresour. Technol. 2008;99:205–209. [PubMed]

73. Arutchelvan V., Kanakasabai V., Elangovan R., Nagarajan S., Muralikrishnan V. Kinetics of high strength phenol degradation using *Bacillus brevis*. J. Hazard. Mater. 2006;129:216–222. [PubMed]

74. Santos P.M., Benndorf D., Sa-Correia I. Insights into *Pseudomonas putida* KT2440 response to phenol-induced stress by quantitative proteomics. Proteomics. 2004;4:2640–2652. [PubMed]

75. Almiron M., Link A.J., Furlong D., Kolter R. A novel DNA-binding protein with regulatory and protective roles in starved *Escherichia coli*. Genes Dev. 1992;6:2646–2654. [PubMed]

76. Wei X., Mingjia H., Xiufeng L., Yang G., Qingyu W. Identification and biochemical properties of Dps (starvation-induced DNA binding protein) from cyanobacterium *Anabaena* sp. PCC 7120. IUBMB Life. 2007;59:675–681. [PubMed]

77. Harrison C. GrpE, a nucleotide exchange factor for DnaK. Cell Stress Chaperones. 2003;8:218–224.[PMC free article] [PubMed]

78. Calloni G., Chen T., Schermann S.M., Chang H.C., Genevaux P., Agostini F., Tartaglia G.G., Hayer-Hartl M., Hartl F.U. DnaK functions as a central hub in the *E. coli* chaperone network. Cell Rep. 2012;1:251–264. [PubMed]

79. Gallegos M.T., Williams P.A., Ramos J.L. Transcriptional control of the multiple catabolic pathways encoded on the TOL plasmid pWW53 of *Pseudomonas putida* MT53. J. Bacteriol. 1997;179:5024–5029.[PMC free article] [PubMed]

80. Arenghi F.L., Pinti M., Galli E., Barbieri P. Identification of the *Pseudomonas stutzeri* OX1 toluene-o-xylene monooxygenase regulatory gene (touR) and of its cognate promoter. Appl. Environ. Microbiol. 1999;65:4057–4063. [PMC free article] [PubMed]

81. Tropel D., van der Meer J.R. Bacterial transcriptional regulators for degradation pathways of aromatic compounds. Microbiol. Mol. Biol. Rev. 2004;68:474–500. [PMC free article] [PubMed]

82. Gallegos M.T., Schleif R., Bairoch A., Hofmann K., Ramos J.L. Arac/XylS family of transcriptional regulators. Microbiol. Mol. Biol. Rev. 1997;61:393–410. [PMC free article] [PubMed]

83. Schleif R. AraC protein, regulation of the l-arabinose operon in *Escherichia coli*, and the light switch mechanism of AraC action. FEMS Microbiol. Rev. 2010;34:779–796. [PubMed]

84. Khlebnikov A., Risa O., Skaug T., Carrier T.A., Keasling J.D. Regulatable arabinose-inducible gene expression system with consistent control in all cells of a culture. J. Bacteriol. 2000;182:7029–7034.[PMC free article] [PubMed]

85. Wolin S.L., Belair C., Boccitto M., Chen X., Sim S., Taylor D.W., Wang H.W. Non-coding Y RNAs as tethers and gates: Insights from bacteria. RNA Biol. 2013;10:1602–1608. [PMC free article] [PubMed]

86. Chen X., Sim S., Wurtmann E.J., Feke A., Wolin S.L. Bacterial noncoding Y RNAs are widespread and mimic tRNAs. RNA. 2014;20:1715–1724. [PMC free article] [PubMed]

87. Linger J.G., Vardon D.R., Guarnieri M.T., Karp E.M., Hunsinger G.B., Franden M.A., Johnson C.W., Chupka G., Strathmann T.J., Pienkos P.T., et al. Lignin valorization through integrated biological funneling and chemical catalysis. Proc. Natl. Acad. Sci. U. S. A. 2014;111:12013–12018. [PMC free article][PubMed]

88. Dunlop M.J., Dossani Z.Y., Szmidt H.L., Chu H.C., Lee T.S., Keasling J.D., Hadi M.Z., Mukhopadhyay A. Engineering microbial biofuel tolerance and export using efflux pumps. Mol. Syst. Biol. 2011;7:487. [PMC free article] [PubMed]

89. Foo J.L., Leong S.S. Directed evolution of an *E. coli* inner membrane transporter for improved efflux of biofuel molecules. Biotechnol. Biofuels. 2013;6:81. [PMC free article] [PubMed]

90. Fisher M.A., Boyarskiy S., Yamada M.R., Kong N., Bauer S., Tullman-Ercek D. Enhancing tolerance to short-chain alcohols by engineering the *Escherichia coli* AcrB efflux pump to secrete the non-native substrate n-butanol. ACS Synth. Biol. 2014;3:30–40. [PubMed]